7-1-2016

Energetics Across Ecological Scales

John M. Grady

John M. Grady

Candidate

Biology

Department

This dissertation is approved, and it is acceptable in quality and form for publication:

Approved by the Dissertation Committee:

Dr. Felisa Smith , Chairperson

Dr. James Brown

Dr. Christopher Witt

Dr. Richard Sibly

Energetics Across Ecological Scales

by

John M. Grady

M.S. Plant Biology, North Carolina State University, 2010
B.S. Ecology & Evolutionary Biology,
University of Arizona, 2007

DISSERTATION

Submitted in Partial Fulfillment of the
Requirements for the Degree of

Doctor of Philosophy
Biology

The University of New Mexico
Albuquerque, New Mexico

July 2016

Acknowledgements

I am deeply indebted to my advisor Felisa Smith, and my 'spiritual advisor' Jim Brown. Both have contributed greatly to my intellectual development and have opened doors in my career so that I can pursue the science I love. I must also acknowledge my parents, John and Veronica Grady, who have supported my journey all these years. It was your job, but you did it so well. Finally, I would like to thank Nature, or the 'God of Evolution' as my mother puts it. You can't hear me, but it still feels right to acknowledge the source of my inspiration. Thank you all.

Energetics Across Ecological Scales

by

John M. Grady

B.S. Ecology & Evolutionary Biology, University of Arizona, 2007
M.S. Plant Biology, North Carolina State University, 2010
Ph.D. Biology University of New Mexico, 2016

Abstract

Energy is the common currency of ecological interactions. In this dissertation, I consider ecological energetics at different temporal, spatial and organizational scales. In my first chapter, I examine the energetics and thermoregulation of enigmatic taxon: dinosaurs. From fossil evidence and assessment of living vertebrates I conclude that many non-avian dinosaurs were likely thermally intermediate, or 'mesothermic'. In my second chapter I detail the empirical evidence gathered to buttress my claim of dinosaur mesothermy. In my third chapter, I show how ecosystem rates of carbon flux, gross primary production and total biomass can be linked to individual body size. In my fourth and final chapter I explore how differences in metabolism and thermoregulation lead to predictable difference in marine predator biogeography, diversity and food consumption at ecosystem scales. A focus on organismal energetics offers insight into ecological interactions across space and time.

Table of Contents

Chapter I

‘Evidence for mesothermy in dinosaur’

Dinosaurs have long captured the public and scientific imagination, and debate has raged as to whether they were more like endothermic (‘warm-blooded’) mammals and birds or ectothermic (‘cold-blooded’) reptiles and fish. In this chapter, I examine growth rates of dinosaurs derived from fossil bones and compare this to growth and metabolism in living vertebrates. I show that predictable relationships are observed between growth, metabolic rates, and thermoregulation. Somewhat surprisingly, Mesozoic dinosaurs grew neither like endotherms or ectotherms. Rather, their growth rates most resembled thermally intermediate taxa – tuna, lamnid sharks, echidnas – that we have dubbed ‘mesotherms’ (from the Greek *mesos* for ‘middle’; and *thérmē* for ‘heat’). The implication, then, is that most dinosaurs were likely mesotherms as well, a successful thermal and metabolic strategy in the absence of endothermic competitors. The combined use of fossil markers of growth and metabolic scaling principles offers a promising route for resolving some of the oldest mysteries in paleontology.

areas of downwelling across the 660 is consistent with the occurrence of dehydration melting as observed in our laboratory experiments. An alternative bulk-compositional origin of low velocities near the top of the lower mantle is segregated basalt that may be neutrally buoyant (*23*) and would reduce seismic velocities (*24*).

However, long-term accumulation of basalt near the top of the lower mantle is not expected to be preferentially present where there is downwelling across the 660 and absent where there is not. The areas of downward flow across 660 do not all coincide with local presence of subducted slabs, so a direct link to composition of the sinking Farallon slab cannot explain the negative velocity gradients below 660. Assuming that the velocity reductions result from partial melt, and that the shear-velocity decrease per percent of melt is between 2.6 and 3.8%, as predicted for partial melt near 400-km depth (*25*), then 0.68 to 1% melt could explain a 2.6% shear velocity reduction indicated by negative *Ps* conversions with amplitude of 2% in the CCP image.

Prediction of partial melt percentages at 660-km depth for various H_2O contents requires knowledge of water partition coefficients between minerals and melts at relevant pressure-temperature (*P-T*) conditions in the peridotite-saturated compositional system. At present, experiments in the hydrous peridotite system at conditions near the 660 have not been performed. However, using experimental results for partial melting near the 410-km discontinuity (410) in a bulk peridotite system with 1 wt % H_2O indicates that ~5% partial melt at 410 km is expected (*26*, *27*) where the partition coefficient of H_2O between wadsleyite and olivine is at least 5:1 (*11*). We can expect at least 5% partial melt in a bulk 1 wt % H_2O peridotite system where the partition coefficient between ringwoodite and silicate perovskite is 15:1 (*11*). Thus, production of up to 1% melt by dehydration melting of hydrous ringwoodite viscously entrained into the lower mantle is feasible.

The density of hydrous melt near the top of the lower mantle is uncertain, but it is likely buoyant with respect to the top of the lower mantle (*28*). Hence, we expect that the velocity decreases imaged beneath the 660 are transient features resulting from ongoing downward flow through the 660 that is driven by sinking slabs in the lower mantle. Eventually, the slightly buoyant hydrous melt would percolate upward, returning H_2O to the transition zone (*4*). Dehydration melting has also been suggested to occur where hydrous wadsleyite upwells across the 410 and into the olivine stability field (*3*, *27*). Experiments indicate that hydrous melt is gravitationally stable atop the 410 (*28*), so once melt is generated, it may remain or spread laterally rather than maintaining a clear correlation with ongoing vertical flow patterns. Seismic detections of a low-velocity layer atop the 410 are common but laterally sporadic beneath North America and globally (*29*, *30*). The combination of dehydration melting driven by downwelling across the 660 and upwelling across the 410 could create a long-term H_2O trap in the transition zone (*4*).

REFERENCES AND NOTES

1. A. E. Saal, E. H. Hauri, C. H. Langmuir, M. R. Perfit, *Nature* **419**, 451–455 (2002).
2. J. R. Smyth, *Am. Mineral.* **72**, 1051 (1987).
3. D. L. Kohlstedt, H. Keppler, D. C. Rubie, *Contrib. Mineral. Petrol.* **123**, 345–357 (1996).
4. D. Bercovici, S. Karato, *Nature* **425**, 39–44 (2003).
5. D. G. Pearson *et al*., *Nature* **507**, 221–224 (2014).
6. H. Zhu, E. Bozdag, T. S. Duffy, J. Tromp, *Earth Planet. Sci. Lett.* **381**, 1–11 (2013).
7. A. Kelbert, A. Schultz, G. Egbert, *Nature* **460**, 1003–1006 (2009).
8. N. Bolfan-Casanova, H. Keppler, D. C. Rubie, *Geophys. Res. Lett.* **30**, 1905 (2003).
9. M. Murakami, K. Hirose, H. Yurimoto, S. Nakashima, N. Takafuji, *Science* **295**, 1885–1887 (2002).
10. K. Litasov *et al*., *Earth Planet. Sci. Lett.* **211**, 189–203 (2003).
11. T. Inoue, T. Wada, R. Sasaki, H. Yurimoto, *Phys. Earth Planet. Inter.* **183**, 245–251 (2010).
12. Materials and methods are available on *Science* Online.
13. S. D. Jacobsen, J. R. Smyth, H. A. Spetzler, C. M. Holl, D. J. Frost, *Phys. Earth Planet. Inter.* **143-144**, 47–56 (2004).
14. R. A. Kerr, *Science* **340**, 1283–1285 (2013).
15. J. P. Mercier, M. G. Bostock, A. M. Baig, *Geophysics* **71**, SI95–SI102 (2006).
16. B. Schmandt, K. G. Dueker, E. D. Humphreys, S. M. Hansen, *Earth Planet. Sci. Lett.* **331-332**, 224–236 (2012).
17. B. Tauzin, R. D. van der Hilst, G. Wittlinger, Y. Ricard, *J. Geophys. Res. Solid Earth* **118**, 2307–2322 (2013).
18. J. Ritsema, A. Deuss, H. J. van Heijst, J. H. Woodhouse, *Geophys. J. Int.* **184**, 1223–1236 (2011).
19. T. W. Becker, C. Faccenna, E. D. Humphreys, A. R. Lowry, M. S. Miller, *Earth Planet. Sci. Lett.* (2014).
20. N. A. Simmons, A. M. Forte, S. P. Grand, *Geophys. J. Int.* **177**, 1284–1304 (2009).
21. B. Steinberger, *Phys. Earth Planet. Inter.* **118**, 241–257 (2000).
22. A. M. Forte, R. Moucha, N. A. Simmons, S. P. Grand, J. X. Mitrovica, *Tectonophysics* **481**, 3–15 (2010).
23. C. T. A. Lee, W. P. Chen, *Earth Planet. Sci. Lett.* **255**, 357–366 (2007).
24. W. B. Xu, C. Lithgow-Bertelloni, L. Stixrude, J. Ritsema, *Earth Planet. Sci. Lett.* **275**, 70–79 (2008).
25. S. Hier-Majumder, A. Courtier, *Earth Planet. Sci. Lett.* **308**, 334–342 (2011).
26. M. M. Hirschmann, T. Tenner, C. Aubaud, A. C. Withers, *Phys. Earth Planet. Inter.* **176**, 54–68 (2009).
27. T. J. Tenner, M. M. Hirschmann, A. C. Withers, P. Ardia, *Contrib. Mineral. Petrol.* **163**, 297–316 (2012).
28. T. Sakamaki, A. Suzuki, E. Ohtani, *Nature* **439**, 192–194 (2006).
29. B. Schmandt, K. G. Dueker, S. M. Hansen, J. J. Jasbinsek, Z. Zhang, *Geochem. Geophys. Geosyst.* **12**, Q08014 (2011).
30. B. Tauzin, E. Debayle, G. Wittlinger, *Nat. Geosci.* **3**, 718–721 (2010).

ACKNOWLEDGMENTS

Seismic data were acquired from the IRIS Data Management Center. This work was supported by NSF grants EAR-0748707 to S.D.J. and EAR-1215720 to T.W.B., and by the David and Lucile Packard Foundation and Carnegie/DOE Alliance Center (CDAC) to S.D.J. Portions of this work were performed at GSECARS (Sector 13), Advanced Photon Source (APS), Argonne National Laboratory. GSECARS is supported by the NSF (EAR-1128799) and U.S. Department of Energy (DOE) (DE-FG02-94ER14466). Use of the APS was supported by the DOE-BES (Basic Energy Sciences) (DE-AC02-06CH11357). Portions of this work were performed at beamline U2A of the National Synchrotron Light Source (NSLS), Brookhaven National Laboratory. U2A is supported by COMPRES (Consortium for Materials Properties Research in Earth Sciences) under NSF Cooperative Agreement EAR 11-57758 and DOE-NNSA (National Nuclear Security Administration) (DE-FC-52-08NA28554, CDAC). Use of the NSLS was supported by the DOE-BES (DE-AC02-98CH10886). We thank S. Demouchy, D. J. Frost, E. H. Hauri, M. M. Hirschmann, F. Langenhorst, J. F. Lin, G. Shen, V. B. Prakapenka, and J. R. Smyth for discussions and help with experiments. B.S. and S.D.J. designed the research and wrote the paper. B.S. conducted the seismological research, and S.D.J. performed the experiments. T.W.B. produced the mantle circulation models, Z.L. contributed to the FTIR experiments, and K.G.D. contributed to seismic imaging. All authors participated in data interpretation and contributed to the manuscript.

SUPPLEMENTARY MATERIALS

www.sciencemag.org/content/344/6189/1265/suppl/DC1
Materials and Methods
Figs. S1 to S4
References (*31*–*38*)
Additional Data Tables S1 to S3

13 March 2014; accepted 12 May 2014
10.1126/science.1253358

DINOSAUR PHYSIOLOGY

Evidence for mesothermy in dinosaurs

John M. Grady,[1]* Brian J. Enquist,[2,3] Eva Dettweiler-Robinson,[1] Natalie A. Wright,[1] Felisa A. Smith[1]

Were dinosaurs ectotherms or fast-metabolizing endotherms whose activities were unconstrained by temperature? To date, some of the strongest evidence for endothermy comes from the rapid growth rates derived from the analysis of fossil bones. However, these studies are constrained by a lack of comparative data and an appropriate energetic framework. Here we compile data on ontogenetic growth for extant and fossil vertebrates, including all major dinosaur clades. Using a metabolic scaling approach, we find that growth and metabolic rates follow theoretical predictions across clades, although some groups deviate. Moreover, when the effects of size and temperature are considered, dinosaur metabolic rates were intermediate to those of endotherms and ectotherms and closest to those of extant mesotherms. Our results suggest that the modern dichotomy of endothermic versus ectothermic is overly simplistic.

Over the past few decades, the original characterization of dinosaurs by early paleontologists as lumbering, slow-metabolizing ectotherms has been challenged. Recent studies propose that dinosaurs were capable of an active lifestyle and were metabolically similar to endothermic mammals and birds (*1*–*3*). This debate is of more than heuristic interest; energy consumption is closely linked to life history, demographic, and ecological traits (*4*). Extant endothermic mammals and birds possess metabolic rates ~5 to 10 times higher than

those of reptiles and fish (*5*, *6*), but characterizing the metabolic rates of dinosaurs has been difficult.

A promising method for inferring paleoenergetics comes from studies of ontogenetic growth, in which age is determined from annual rings in bone cross sections and mass is determined from bone dimensions. Ultimately, growth is powered by metabolism, and rates of growth and energy use should correspond. Pioneering work by Erickson and others has led to a growing body of literature on dinosaur growth and generated important insights (*7*, *8*). However, many analyses were hampered by small samples, an outdated comparative data set, and the lack of an appropriate energetic framework. Increasing data availability permits a reassessment of dinosaur growth against a broader spectrum of animals, standardized for environmental temperature. Further, recent advances in metabolic theory provide a theoretical framework for evaluating metabolic rate on the basis of growth.

We used a comparative approach to characterize the energetics of dinosaurs and other extinct taxa. We examined the empirical and theoretical relationship between growth and resting metabolic rate, using a broad database of major vertebrate clades (*9*), and used our results to examine the energetics of Mesozoic dinosaurs. From empirical studies, we constructed ontogenetic growth curves and determined a maximum rate of growth for each species. Environmental temperature was standardized by only considering growth rates in ectotherms from tropical and subtropical climates or from laboratory settings between 24° and 30°C, comparable to temperatures experienced by dinosaurs during the Mesozoic (*10*). Data for dinosaur growth were taken from published reports that provided a minimum of five measurements of size and age. All metabolic rates were converted to watts (W). Where multiple metabolic or maximum growth rates for a species were recorded, the geometric mean was determined. Overall, our data set includes ~30,000 values and was used to characterize growth for 381 species, including 21 species of Mesozoic dinosaurs, 6 extinct crocodilians, and a Cretaceous shark (table S1). Dinosaurs are well represented both temporally (late Triassic to end-Cretaceous) and taxonomically (Theropoda, Sauropodomorpha, Ornithopoda, and Ceratopsia). Values for resting metabolic rates were compiled from the literature and standardized to a common temperature of 27°C (table S1). We performed phylogenetic independent contrasts (PICs) in addition to conventional ordinary least-squares regression (OLS) and standardized major axis regression (table S2).

Data show, within and across species, that resting metabolic rate B scales with body mass m as a power function, $B = B_0 m^{\alpha}$, where B_0 is

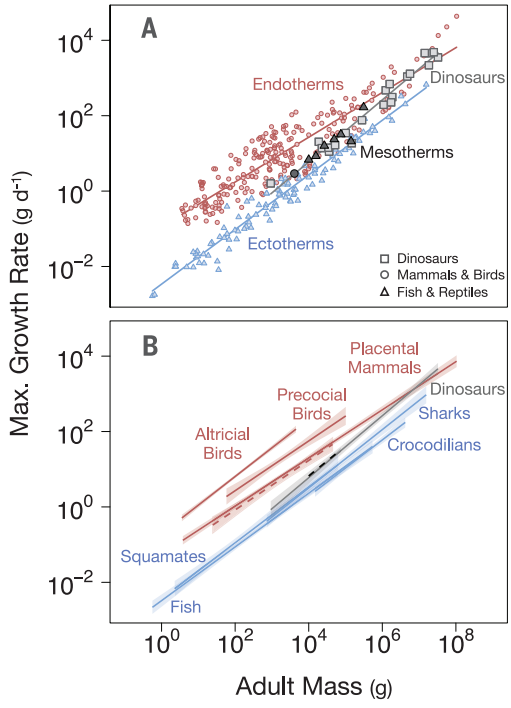

Fig. 1. The scaling of maximum growth rate in vertebrates. (**A**) Growth rates of thermoregulatory guilds. Red indicates endothermy; blue, ectothermy, gray, dinosaurs; and black, mesothermy. (**B**) Vertebrate taxa scaling with 95% confidence bands. The red dashed line indicates marsupials, and the black dashed line is tuna; all other taxa are labeled. See table S2 for regression parameters and statistics.

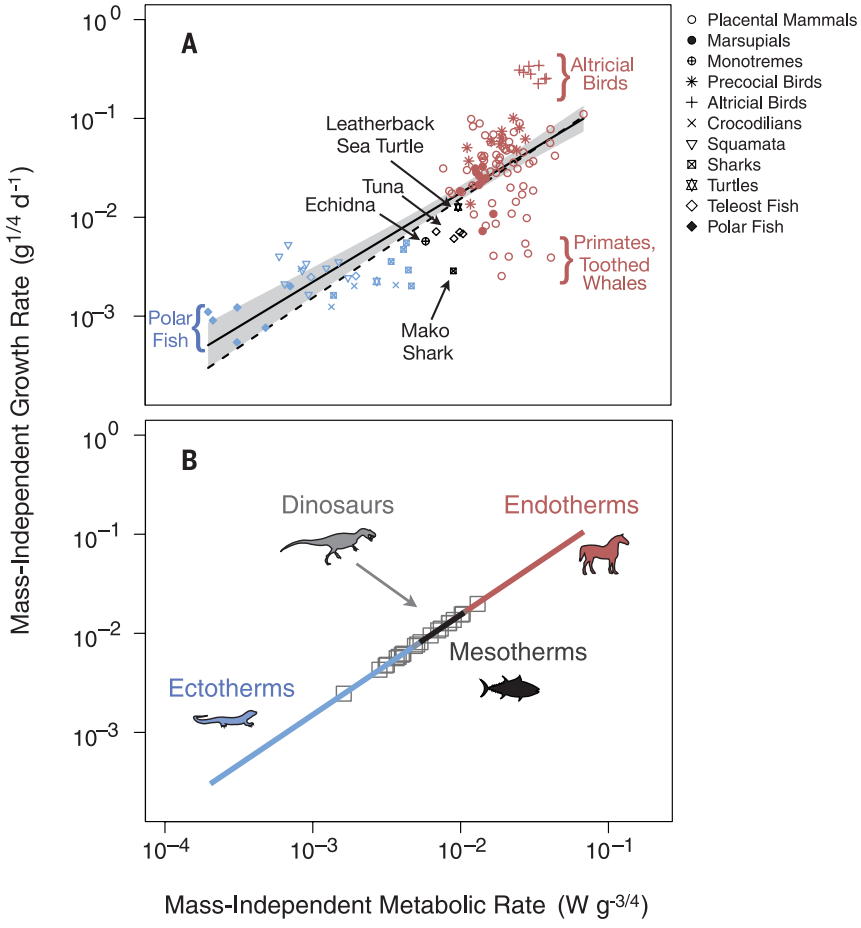

Fig. 2. Vertebrate growth energetics. (**A**) Relationship between growth and resting metabolic rate for vertebrates. The dashed line is the theoretical prediction; the solid line represents an OLS fitted regression with 95% confidence bands. (**B**) Predicted energetics of dinosaurs. Dinosaur rates (open squares) from Eq. 2 are plotted on the theoretical line. The ranges in metabolic rates occupied by extant endotherms, mesotherms, and ectotherms are indicated by color.

[1]Department of Biology, University of New Mexico, Albuquerque, NM 87131, USA. [2]Department of Ecology and Evolutionary Biology, University of Arizona, Tucson, AZ 85721, USA. [3]The Santa Fe Institute, USA, 1399 Hyde Park Road, Santa Fe, NM 87501, USA.
*Corresponding author. E-mail: jgrady@unm.edu

a normalization constant representing mass-independent metabolic rate, and α is ~3/4 and ranges from 0.65 to 0.85 (*11*, *12*). Growth rate varies over ontogeny, but use of the maximum growth rate (G_{max}) standardizes growth and permits interspecific comparisons. Empirical evidence (*13*) indicates that G_{max} scales similarly to B, where $G_{max} = G_0 M^{\alpha}$. This suggests that $B \propto G_{max}^{1}$ and thus that metabolic rate may be inferred from growth. However, the relationship between G_{max} and B across major vertebrate taxa has received little attention, and many uncertainties exist. For instance, Case (*13*) reported that fish G_{max} was an order of magnitude lower than that of reptiles, despite similarities in metabolic and thermoregulatory lifestyle (*6*).

Theoretical assessments of growth complement a strictly empirical approach and can strengthen paleontological inferences. An ontogenetic growth model based on metabolic scaling theory (MST) quantifies the linkages between G_{max} and metabolic rate from first principles of allometry and conservation of energy (*14*, *15*). According to MST (*9*), the relationship between B (W) and G_{max} (g day^{-1}) at final adult mass M is

$$B_M = cG_{max}^{1} \quad (1)$$

where $c \approx 0.66$ (W g^{-1} day). To observe the mass-independent relationship and compare energetic groups, we divide both sides by M^{α}, yielding

$$B_0 = cG_0 \quad (2)$$

To calculate metabolic rate at any ontogenetic mass m from the observed maximum growth rate, we combine Eqs. 1 and 2

$$B_m = cG_0 m^{3/4} \quad (3)$$

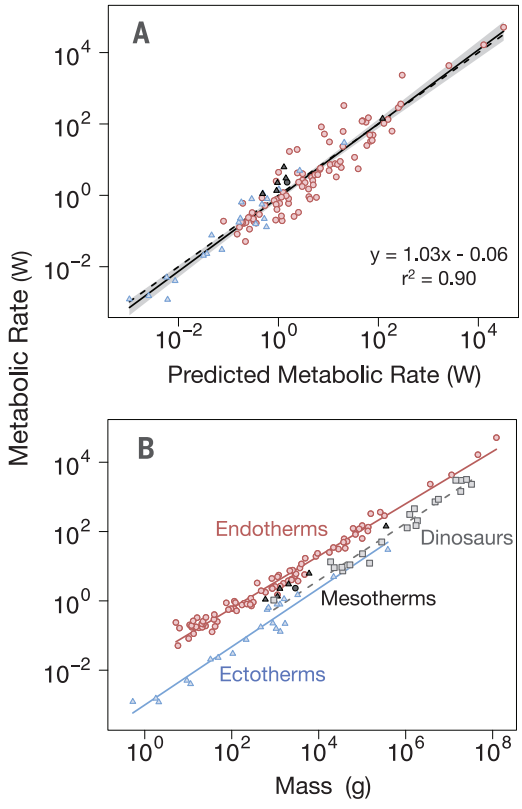

Fig. 3. Resting metabolic rates in vertebrates. (**A**) Predicted metabolic rates compared to observed rates. The solid line is the fitted regression, with shaded 95% confidence bands; the dashed line is the theoretical fit. (**B**) Metabolic scaling of vertebrates. Dinosaur resting metabolic rates are predicted from growth (dashed line); all other fits are predicted from empirical data. Endotherms: $y = 0.019x^{0.75}$, $r^2 = 0.98$, $n = 89$; Ectotherms (27°C): $y = 0.00099x^{0.84}$, $r^2 = 0.95$, $n = 22$; Dinosaurs: $y = 0.0020x^{0.82}$, $r^2 = 0.96$, $n = 21$. $P < 0.001$ for all regressions.

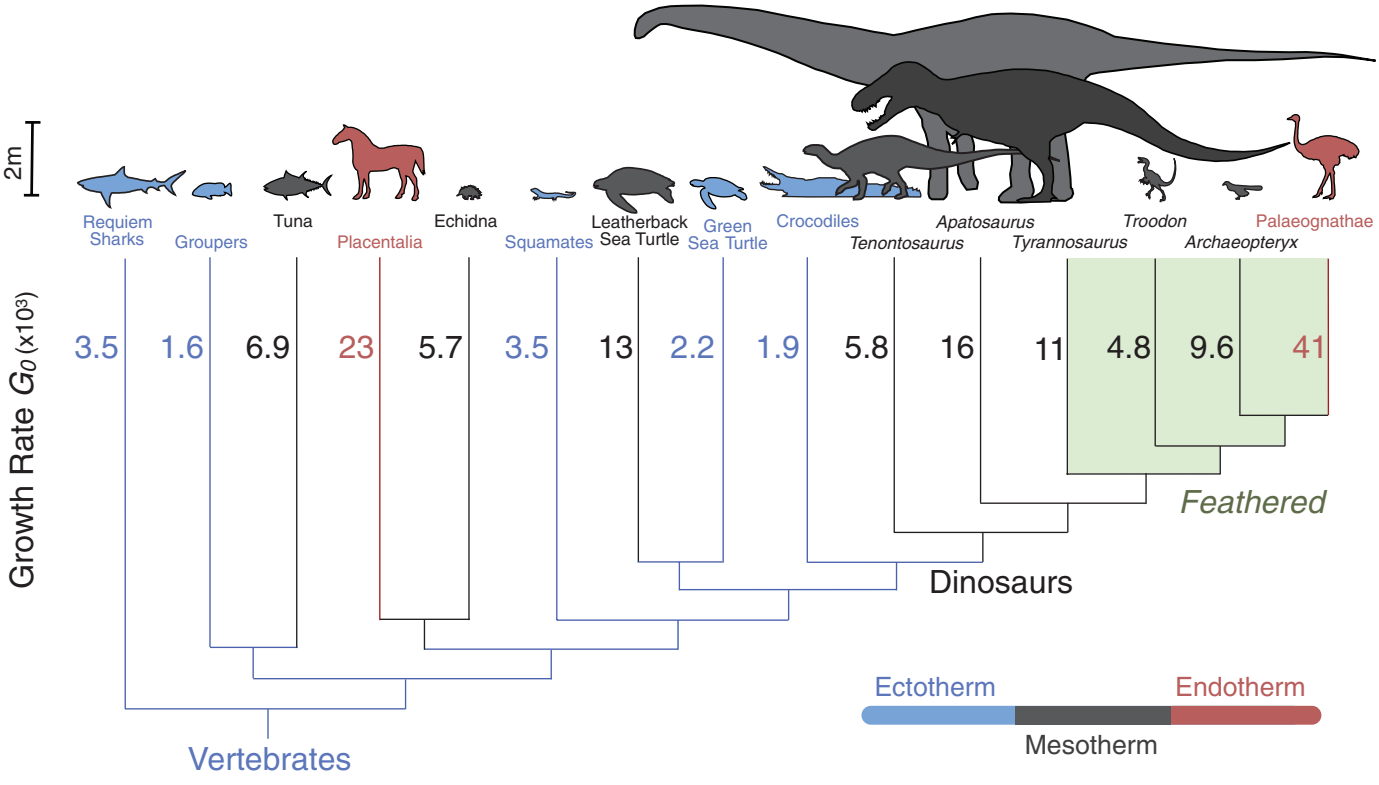

Fig. 4. Phylogeny of mass-independent growth rates (g$^{1/4}$ day^{-1}). Color signifies thermoregulatory state; branch lengths are not standardized for divergence times. Green shading indicates feathered coelurosaurian dinosaurs.

MST makes the following theoretical predictions regarding growth and metabolic rate:

(1) G_{max} scales as M^{α}, where $\alpha \sim 3/4$.

(2) B scales isometrically with G_{max} if masses are standardized (*9*). Regression of B against G_{max} yields a slope of 1 and an intercept of ≈ 0.66.

(3) Plotting G_0 against B_0 will reveal distinct energetic clusters corresponding to endotherms and ectotherms. High-power endotherms will exhibit an elevated G_0 and B_0, and ectothermic organisms the converse. Thermally intermediate taxa, termed mesotherms, such as tuna and lamnid sharks (*16*), should fall between the upper and lower quadrats. The predicted slope and intercept are 1 and 1.52, respectively. Similar clustering is observed if G_{max} and B residuals are plotted.

(4) $B_{predicted} = B_{observed}$ in extant animals, where $B_{predicted}$ is calculated from Eq. 3.

Our analyses find broad support for all four predictions. First, growth scales with mass as ~3/4, although taxonomic variation is observed (Fig. 1 and fig. S1, mean $\alpha_{OLS} = 0.73$; mean $\alpha_{PIC} = 0.69$, table S2). This indicates that larger species acquire their bulk by accelerating their maximum growth rate proportionate to $\sim M^{3/4}$. Second, G_{max} is a strong predictor of B, where $B_M = 0.56 G_{max}^{1.03}$, which is close to theoretical predictions [figs. S3 and S4; slope confidence interval (CI) = 0.97 to 1.10; intercept CI = 0.47 to 0.97; coefficient of determination (r^2) = 0.90, n = 118]. Third, we find that the observed relationship between mass-independent growth and metabolic rates corresponds closely to predicted values (slope = 0.90, CI = 0.77 to 1.03; intercept = 1.10, CI = 0.59 to 2.06, r^2 = 0.61, n = 124). Ectothermic species fall in the lower left quadrat; endotherms in the upper right; and thermally intermediate taxa, including tuna, a lamnid shark, the leatherback turtle, and a prototherian mammal, fall between values for endo- and ectotherms (Fig. 2 and figs. S1, S2, and S5). These results are robust; the inclusion of cold-water fish, with reduced growth and metabolic rates, simply extends the lower portion of the regression line. Furthermore, the ratio G_0/B_0 (g J^{-1}), a measure of efficiency in converting energy to biomass, does not differ significantly between endo- and ectotherms, indicating that energy allocation to growth does not vary with thermoregulatory strategy (t statistic = 0.46, P = 0.64, fig. S6). Finally, regression of observed against calculated metabolic rates does not differ significantly from unity (Fig. 3A; slope CI = 0.97 to 1.10; intercept CI = −0.14 to 0.02). We can therefore predict dinosaur resting metabolic rates from growth rate, using either a theoretical model (Eq. 3) or an empirically determined equation (*9*)

$$B_M = 0.6\, G_{max} \quad (4)$$

Our analyses are robust to variation in the scaling exponent, phylogenetic correction, inclusion of captive versus wild animals, critiques of dinosaur growth studies, and uncertainty in estimating M and metabolic temperature (*9*).

Our results find that mass-independent growth rates in dinosaurs were intermediate to, and significantly different from, those of endothermic and ectothermic taxa (table S2). Although some dinosaur growth rates overlap with high-power ectotherms or low-power endotherms, they cluster closest to energetically and thermally intermediate taxa, such as tuna (Fig. 2). Further, our analyses uphold the somewhat surprising finding that feathered dinosaurs, including protoavian *Archaeopteryx* (*17*), did not grow markedly differently from other dinosaurs (Fig. 4). It appears that modern avian energetics did not coincide with feathers or flight, which is consistent with fossil evidence that modern bone histology in birds did not appear until the late Cretaceous (*18*).

At the largest body masses, the growth rates of the largest dinosaurs and mammals overlap (Fig. 1B). This pattern is driven by two factors. First, dinosaurs have a relatively high slope (α_{OLS} = 0.82, but α_{PIC} = 0.76). This value is consistent with suggestions of thermal inertia for larger taxa; the removal of sauropods yields a reduced OLS slope of 0.77. Second, significantly reduced growth rates are observed in several large mammalian taxa, particularly primates, elephants, and toothed whales, whereas small shrews and rodents have relatively high rates, leading to a low overall slope for placental mammals (α_{OLS} = 0.64, α_{PIC} = 0.63; table S2 and fig. S11). The slow growth of many large endothermic mammals is associated with large brain size and low juvenile mortality (*19*, *20*); this is unlikely to be relevant to most dinosaurs.

Our results highlight important similarities and differences from previous studies. For example, our work agrees with assessments by Erickson (*7*, *17*) that dinosaurs grew at rates intermediate to most endo- and ectotherms. However, we find considerably more similarity in ectothermic growth rates than reported by Case (*13*) and significantly higher growth rates for fish (~seven times higher), marsupials (~four times higher) and precocial birds (~two times higher; fig. S8). We attribute these differences to enhanced sampling and standardization of the thermal environment for ectotherms (e.g., Case included temperate fish). Moreover, our expansion of the comparative growth framework indicates that dinosaurs grew and metabolized at rates most similar to those of active sharks and tuna (Fig. 2 and fig. S1), rather than those of endothermic marsupials, as has been suggested (*17*).

Past work has often struggled to fit dinosaurs into a simple energetic dichotomy; our work suggests that an intermediate view (*17*, *21*) is more likely. Although dinosaur growth rates vary, they cluster most closely to those of thermally intermediate taxa (Figs. 1 and 2), which we term mesotherms. Mesothermic tuna, lamnid sharks, and the leatherback turtle rely on metabolic heat to raise their body temperature (T_b) above the ambient temperature (T_a) but do not metabolically defend a thermal set point as endotherms do (*16*, *22*). This reliance on metabolic heat distinguishes them from other large homeothermic reptiles, such as crocodiles (*23*), which bask to elevate T_b. The echidna, while maintaining a set point of ~31°C, shows remarkable lability, because T_b values can range over 10°C while it is active (*24*). Unlike hibernating mammals or torpid hummingbirds, this variability is externally imposed. Collectively, these animals are distinguished from endotherms and ectotherms by a weak or absent metabolic defense of a thermal set point but sufficient internal heat production to maintain $T_b > T_a$ when T_a is low [see (*9*) for further discussion]. Although some feathered dinosaurs may have been endotherms, they would have been uniquely low-powered compared to extant birds and mammals. We suggest that mesothermy may have been common among dinosaurs, ranging from modest metabolic control of T_b, as seen in furred echidnas, to the absent metabolic defense observed in tuna and leatherback turtles. Analysis of fossil isotopes, which can shed light on body temperatures, will be useful in testing this hypothesis. In particular, attention to neonate and juvenile dinosaurs in seasonally cool environments, such as polar regions, may help distinguish among thermoregulatory states.

Dinosaurs dominated the flux of matter and energy in terrestrial ecosystems for more than 135 million years. Consequently, our results have important implications for understanding ancient Mesozoic ecosystems. We emphasize the primary importance of comparative energetics for integrating form, function, and diversity. Knowing only two facts from the fossil record—adult mass and maximum growth rate—we show that the metabolic rates of extinct clades can be predicted with accuracy. Such an approach will be useful in resolving the energetics of metabolically ambiguous taxa, such as pterosaurs, therapsids, and Mesozoic birds.

REFERENCES AND NOTES

1. K. Padian, A. J. de Ricqlès, J. R. Horner, *Nature* **412**, 405–408 (2001).
2. P. M. Sander *et al.*, *Biol. Rev. Camb. Philos. Soc.* **86**, 117–155 (2011).
3. R. A. Eagle *et al.*, *Science* **333**, 443–445 (2011).
4. J. H. Brown, J. F. Gillooly, A. P. Allen, V. M. Savage, G. B. West, *Ecology* **85**, 1771–1789 (2004).
5. P. Else, A. Hulbert, *Am. J. Physiol. Regul. Integr. Comp. Physiol.* **240**, R3–R9 (1981).
6. J. F. Gillooly, J. H. Brown, G. B. West, V. M. Savage, E. L. Charnov, *Science* **293**, 2248–2251 (2001).
7. G. M. Erickson, K. C. Rogers, S. A. Yerby, *Nature* **412**, 429–433 (2001).
8. A. H. Lee, S. Werning, *Proc. Natl. Acad. Sci. U.S.A.* **105**, 582–587 (2008).
9. See the supplementary materials.
10. F. Seebacher, *Paleobiology* **29**, 105–122 (2003).
11. R. H. Peters, *The Ecological Implications of Body Size* (Cambridge Univ. Press, Cambridge, MA, 1983).
12. C. R. White, N. F. Phillips, R. S. Seymour, *Biol. Lett.* **2**, 125–127 (2006).
13. T. J. Case, *Q. Rev. Biol.* **53**, 243–282 (1978).
14. G. B. West, J. H. Brown, B. J. Enquist, *Nature* **413**, 628–631 (2001).
15. C. Hou *et al.*, *Science* **322**, 736–739 (2008).
16. D. Bernal, K. A. Dickson, R. E. Shadwick, J. B. Graham, *Comp. Biochem. Physiol. A Mol. Integr. Physiol.* **129**, 695–726 (2001).
17. G. M. Erickson *et al.*, *PLOS ONE* **4**, e7390 (2009).
18. A. Chinsamy, *Mesozoic Birds: Above the Heads of Dinosaurs* (Univ. of California Press, Berkeley, CA, 2002), pp. 421–431.

19. E. L. Charnov, D. Berrigan, *Evol. Anthropol.* **1**, 191–194 (1993).
20. K. Isler, C. P. van Schaik, *J. Hum. Evol.* **57**, 392–400 (2009).
21. R. Reid, in *The Complete Dinosaur*, M. K. Brett-Surman, T. R. Holtz, J. O. Farlow, Eds. (Indiana Univ. Press, Bloomington, IN, 2012), pp. 873–24.
22. F. V. Paladino, M. P. O'Connor, J. R. Spotila, *Nature* **344**, 858–860 (1990).
23. F. Seebacher, G. C. Grigg, L. A. Beard, *J. Exp. Biol.* **202**, 77–86 (1999).
24. P. Brice, G. C. Grigg, L. A. Beard, J. A. Donovan, *Aust. J. Zool.* **50**, 461–475 (2002).

ACKNOWLEDGMENTS

This work was supported by a fellowship from the Program in Interdisciplinary Biological and Biomedical Sciences at the University of New Mexico (grant no. T32EB009414 from the National Institute of Biomedical Imaging and Bioengineering to F.A.S. and J. H. Brown). B.J.E. was supported by an NSF CAREER and ATB Award (EF 0742800). We thank C. White and two anonymous reviewers for valuable feedback on our manuscript and N. Milan for assistance with the figures. Data are available in the supplementary materials.

SUPPLEMENTARY MATERIALS

www.sciencemag.org/content/344/6189/1268/suppl/DC1
Figs. S1 to S15
Tables S1 to S4
References (*25*–*396*)

10 March 2014; accepted 8 May 2014
10.1126/science.1253143

NONHUMAN GENETICS

Strong male bias drives germline mutation in chimpanzees

Oliver Venn,[1] Isaac Turner,[1] Iain Mathieson,[1]* Natasja de Groot,[2] Ronald Bontrop,[2] Gil McVean[1]†

Germline mutation determines rates of molecular evolution, genetic diversity, and fitness load. In humans, the average point mutation rate is 1.2×10^{-8} per base pair per generation, with every additional year of father's age contributing two mutations across the genome and males contributing three to four times as many mutations as females. To assess whether such patterns are shared with our closest living relatives, we sequenced the genomes of a nine-member pedigree of Western chimpanzees, *Pan troglodytes verus*. Our results indicate a mutation rate of 1.2×10^{-8} per base pair per generation, but a male contribution seven to eight times that of females and a paternal age effect of three mutations per year of father's age. Thus, mutation rates and patterns differ between closely related species.

Accurate determination of the rate of de novo mutation in the germ line of a species is central to the dating of evolutionary events. However, because mutations are rare events, efforts to measure the rate in humans have typically been indirect, calculated from the incidence of genetic disease or sequence divergence (*1*–*4*). However, high-throughput sequencing technologies have enabled direct estimates of the mutation rate from comparison of the genome sequence of family members (*5*–*8*). Unexpectedly, these studies have indicated a mutation rate of, on average, ~1.2×10^{-8} per base pair per generation, or ~0.5×10^{-9} per base pair per year, approximately half that inferred from phylogenetic approaches (*1*, *9*). Moreover, they have demonstrated a substantial male bias to mutation, such that three to four times as many autosomal mutations occur in the male compared to the female germ line (*6*, *7*). Male bias is largely caused by an increase in the rate of paternal but not maternal mutation with the age of the parent; approximately two additional mutations per year of father's age at conception (*7*). This difference is consistent with ongoing cell division in the male germ line but not in females (*10*).

An alternative approach for estimating the extent of male bias is to compare rates of sequence divergence on the autosomes (which spend equal time in the male and female germ lines) and the X chromosome (which spends two-thirds of the time in females) (*2*, *11*). Such indirect approaches broadly agree with direct estimates in humans, but suggest that male bias may be stronger in chimpanzees (*12*). To test this hypothesis, we sequenced the genomes of nine members of a three-generation pedigree of Western chimpanzees, *Pan troglodytes verus* (Fig. 1A and fig. S1). One trio was sequenced at high depth (average 51×), while other family members were sequenced to an average of 27× (table S1). We inferred the structure of recombination and transmission across the pedigree (Fig. 1B), which enabled us to detect de novo point mutations in regions of high sequence complexity and to remove artifacts caused by mismapping, sequence that is absent from the reference genome, and reference misassembly (*13*).

We used a probabilistic approach that, at a given site, compared the likelihood of different models for genetic variation inconsistent with the inferred transmission: genotyping error at a segregating variant, de novo mutation, single-gene conversion event, segregating deletion and erroneous call (Fig. 1C). The design was expected to enable haplotype phasing through transmission for 99.2% of sites that were heterozygous in the founders and 87.5% of de novo mutation events inherited by chimpanzee F (Fig. 1A). Read-based phasing was used to phase de novo events in other offspring, and we performed independent validation to assess the accuracy of de novo variant calls. The false-negative rate was estimated from allele-dropping simulations (*13*).

Across the genomes of the nine pedigree members, we called 4.1 million variants [single-nucleotide polymorphisms (SNPs) and short insertions and deletions (indels)] using a mapping-based approach and 3.0 million variants using an assembly-based approach (*14*). Genotype data confirmed expected pedigree relationships (fig. S2). The intersection of call sets (1.6 million sites with a transition-transversion ratio of 2.2) established the underlying structure of recombination and transmission across the pedigree with a robust version of the Lander-Green algorithm (fig. S3). Briefly, this is a two-stage strategy of identifying dominant inheritance vectors over 1-Mb intervals, followed by fine-mapping of cross-over breakpoints, which guards against problems caused by false-positive variants and genotyping errors (*13*). Across the pedigree, we identified 375 cross-over events, with a distribution similar to that of human homologs, with the exception of human chromosome 2, which is a fusion of the chimpanzee chromosomes 2A and 2B (*15*) (Fig. 2A, fig. S4, and tables S2 and S3).

Overall, we estimate the sex-averaged autosomal genetic map length to be 3150 cM [95% equal-tailed probability interval (ETPI) 2850 to 3490], compared to 3505 cM in humans (*16*, *17*). On the X chromosome, we detected nine cross-over events in the non-pseudoautosomal (non-PAR) region, indicating a female-specific genetic map length of 160 cM (95% ETPI 83 to 300), compared to 180 cM in humans. On the pseudoautosomal region (PAR), we detected four male cross-overs, giving a male-specific estimate of 34 cM (95% ETPI 28 to 180; tables S4 and S5), in agreement with estimates in humans (*13*). Males have 58% of the autosomal cross-over events of females and, unlike females, show an increase in cross-over frequency toward the telomere (Fig. 2B), similar to humans (fig. S5). We also observed a decrease in cross-over frequency with maternal (2.65 cM per year, linear model $P = 0.025$), but not paternal age (Fig. 2C). However, this observation could be explained by between-female variation (linear model $P = 0.13$, allowing for a maternal effect). The median interval size to which cross-over events can be localized is 7.0 kb, with 95% of all intervals localized to within 80 kb (excluding complex cross-over events), with cross-over events enriched in regions inferred to have

[1]Wellcome Trust Centre for Human Genetics, Roosevelt Drive, Oxford, OX3 7BN, UK. [2]Biomedical Primate Research Centre, Lange Kleiweg 161, 2288 GJ Rijswijk, Netherlands. *Present address: Department of Genetics, Harvard Medical School, 77 Avenue Louis Pasteur, Boston, MA 02115 USA. †Corresponding author. E-mail: mcvean@well.ox.ac.uk

Chapter II

Supporting Materials, Methods and Results for

'Evidence for mesothermy in dinosaurs'

The topic of dinosaur energetics and thermoregulation has long generated interest and debate in the paleontology community. The answer that we put forward – that dinosaurs are thermally and energetically intermediate – is bold and requires clear and compelling justification. While we certainly offer justification in the main publication, space constrained our ability to elaborate on the data, methods, and results. The following supplemental section, published along with the main manuscript, goes into greater detail in how the data was compiled, results assessed, and conclusions formed.

In this chapter I offer a general definition and explanation for the freshly coined term 'mesothermy,' which we felt best described the thermoregulatory strategy for most non-avian dinosaurs, as well as some extant, thermally-intermediate taxa. I discuss our methods for calculating maximum ontogenetic growth rates in vertebrates, and how growth rate links to resting metabolism and thermoregulation both empirically and theoretically. I also compare our work to prior findings, and make use of sensitivity analyses to show the robustness of the results. Finally, I provide detailed descriptions of our scaling patterns as well as the species-level data on growth and metabolic rates used in our calculations.

www.sciencemag.org/content/344/6188/1268/suppl/DC1

Supplementary Materials for

Evidence for mesothermy in dinosaurs

John M. Grady,* Brian J. Enquist, Eva Dettweiler-Robinson, Natalie A. Wright, Felisa A. Smith

*Corresponding author. E-mail: jgrady@unm.edu

Published 13 June 2014, *Science* **344**, 1268 (2014)
DOI: 10.1126/science.1253143

This PDF file includes:

Materials and Methods

I. Mesothermy

Most vertebrates today are classified as either endotherms ('warm-blooded') or ectotherms ('cold-blooded'). Endothermic mammals and birds rely on internal metabolic heat to stay warm, whereas ectothermic fish and reptiles rely on external sources, such as solar energy. Endothermy and ectothermy might simply be regarded as two poles along a continuum, reflecting differences in the contribution of internal heat to body temperature (T_b). By this definition, a strict endotherm (100% endothermy) relies solely on internal heat to set its T_b and a strict ectotherm (0% endothermy) relies solely on external heat sources. An intermediate organism would use both internal and external sources. However, this classification belies biological reality. No mammal or bird today relies entirely, or even mostly, on internal heat. In the absence of environmental heat, at –273 ºC, all endotherms would quickly perish. In tropical environments, in particular, the contribution of ambient temperature (T_a) to endotherm body temperature far exceeds 50%.

Instead, the relevant conceptual difference between endo- and ectotherms is the degree of metabolic control over body temperature. Mammals and birds metabolically increase heat production to maintain a constant body temperature when T_a falls below T_b, leading to stable T_b values. In addition, endotherms typically possess insulation in the form of fur, fat or feathers to aid heat conservation. In contrast, reptiles and fish are characterized by the relative unimportance of metabolic heat in contributing to T_b. Consequently, ectotherms show a declining T_b and metabolic rate when T_a falls, unless other external sources of heat are found (e.g., solar basking). Endotherms can relax thermal control – e.g., hibernation or aestivation to conserve energy – or alter the preferred T_b – for instance, varying T_b with their circadian rhythm (*25*). This 'regulated poikilothermy' of many endotherms is consistent with the high degree of metabolic control that characterizes mammalian and avian thermoregulation.

Today, there is relatively little overlap in the vertebrate world between endothermic and ectothermic lifestyles. For this reason, the terms 'endothermy' and 'ectothermy' are practical, broadly employed designations in vertebrate biology. However, some middle ground does exist. Marine biologists recognize that certain fish, particularly tuna and lamnid sharks, can maintain a body temperature up to 10–20 ºC higher than the surrounding water (*16*). This is accomplished with elevated metabolic rates and the heat-conserving effects of large body size, countercurrent circulation, and the redistribution of organs. Thus, like endotherms, metabolic heat is used to maintain high body temperatures ($T_b > T_a$). For this reason, these species are often described as 'warm-blooded' or 'endothermic'. Similarly, some large sea turtles, such as the leatherback sea turtle, possess elevated body temperatures, relying on their large bulk to conserve metabolic heat (*22*). However, these species differ in important ways from endothermic mammals and birds. First, they are born ectothermic and match ambient water temperatures

throughout early ontogeny (*26*), presumably reflecting the high surface area/volume ratio of small juveniles that leads to rapid heat loss. Second, they are capable of being active at a range of body temperatures, especially low temperatures, unlike hibernating mammals and birds. Third, and most importantly, there is little evidence that tuna, lamnid sharks or sea turtles increase their metabolic rate as T_b falls. For instance, diving to lower, colder depths generally leads to a corresponding decline in T_a and metabolic rate, even as T_b remains above T_a (*16*). The failure to metabolically defend a core body temperature leads to externally imposed thermal lability – in stark contrast to most mammals and birds.

Some mammals have low and variable body temperatures as well, particularly among tropical myrmecophagous species. A well-documented case is that of the echidna. Echidnas are egg-laying, insectivorous monotremes distributed across Australasia. They possess a very low body temperature (~31 ºC), and differ from their other monotreme relative, the platypus, by showing much weaker regulation of T_b. Echidna T_b has been documented to range over 10 ºC in the course of a day (*24, 27*). This variation is not due to torpor or circadian rhythms but rather, reflects ambient temperature and activity level. Unlike tuna and lamnid sharks, echidnas do maintain a thermal set point, but their internal regulation of T_b is weak, leading to significant thermal lability. Notably, echidnas have very low metabolic rates, ~¼ that of a placental mammal (*27*), and this likely limits their capacity to thermoregulate.

Although the species described here originate from different branches of the evolutionary tree, they all share similar thermoregulatory features. Mesothermy can therefore be defined by the following criteria:

1. *$T_b > T_a$ via metabolic heat production, when T_a is below the preferred range.*

2. *A constant T_b is not metabolically defended while active, as in the case of tuna, or only weakly defended, as observed in the echidna. This may lead to daily or seasonal thermal lability, particularly in small-bodied forms.*

For tuna, lamnid sharks, and leatherback turtles, it is clear that mesothermy is not simply an arbitrary convergence zone between endotherms and ectotherms. Their inability to metabolically defend a thermal set point qualitatively differentiates mesotherms from endotherms, while their reliance on metabolic heat to elevate T_b differentiates them from ectotherms. Echidnas can be regarded as near the intersection of mesothermy and endothermy, as they demonstrate a modest metabolic defense of a thermal set point, like endotherms, but also show externally driven T_b lability and low rates of heat generation, like mesotherms. We group them with mesotherms here to reflect their unusual thermal lability (*27*), which is likely related to their low metabolic rate. In addition, like other mesotherms – and in contrast to other mammals and birds – echidnas have a remarkable ability to be active several degrees below their preferred body temperature. They represent a useful model when considering dinosaur thermoregulation, particularly feathered species.

Large body size plays an important role among mesotherms in limiting heat loss, because greater bulk leads to lower surface area/volume. It is no coincidence that the greatest T_b – T_a differentials occur in larger mesotherms, such as bluefin tuna. As all animals produce metabolic heat, it is likely that at a sufficiently large size, ectotherms will grade into mesotherms. Nonetheless, extant mesotherms are not equivalent to inertial homeotherms, i.e., ectothermic organisms whose large size dampens T_b fluctuation. Large crocodiles, for instance, rely on basking rather than metabolic heat to increase their body temperatures (*23*). This is true for large lizards as well, such as the Komodo dragon, which occupies open, sunny habitats (*28, 29*). These inertial homeotherms are still ectothermic, as external sources of heat are important in elevating T_b. It also bears noting that many large sharks are typical ectotherms as well, despite their bulk (*30, 31*). Unlike mesotherms, these large ectotherms show lower rates of heat generation and conservation.

We are hopeful introduction of the term 'mesothermy' will serve three functions: 1. Highlight important similarities and differences between animals like tuna, leatherback sea turtles, echidnas and endo/ectotherms, 2. Clarify the relationship between energy use and thermoregulation, particularly at the intersection of endo/ectothermy, and 3. Stimulate a closer examination of living mesotherms and their relevance to paleobiology.

II. Methods Summary

Data on growth and metabolic rates were compiled from the literature, and graphical data plots were digitized using GraphClick 3.0 (*32*). To reduce uncertainty, data for dinosaur growth were taken from published reports that provided a minimum of five measurements of size and age. Following Peters (*11*), metabolic rates were converted to watts from ml O_2 s^{-1} or mg O_2 s^{-1} by multiplying by 20.1 and 14.1, respectively. Where multiple metabolic rates for a species were reported, the geometric mean was determined. In instances where only length units were reported, equations relating length to mass were employed to estimate growth rates. For crocodilians, the formula total length (TL) equals twice the snout-vent length (SVL) was used to facilitate conversions (*33*). Growth and metabolic rates are reported in table S1, and length-mass equations and references in table S3. All reported growth rates are standardized to modern temporal units (1 day = 86,400 seconds). Statistical calculations were performed in R 3.1.0 (*34*) and JMP 9.0.1 (*35*).

The MST ontogenetic growth model defines growth rate as a function of resting metabolic rate (*15*), which is similar to basal or standard metabolic rate but includes the costs of digestion. An accurate, average resting metabolic rate would integrate changes in metabolic rate from digestion over time, but this is difficult and little data is available. Resting metabolic rate is quite close to basal metabolic rate in mammals (~20% increase) (*15*), and these terms are often used interchangeably. Therefore, we do not distinguish the

two, but note that virtually all data used here are based on measurements of basal metabolic rate of endotherms, or standard metabolic rate in ectotherms, as measured by oxygen consumption during postabsorptive condition at rest. For a few large whales – *Physeter catodon*, *Balaenoptera musculus*, and *B. physalus* – basal metabolic rates were estimated from lung capacity (*36*). As standard metabolic rates for ectotherms are recorded at a variety of temperatures, affecting the metabolic rate, we standardized rates by employing a Boltzmann-Arrhenius correction factor (*6*) to facilitate comparison. Here, metabolic rate B for an organism of mass m and temperature T_0 (in kelvins) can be adjusted to another temperature T:

$$B_T = B_{T0} e^{-E/k(1/T - 1/T0)}$$

where E is the 'activation energy' at ~0.65 eV, and k is Boltzmann's constant (8.62E-5 eV K^{-1}). This formulation is statistically similarly to a Q_{10} adjustment of 2.5, but is preferred here for its generality and underpinnings in statistical thermodynamics (*6, 37*). While more precise measures may be used by empirically determining taxon-specific temperature shifts, the difference between the two adjustments is relatively small in vertebrates (≤10%) (*38*). Resting metabolic rates of tropical ectotherms were adjusted to 27 ºC, but other temperatures are considered as well (see figs. S2, S7).

Ontogenetic growth data were fit using three common nonlinear models: the von Bertalanffy, logistic, and Gompertz. These models generate estimates of final asymptotic mass and an instantaneous growth coefficient, permitting calculation of maximum growth rate. We calculated growth parameters using the minpack.lm package (*39*) in R (*34*), which uses a Levenberg-Marquardt least squares criterion. Akaike Information Criterion (AIC) was used to assess model fit, using the qpcR package (*40*) in R. The Gompertz model was consistently low for all AICc metrics (table S4); therefore, growth rates presented here are derived from the Gompertz model unless otherwise noted. Where growth rates from multiple populations or sexes were reported, growth curves were fit separately, and the geometric mean of final mass M and G_{max} were reported.

To ensure that our results were not driven by phylogenetic inertia, we performed linear regressions of phylogenetic independent contrasts of body mass by maximum growth rate for each major taxon using the package ape in R (*41*). We obtained phylogenetic trees from the literature for the following clades: mammals (*42*), birds (*43*), squamates (*44*), teleost fishes (*45*), and sharks (*46*). Some trees were missing taxa included in our study. In these cases, we patched taxa into the tree following the methods of Sibly et al. (2012) (*47*). Phylogenetic trees for squamates, teleost fish and sharks were not ultrametric; in these cases we forced them to become ultrametric using the chromos function in ape with lambda set to 0.1. Varying lambda settings did not significantly alter the results of phylogenetic independent contrasts analyses. Because phylogenetic trees that included all of our study taxa were not available in the literature for dinosaurs and crocodiles, we built our own by constructing trees for dinosaurs and crocodiles using recent cladistics studies (*48-54*) with unscaled branch lengths (fig. S15).

We used these trees to calculate phylogenetic independent contrasts (PICs) of body mass and maximum growth rates for each taxon. We performed ordinary OLS and SMA regression of PICs for maximum growth rate using the R package lmodel2 (*26*). Linear regression analyses of these PICs indicate that our results are not driven by phylogenetic inertia. Slopes for PIC regressions are generally very similar to slopes for non-phylogenetic regressions, almost always falling within the 95% confidence intervals for non-phylogenetic regression slopes (table S2).

Below we plot some of the main figures with greater taxonomic detail:

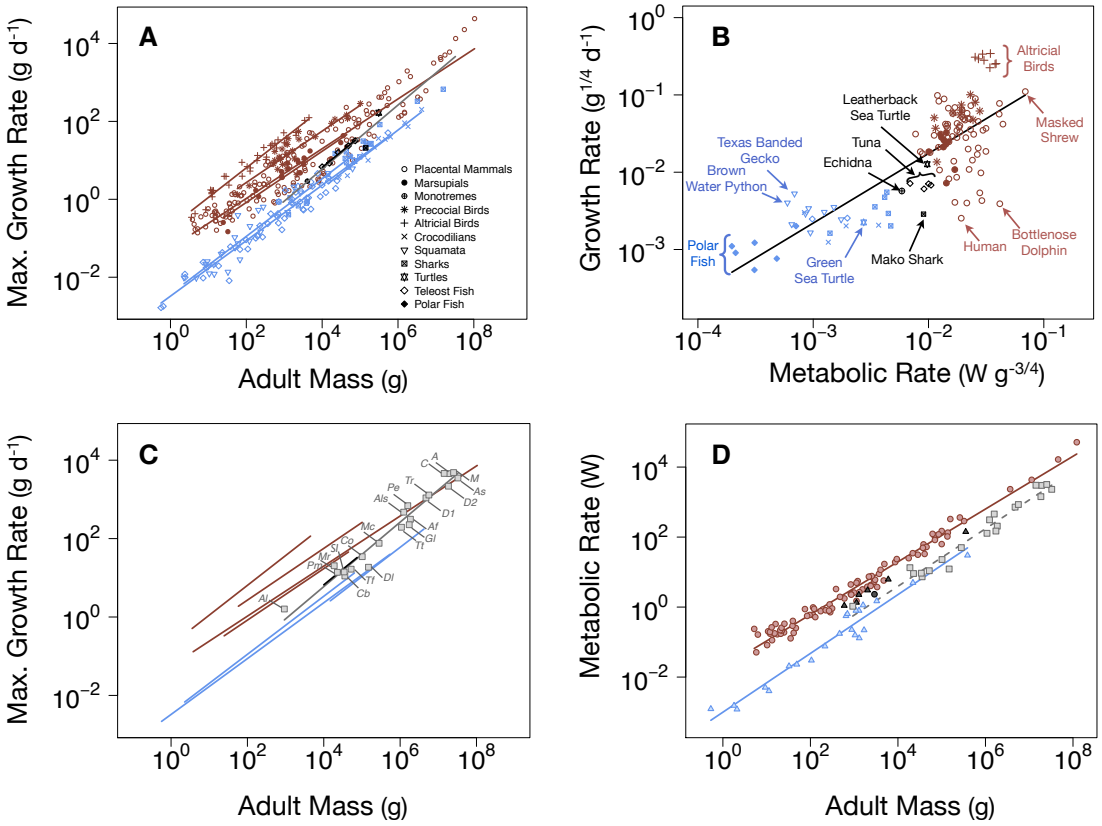

Fig. S1. Some of the main plots in greater taxonomic detail. In **B**, The slope of the standardized major axis fit (not shown) is 1.16 (CI: 1.00 – 1.34), not significantly different from isometry. In **C**, the abbreviations represent the following dinosaur species *Al*: *Archaeopteryx lithographica* (basal bird), *Pm*: *Psittacosaurus mongoliensis*, *Cb*: *Coelophysis bauri*, *Mr*: *Megapnosaurus rhodesiensis*, *Sl*: *Saurornitholestes langstoni*, *Tf – Troodon formosus*, *Dl*: *Dysalotosaurus lettowvorbecki*, *Co*: *Citipati osmolskae*, *Mc – Massospondylus carinatus*, *Tt – Tenontosaurus tilletti*, *Gl – Gorgosaurus libratus*, *Als – Albertosaurus sarcophagus*, *Af – Allosaurus fragilis, Tr – Tyrannosaurus rex*, C – *Camarosaurus* sp, D1 – Diplodocid sp. 1, D2 – Diplodocid sp. 2, *A – Apatosaurus* sp., *As – Alamosaurus sanjuanensis, M* – Mamenchisaurid sp.

To evaluate the metabolic status of dinosaurs, which lived in warm habitats, it is useful to compare their growth rates to tropical ectotherms/mesotherms and endotherms. By

plotting G_0 against B_0 we can compare dinosaurs to extant groups. We have standardized ectotherms temperatures to an ambient temperature of 27 ºC to facilitate comparison with dinosaurs, but our results are not qualitatively affected by variation in standardized temperature between 25 – 30 ºC (fig. S2). The mesothermic echidna was measured at thermoneutral conditions, which corresponds to an internal temperature of 31 ºC. We did not attempt to correct this to 27 ºC, as this elevated temperature represents a useful signal of its metabolic status. Mesothermic fish and reptiles begin their lives as effective ectotherms, only increasing T_b at larger sizes (*26*). For this reason, we adjusted the metabolic rates of small tuna and the mako shark to 27 ºC (see table S2).

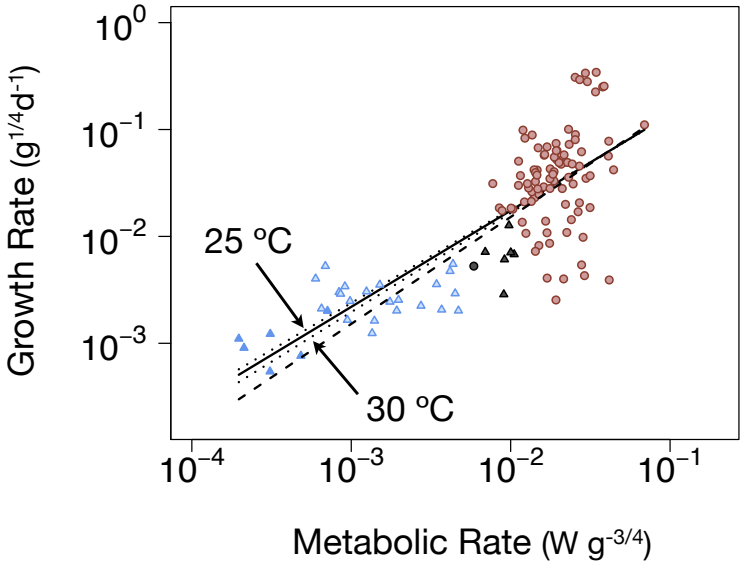

Fig. S2. Plotting ectotherm and small mesotherm metabolic rates adjusted to 25 or 30 ºC (dotted lines), rather than 27 ºC (solid line with 95% confidence band), has little effect on the fit of the data. The theoretical line is dashed.

III. Predicting Metabolic Rate from Growth

The MST ontogenetic growth model quantifies how growth relates to metabolic rate in an organism. The MST assumes, and research indicates (*55*), that scaling of resting metabolic rate B in relation to mass m over ontogeny generally follows a power function of the form:

$$B = B_0 m^{\alpha}$$

where $\alpha = ¾$. Maximum growth rate G_{max} can be determined by assessing growth rate at the point of inflection, at $(¾)^4 M$, or $\sim 1/3 M$, where M is final (asymptotic) mass. Based on its energetic formulation (*14, 15, 55*), this yields:

$$B_M = E_m\,(256/27) G_{max}$$

where G_{max} is in units g s^{-1}, B_M is metabolic rate in watts (W), at mass M (g), and E_m is the energy required to construct one gram of biomass, calculated at ~6000 J g^{-1} (*55*). More simply, $B_M = cG_{max}$, where c = $E_m(256/27)$. Since G_{max} scales as a power function (Fig. 1b) it can also be written as $G_{max} = G_0 M^{\alpha}$. Dividing both sides by M^{α} removes mass dependence, yielding:

$$B_0 = cG_0$$

It is convenient to write G_{max} in units of g d^{-1} rather than g s^{-1}. Converting seconds to days and rounding two decimal places, c = 0.66 W d g^{-1} (if G_{max} is kg yr^{-1}, c becomes 0.24). B at mass m can be predicted by multiplying both sides by m^{α}:

$$B_m = cG_0 m^{\alpha}$$

or $B_m \approx 0.66 G_0 m^{3/4}$. The advantage of this formulation, compared to $B_M = cG_{max}$, is that metabolic rate can be predicted for any organism at any mass (m), not just at its final mass (M). Since differences in model estimation of G_{max} are relatively small when growth curves are well characterized, G_{max} calculated from other models can be substituted in this equation with little loss of accuracy.

For empirical comparisons of B and G_{max} scaling, it is important that metabolic mass is standardized with respect to final mass (i.e. metabolic mass = M, or a standard fraction of M). To make the mass-dependence equivalent, we standardize G_{max} to the metabolic mass m_{met}, recalculating G_{max} as:

$$G_{max(R)} = G_0 m_{met}^{3/4}$$

For many large ectotherms, B is often measured at masses $\ll M$ (see table S2). Therefore, a standardized comparison of $G_{max(R)}$ and B is necessary. We plot B against $G_{max(R)}$ for endotherms, ectotherms, and all species in fig. S3. The fitted line does not differ significantly from isometry or the theoretical fit for all groups.

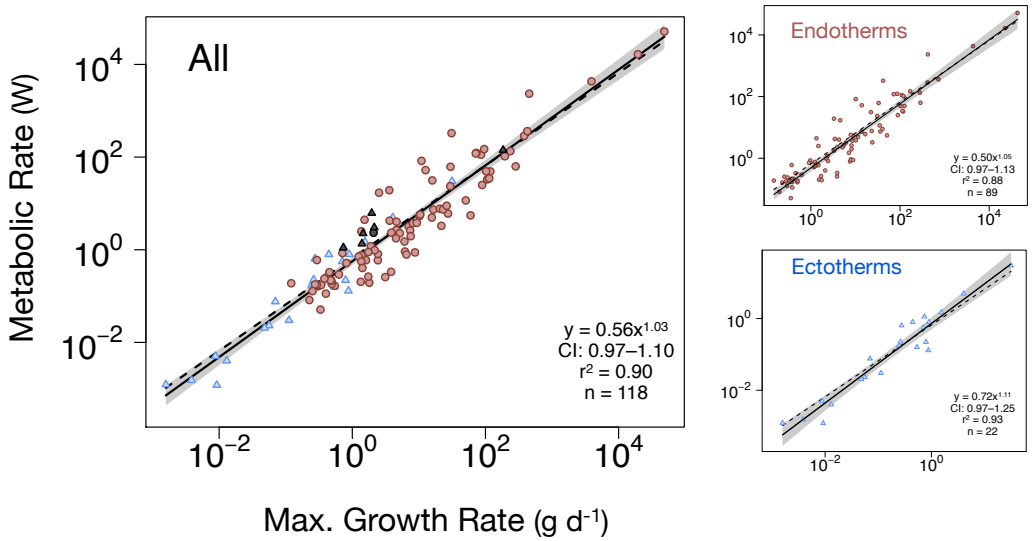

Fig. S3. Empirical resting metabolic rates are plotted against $G_{max(R)}$ for all species, endotherms, and ectotherms. The dashed line represents the theoretically predicted relationship from MST, the solid line is the fitted regression with a 95% confidence band. Note the close correspondence to the predicted relationship, $B \approx 0.66 G_{max}^{1}$.

Among endotherms, metabolic rates are typically measured on adults that have stopped growing. Therefore, $m_{met} \approx M$, and G_{max} can be compared directly to B, relying on no assumptions of the value of α. Again, the observed scaling does not differ significantly from isometry, nor the predicted fit (fig. S4).

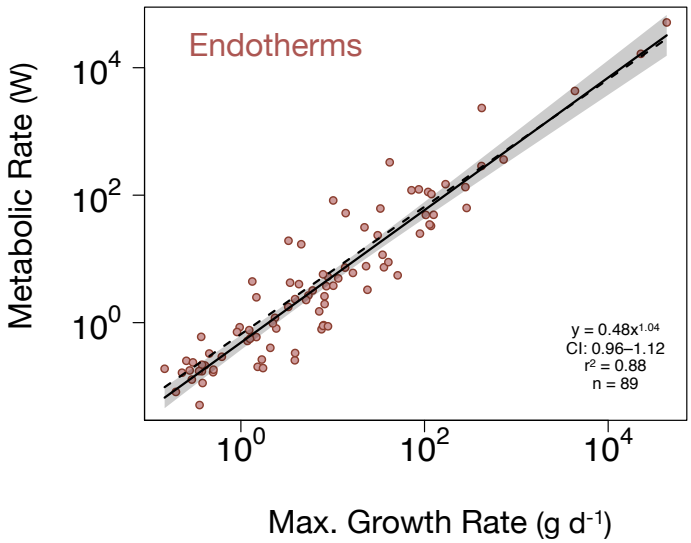

Fig. S4. Observed basal metabolic rates B are plotted against observed G_{max} for all endotherms.

These equations provide a useful way to predict dinosaur metabolic rates empirically, with limited theoretical assumptions. From figs. S3 and S4, an approximate empirical

formula for converting growth (g d^{-1}) to metabolic rate (W) at asymptotic size M can be determined: $B_M \approx 0.6G_{max}$. To predict rates for juveniles (at mass m), this can be written as:

$$B_m \approx (0.6)G_0 m^{\alpha}$$

where $\alpha \sim ¾$, and G_0 is in units of grams and modern days (where 1 day = 86,400 s). For paleostudies, it may be useful to determine G_{max} in units kg yr^{-1}, in which case $B_M \approx 0.3G_{max}$, or:

$$B_m \approx (0.3)G_0 m^{\alpha}$$

If maximum growth rates are unknown, metabolic rates can be predicted from body size (see Fig. 3b).

Uncertainty in α

If metabolic mass ≈ M, maximum growth rate and metabolic rate can be regressed and examined for isometry without assumptions of the value of α (e.g., fig. S4). But to compare or predict metabolic rate from growth rate at any ontogenetic mass, some assumptions of the proper value of α must be made. In principle, α could vary between taxa, and our formulation would hold, so long as α for growth rate and metabolic rate were equivalent within taxa.

We used the value ¾ as a reasonable approximation of a common or average α, due to its broad use and empirical support in the literature (*4, 11, 55, 56*), its theoretical arguments (*57, 58*), and the relatively small variation observed between vertebrate groups ~(0.65 – 0.85) (*59*). However, some have found ⅔ to be a better fit for certain taxa (*12*), or emphasized the variation between groups (*59, 60*). If we calculate G_0 and B_0 assuming α = ⅔, we observe qualitatively similar patterns. In addition, analysis of growth and metabolic residuals, which makes no assumptions of α, reproduces the distinct clustering of ectotherms and endotherms, with mesotherms intermediate (fig. S5). This indicates our approach is robust to variation and assumptions of a specific value of α.

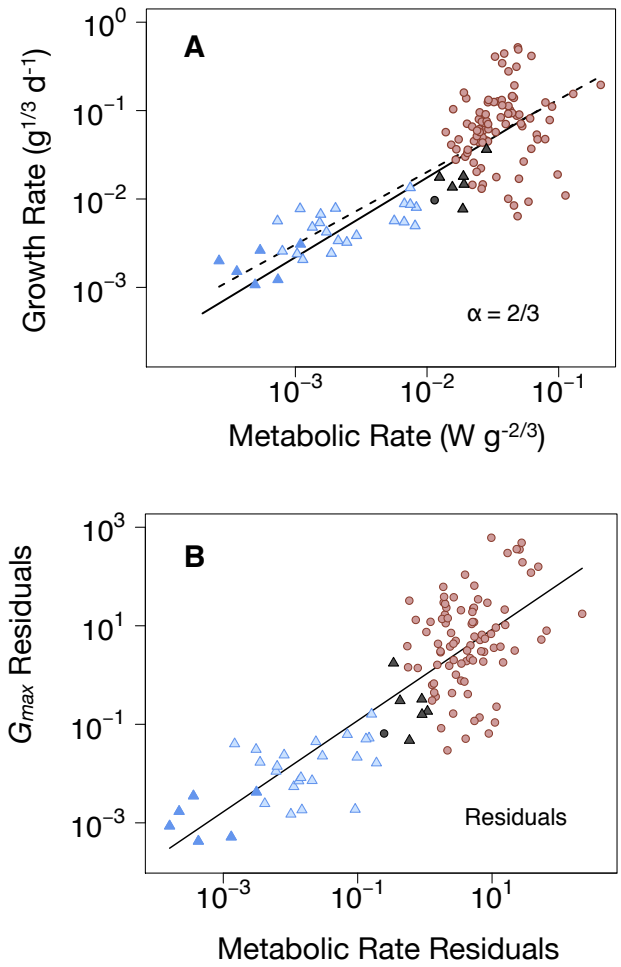

Fig. S5. Evaluation of α**.** In **A**, we plot B_0 vs. G_0, assuming α = ⅔. The solid line is the fitted regression, the dashed is the fitted regression based on ¾ scaling. In **B**, we plot the OLS mass residuals of growth and metabolic rate.

Generality of Growth Energetics

We also examined the log ratio of (G_0/B_0) between endo- and ectotherms, a measure of the metabolic energy allocated to growth. There is no significant difference between the two (t = 0.46, p = 0.68, df = 110), suggesting thermoregulation does not influence the allocation pattern, although taxonomic affiliation and lifestyle may be important.

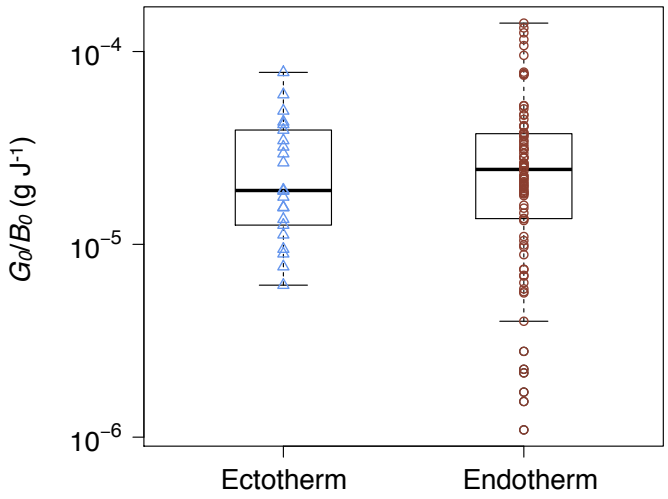

Fig. S6. The ratio of mass-independent growth rate G_0 (g$^{1/4}$ s^{-1}) and mass-independent metabolic rate B_0 (W g$^{-3/4}$) is plotted. Although observed variation is higher in endotherms (e.g. fast-growing altricial birds and slow-growing primates), the means for both thermoregulatory groups are not significantly different (p = 0.68).

Dinosaur Metabolic Rates and Thermoregulation

In Fig. 3b, we compared dinosaur predicted rates to empirical rates in ectotherms, standardized at 27 ºC. However, it has been argued that dinosaurs may have had higher body temperatures, simply by virtue of their large bulk (*61*). If we plot ectotherm metabolic rates standardized to 35 ºC, they overlap with resting metabolic rates of dinosaurs. These values are also close to that observed in mesotherms. While inertial homeothermy likely played role in dinosaurs, their elevated growth rates, higher aerobic capacity, and ability to survive in seasonally cold habitats indicates that mesothermy was probably more common than ectothermic homeothermy. Further, smaller dinosaurs grew significantly faster than similarly sized ectotherms, such as the Komodo dragon.

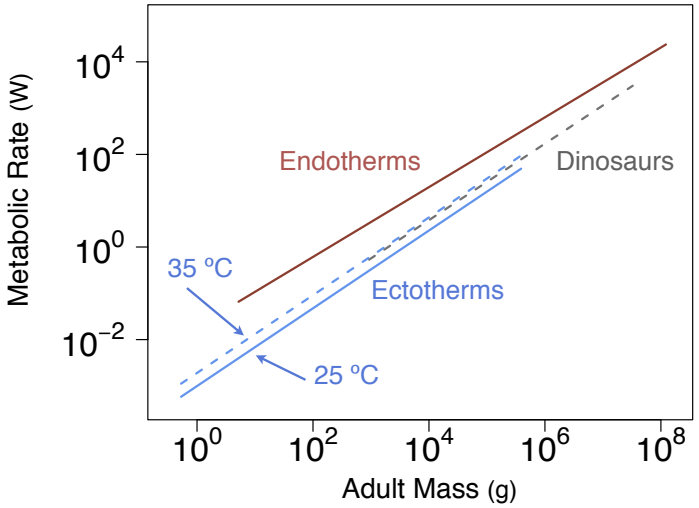

Fig. S7. Empirical metabolic rates for endotherms and ectotherms are shown, where ectotherms rates are standardized to 27 ºC (solid line) and 35 ºC (dotted line). The rate of ectotherms at 35 ºC corresponds to that of dinosaurs.

IV. Comparison to Previous Analyses of G_{max}

For comparison, we show previously published estimates of maximum growth rates of vertebrates. We compare our results with Case (*13*), whose seminal 1978 work was the first to examine the scaling maximum growth rates both within and across taxa. However, his analysis did not distinguish growth in ectotherms at warm or cold ambient temperatures, grouped all reptilian lineages together, did not include sharks (a potential analogue to dinosaurs as large active ectotherms), did not include a phylogenetic correction, and was limited by the paucity of ontogenetic data available at the time. Two published regression lines of dinosaur growth by Erickson (*7, 17*) are also depicted for comparison. Our results show slopes intermediate to Erickson's, but the individual growth rates are somewhat lower for most species.

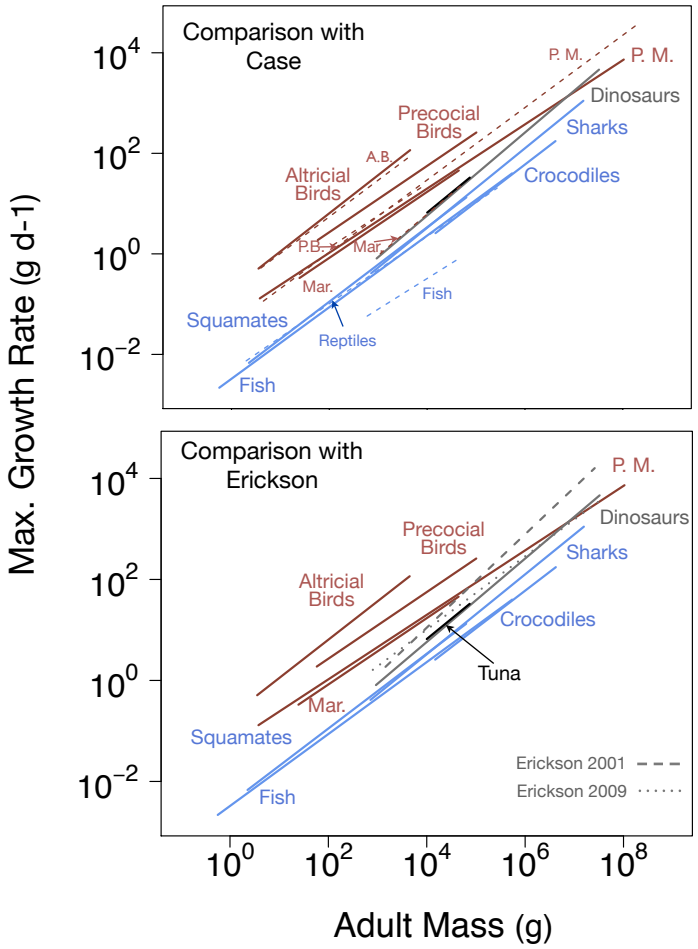

Fig. S8. A. Comparisons with Case (1978) and **B.** Erickson (2001, 2009). Solid lines, with larger text, indicate regression lines from this paper; dashed lines and smaller text indicate those by Case and Erickson. The abbreviations signify: A.B. – Altricial Birds, D. – Dinosaurs, P.B. – Precocial Birds, P.M. – Placental Mammals, Mar. – Marsupials. Reptiles are only reported by Case, and are located between the solid squamate and fish lines. The depictions of Case's regression lines are contracted compared to his publication, but match the ranges for adult masses in his data.

V. Estimating Maximum Growth Rate

We examined growth rate using the following equations:

Gompertz	$m(t) = M[\exp(-e^{(-k(t-t0))})]$	$G_{max} = (kM)(1/e)$
von Bertalanffy	$m(t) = M[1 - e^{(-k(t-t0))}]^3$	$G_{max} = (kM)(4/9)$
Logistic	$m(t) = M/[1 + e^{(-k(t-t0))}]$	$G_{max} = (kM)(1/4)$

where m is mass at time t, M is final adult (asymptotic) mass, k is an instantaneous growth rate constant, and t_0 is a correction term for nonzero birth mass (*62*).

Maximum growth rate is the product of k, M and a model constant. In some instance where M was poorly resolved or biologically unrealistic, literature references were used to determine M. This is the case for many dinosaurs, as fitted estimates will often produce biologically unrealistic values when few non-growing adults are recorded. Where estimates of M for dinosaurs are provided in the growth literature, these values were used. Otherwise they were estimated with least squares fitting.

Length and mass are typically related by allometric equations reflecting geometric similarity (i.e., mass is proportional to length^3). Because of this property, at any age prior to final size, length is a greater fraction of asymptotic length than mass is of asymptotic mass (see fig. S9). When adult sizes and age were not recorded, estimating asymptotic size involves extrapolation beyond the observed size range. To limit extrapolation, whenever length data was provided we determined asymptotic length, and then converted this value to asymptotic mass. The most frequently used formula for length calculation is the von Bertalanffy equation (*33, 63*), where length l at time t is:

$$l(t) = L(l - e^{-k(t-t0)})$$

This formula was used to determine asymptotic length L for all species where length values were provided.

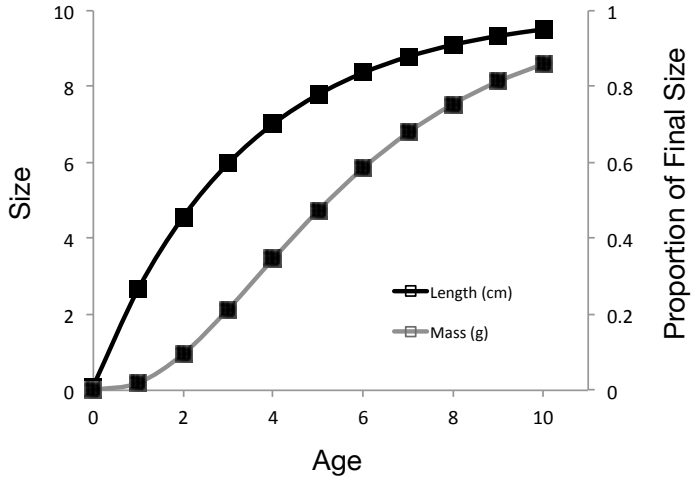

Fig. S9. Growth of mass and length over ontogeny. Here we depict a hypothetical growth curve of an organism, where mass(g) = 0.01l(cm)^3 (an approximately correct relationship, see (*47*)). It is born at 0.1 cm, grows to an asymptotic size of 10 g and 10 cm, with a growth rate constant k = 0.3, following the von Bertalanffy growth curve. On the right axis, relative size (l/L or m/M) is shown. As can be seen, an organism attains a greater fraction of L compared to M at any given time until asymptotic size is reached. For instance, at age 4, 73% of asymptotic length is reached, but only 39% of M. Therefore, estimating L from values of l involves less extrapolation. L is then converted to M to arrive at asymptotic mass.

For one data source, dinosaur limb bone diameters were provided as an estimate of fractional adult size (2 spp). Empirical calculations of long bone diameter indicates that diameter scales as mass$^{0.37}$ (*64*). On this basis we converted bone diameter proportion to a mass proportion by raising the diameter proportion to the 2.73 (0.37^{-1} = 2.73). This was

then multiplied by published values of adult size to calculated mass over ontogeny. This is comparable to estimation using Developmental Mass Extrapolation (*7*). Published sizes of 51.4 kg for *Troodon formosus* and 79.2 kg *Citipati osmolskae* were used (*65*).

Determining Neonate Mass

Mass at birth is the smallest mass along a growth curve and contributes important biological realism by constraining the curve at the lower end. Thus, we were interested in determining birth mass when this value was not provided in the original growth paper. In these cases, we determined birth mass in the following order of priority: First, if mass in endotherms age 2 days or younger was provided, or age 10 days and younger in ectotherms (approximately equivalent values, since ectotherms grow ~5-10x slower), no birth mass was estimated. Second, for species where birth mass was published in other sources, these values were used. Third, if egg dimensions were available, this was converted to neonate mass using suitable conversion equations (*46*). Finally, if none of these options were available, allometric equations relating adult size to neonate mass were employed. For dinosaurs, Dolnik (*66*) provided the following equation:

$$\text{Egg mass} = 0.05(\text{Adult mass})^{0.46}$$

where mass is in kilograms. Egg mass were multiplied by 0.7 (the value for birds (*67*)) to determine neonate mass. Other conversion equations from egg mass to neonate mass can be found in (*67*).

For fish, egg size is approximately invariant with adult mass (*68*). The average egg diameter in fish is 2.3 mm. Neonate size was assumed to be equal to egg mass, at the density of water, or 6.4 mg. Crocodilian neonate mass were typically listed in (*51*). Otherwise, neonate values were estimated from egg mass in g and adult total length (TL) in cm, as described in Thorbjarnarson (*69*):

$$\text{Egg mass} = 0.423\text{TL} + 3.709$$

To standardize adult mass for this calculation, we used the size of the oldest individual in our dataset for that species.

VI. Sensitivity Analyses

It is important to note that ectotherms and endotherms diverge in growth rates by approximately an order of magnitude. Thus, methodological biases that introduce errors as high as 50% will have relatively little impact on our conclusions. Nonetheless, we test for biases that might alter our results.

To check the robustness of our results, we examined the following questions:

1. Do different growth models produce divergent results?
2. Does the scaling assumption of $\alpha = ¾$ scaling produce qualitative differences

than $\alpha = ⅔$?

3. Does uncertainty in the estimation of asymptotic mass affect our results?
4. Does uncertainty in the estimation of neonate mass affect our results?
5. Does inclusion of captive vs. wild animals alter our findings?
6. Do extinct members of a taxon grow like living members?

1. Do different growth models produce divergent results?

To address question 1 we estimated growth parameters with three different models. We note that patterns are qualitatively very similar (below). In all cases, dinosaurs are closest to tuna (black dashed line, center) and are intermediate to extant ectotherms and endotherms.

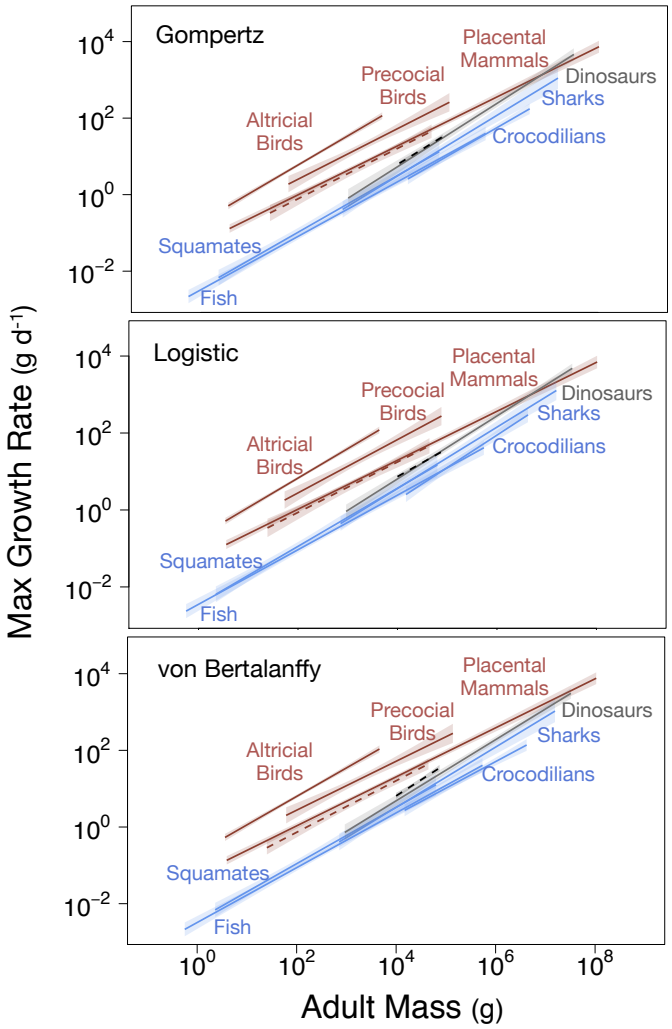

Fig. S10. Sensitivity analysis of growth model choice. The red dashed line is marsupials, the black dashed line is tuna.

2. Does the scaling assumption of $\alpha = ¾$ produce qualitative differences from $\alpha = ⅔$?

In addition to the analyses shown in fig. S5, we also plot G_0 assuming $\alpha = ¾$, and $\alpha = ⅔$. The observed patterns are qualitatively similar.

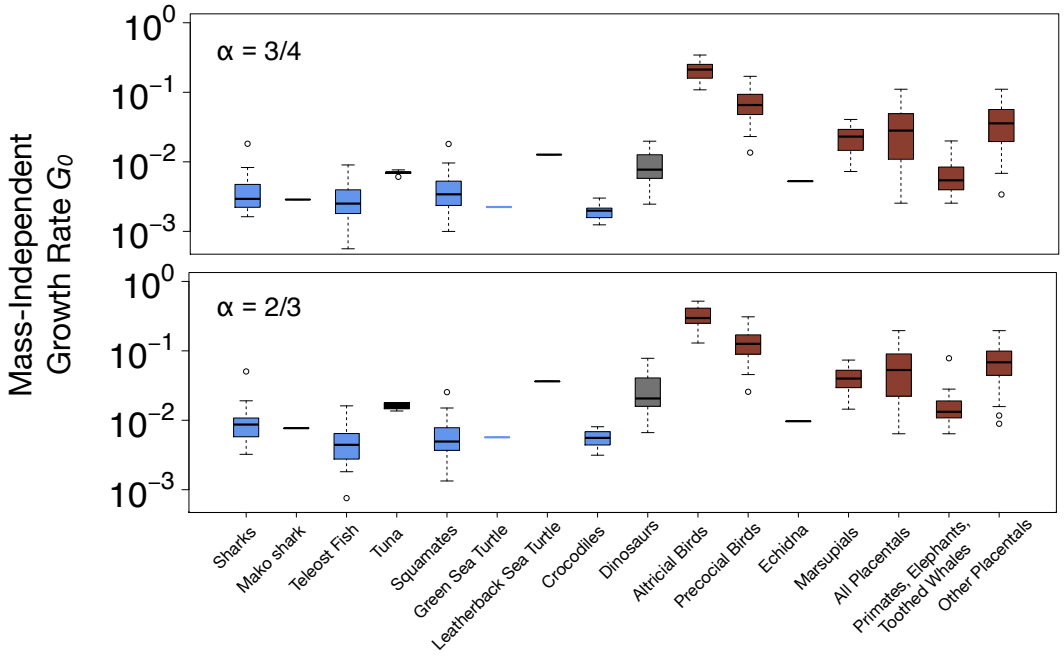

Fig. S11. Sensitivity analysis of α. We permit variations in α in calculating G_0, where $G_0 = G_{max}/M^{\alpha}$ and note that the patterns are qualitatively similar, regardless of the specific value of α. 'Primates' refers to haplorhini primates (e.g., monkeys, apes, tarsiers), which grow markedly slower than strepsirrhini primates (e.g., lemurs, galagos).

3. Does uncertainty in estimation of asymptotic mass affect our results?

For many animals, growth after asymptotic size is reached is not reported. Where growth is still continuing, estimation of final size involves extrapolation and uncertainty. Does this uncertainty influence our results? To address this question, we examined a subset of data where estimation of asymptotic mass was reasonably certain. We defined this as occurring when the Gompertz, von Bertalanffy, and logistic model estimates of asymptotic mass were all within ±10% of the mean asymptotic mass or length. For species where this criterion was met, we plotted growth regressions (dashed) against the full data set (solid). In the case of dinosaurs 6 species met this criterion, ranging in size 15 kg to a 25 tons. The reduced data subset was very similar to the full dataset (fig. S12-A).

4. Do neonate estimates change our results?

To address this question, we recalculated parameter values with birth mass excluded. There is no significant difference between regressions calculated from the full dataset (fig. S12-B).

5. Does inclusion of captive animals alter our findings?

It is reasonable to suppose that captive animals, with a steady food supply and few dangers, should grow faster than wild animals. As dinosaurs were wild, comparative data from wild animals is preferred. We prioritized wild animals over captive and excluded any domesticated animals bred for industrial production (e.g. domestic pigs, cows, chickens). Of the 375 species examined (+ 6 polar fish), 64% were from wild individuals, 35% captive, and 1% both. Some taxa, such as sharks and crocodilians, only involved wild individuals.

Because of the taxonomic and ecological relevance of ratites (as large, precocial, and terrestrial avian dinosaurs) and its low richness, we also examined growth in domesticated rhea (*Rhea Americana*) and emu (*Dromaius novaehollandiae*). These species are produced in relatively new and small markets, and are unlikely to have experienced significant selection for faster growth. They did not grow faster than undomesticated ostriches, and were included in the full dataset.

We plot our full data set (solid lines) against a subset with only wild animals (dashed). There is no significant difference between the two groups (fig. S12-C).

6. Do extinct members of a taxon grow like living members?
If estimates of growth from extinct animals are reasonably accurate, they might be expected to grow in a similar fashion to living, ecologically similar relatives. The extinct taxa analyzed here were comprised of 21 species of Mesozoic dinosaurs, 6 species of crocodilians and 1 shark species. We plotted the crocodilians and sharks together, labeling extinct and extant species. Extinct species, although generally larger, grew in a similar fashion to living members of the taxon (fig. S12-D).

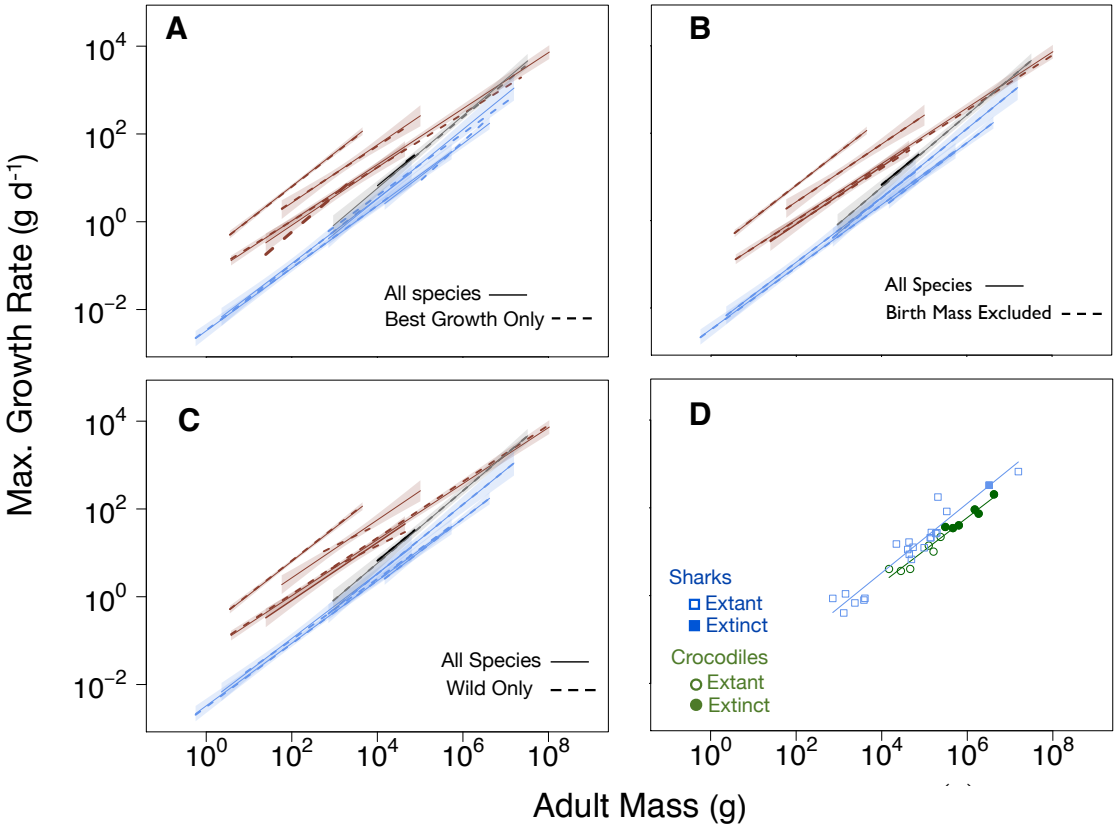

Fig. S12. Sensitivity analyses. For **A**, the sensitivity of asymptotic mass estimates was assessed. We plotted a subset of our data (n = 270 spp out of 375; dashed) where all three models estimates of *M* fell within ± 10% of mean *M*. Solid lines and regression bands are for the full dataset. For dinosaurs, the best fit subset included *Megapnosaurus rhodesiensis*, *Saurornitholestes langstoni*, *Coelophysis bauri*, *Citipati osmolskae*, *Tenontosaurus tilletti,* and a mamenchisaurid sauropod. In **B** and **C**, solid lines represent fits based on our full dataset, dashed lines show the fit when birth mass or captive species are excluded.

VII. Addressing recent methodological concerns with dinosaur growth

In a recent publication (*70*), Myhrvold raised a number of issues regarding published paleontological studies of dinosaur growth curves. Here we discuss briefly on those most salient to our paper. For brevity, we focus on whether the concerns he has raised impact our results, and do not examine in detail the underlying biological issues. Before addressing specific questions, it is important to note that our regression lines for dinosaur had relatively little scatter ($r^2 = 0.96$), so the removal of any specific species deemed problematic should have little impact on our results.

1. Myhrvold discusses two general techniques of aging dinosaurs from their bones, termed the 'longitudinal method' and the 'whole bone method', and discussed their relative merits. Similarly, he discussed approaches to estimating dinosaur body mass from bone dimensions. Two are commonly used – the developmental mass extrapolation

method (*71*), or DME, and allometric equations determined by Anderson (*72*). Without delving into the pros and cons of the various approaches, we simply ask: do these different methodologies alter our results?

To answer this question, we plotted regression line of dinosaur growth derived from data using the respective methods in and compared these to our fit for all data (solid lines, with 95% confidence band). We classified methods as longitudinal vs. whole bone method on the basis of Table 1 in Myhrvold's *PLoS ONE* paper (*70*); classification of DME vs. Anderson was determined from the method description in the original growth papers. There was no significant difference observed between the fits from the whole bone or longitudinal method from our fit through all data (fig. S13–A, B). Maximum growth rates calculated using DME mass calculation were slightly higher than those derived from Anderson's equations, perhaps reflecting the higher allometric slope assumed in DME (3 vs. 2.73). Nonetheless, the results were qualitatively similar the overall fit (fig. S13–C, D), and do not alter our finding that dinosaurs grew intermediate to endo- and ectotherms, and most similar to mesotherms, such as tuna (black, thicker line).

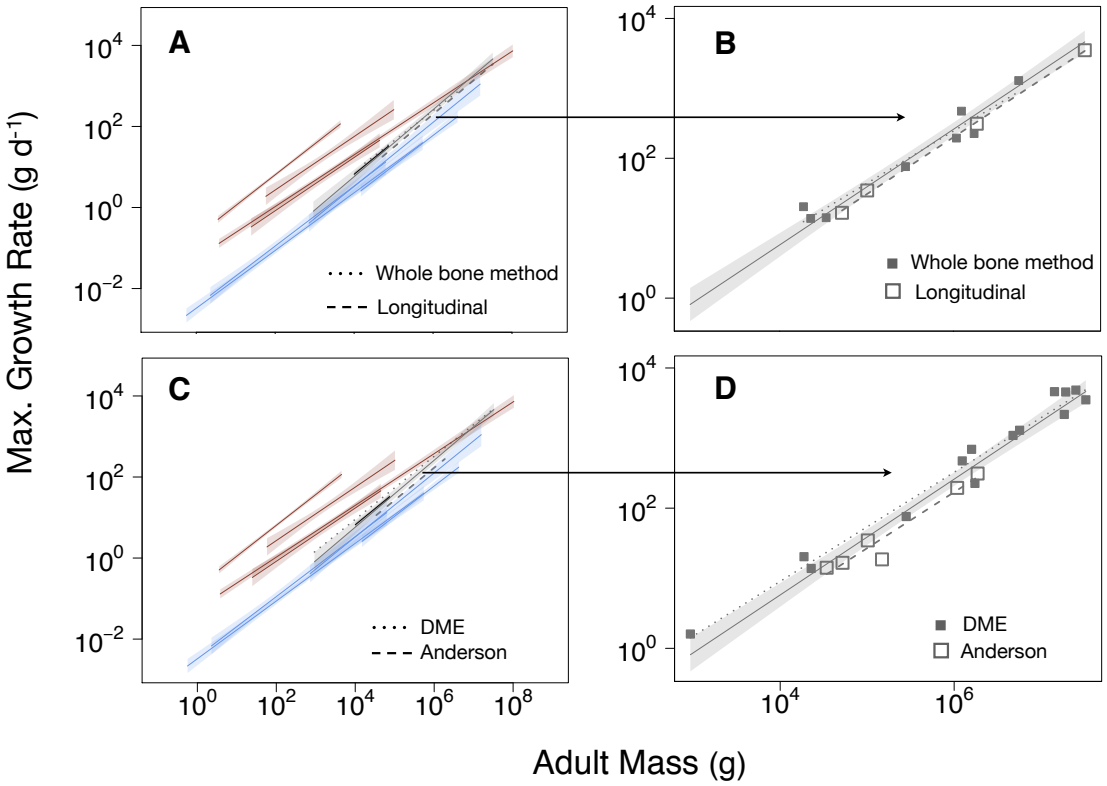

Fig. S13. Comparisons of methodological variation in assessing size and age in dinosaurs. Solid lines, with 95% confidence bands (shaded) represent the regression fit for all data.

2. Myhrvold discussed some issues related to the proper construction of dinosaur growth curves affecting the calculation of maximum growth rates. He noted that measurement error associated with aging involves more uncertainty than that associated with bone size. Consequently, Myhrvold argued growth curves should be constructed with age as the dependent variable, where error is statistically minimized, and bone dimension as the independent variable, where no error is assumed.

We have two concerns with this reasoning. First, assessments of bone length rather than body mass are not particularly relevant to comparative growth and energetic analyses. Growth occurs via cellular addition in a three-dimensional fashion and should be accounted for in units of volume or mass, not in length, particularly when body shapes vary. For instance, a snake may be just as long as an elephant, but it will have over an order of magnitude lower mass, requiring far less energy to grow to maturity. This makes comparisons potentially misleading.

More important, from a statistical perspective, is that statistical error is not equivalent measurement error. Statistical error, which is minimized in least squares regression, is deviation from a fitted line. Measurement error is only one source of this deviation. In a review on regression and scaling (*73*), Warton argued that in scaling analyses, true biological variation is typically a far larger component of statistical error than measurement error. In growth studies, biological variation will occur for many reasons, such as resource availability shifts over ontogeny and the inclusion of multiple individuals, each with varying genetics and environmental histories.

Instead, we suggest that growth curves should be fit to maximize biological realism and predictive accuracy, with consideration to how variation occurs in nature. Most growth curves of wild animals, including paleo studies, are based on measurement of age and size of multiple individuals in a population. As a result, much of the error is due to individual differences, reflecting biological variation in genetics and resource availability. Further, the shape of the growth curve is significant. At adult sizes, growth levels off, forming a horizontal band of data where size is roughly constant even as age increases (fig. S14, left column). Ordinary least squares regression will never fit a vertical line through the center of a vertical band of data, otherwise the residual distances of the data not intersecting the line would be infinite. If we rotate the axes and set age as the dependent variable and length as the independent variable, such a vertical band is formed (fig. S14, center column). To avoid the problem of infinite residuals, asymptotic mass must always be $\geq$ any reported mass. However, asymptotic mass should represent the average final mass in a population. For instance, in a population where adult individuals are no longer growing, about half the adult mass should above the asymptote, and half below.

We can assess the quality of regression strategies by applying each to data from living animals with well-defined curves showing a cessation of growth in adults (fig. S14). In these species, age is inferred on the basis of observed bone rings (like dinosaurs), while

length is directly measured with comparably lower measurement error (also like dinosaurs). These would fit the Myhrvold's criteria for use of age as the dependent variable. To solve, we simply rearrange the growth equation – in this case the von Bertalanffy length equation – to determine age rather than length.

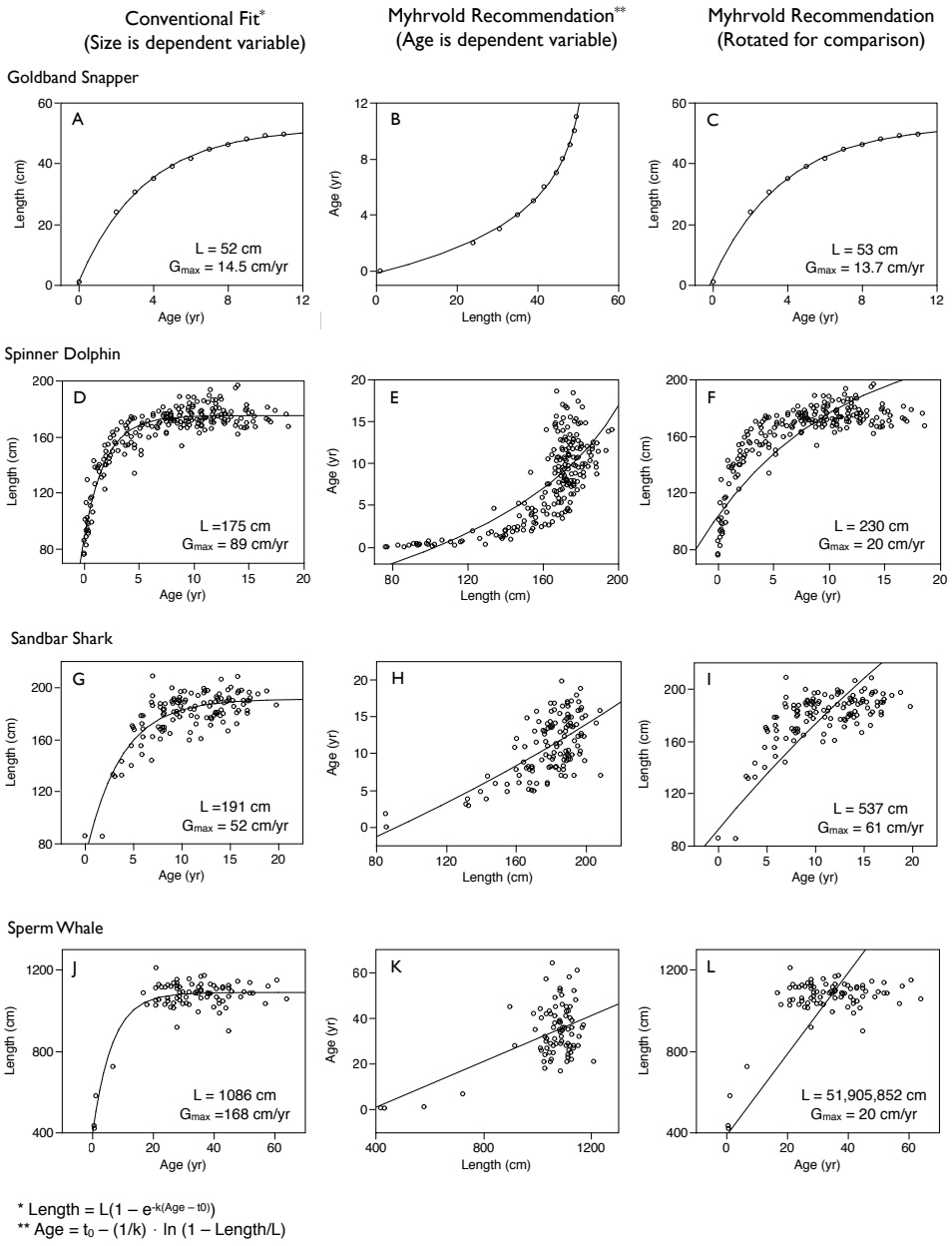

Fig. S14. Choice of dependent variable in growth curves. In the first column we use the von Bertalanffy length equation to plot the conventional fit*, where the dependent variable in the y-axis is size and size variation is minimized. In the middle column we then plot age as the dependent variable in the y-axis**, where age variation is minimized, and in the third column we simply rotate the middle column to facilitate visual comparison with the conventional fit. All growth data are taken from wild animals; maximum growth rate is calculated as kL_{∞}.

It can be seen that for growth curves with low variation, both formulations give similar fits (fig. S14, A–C). However, with more variation, treatment of age as the dependent variable leads to increasingly poor fits by overestimating asymptotic length and underestimating the maximum growth rate (fig. S14, D-L). The performance is particularly poor for the sperm whale, which is predicted to reach a final size of over 500,000 meters, but a maximum growth rate of only 20 cm per year (fig. S14, K, L). In contrast, a realistic final size of 11 meters is readily observed with the conventional approach, with a maximum growth rate of 170 cm/year (fig. S14, J). For this reason, we retain the traditional manner of fitting growth curves, where the independent variable is age, and the dependent variable is size.

3. Myhrvold argues that use of traditional, asymptotic growth curves to fit dinosaurs may be unfounded, as not all animals are determinate growers, *sensu* Sebens (*74*). However, as noted by Sebens, sigmoidal or concave growth towards an asymptote (i.e., $dm/dt \rightarrow 0$) is effectively universal in noncolonial animals, such as vertebrates, and is generally observed unless there is early extrinsic mortality. This pattern includes 'indeterminate' growers (*74*), whose growth patterns are sensitive to environmental conditions. This type of growth is well fit by classical growth curves, such as Gompertz, von Bertalanffy and logistic curves. Over shorter periods of ontogeny, exponential or linear fits may provide a good statistical fit, but these can be misleading, suggesting unlimited growth or impossibly large organisms. Therefore, we do not advocate their use.

Once consideration is limited to biologically realistic models, we agree that is important to use objective statistical measures for model selection. For this reason we selected the Gompertz model on the basis of its low AICc scores for dinosaurs and other taxa (table S4).

4. Myhrvold argues that deficits in available growth data on dinosaurs can lead to problems with the estimation of growth parameters, such as maximum growth rate and final adult size. To reduce parameter uncertainty and statistical overfitting we excluded growth studies with less than 5 data points. This led to the exclusion of some reported rates criticized for being unrealistic (*70, 75*). In addition, in our sensitivity analysis (fig. S12-A) on asymptotic size, only the most complete and best fitting growth curves in dinosaurs were assessed, and these were compared to the full dataset. They did not differ significantly from our full dataset.

5. Myhrvold suggested that reported rates of maximum growth rate of *Tyrannosaurus*, at 769 kg/yr (*76*), was overestimated. Our calculation, at 472 kg/yr (or 1293 g/d), is based on raw data reported by Lee and Werning (*8*), and is quite close to Myhrvold's calculation of 467 kg/yr. Myhrvold also suggests that growth data for *Allosaurus (8)* may actually represent two distinct species. While this is possible, it will require more research by taxonomists. Thus, we retain the published designation of a single species.

Note, however, that removal of *Allosaurus* altogether has almost no affect on the regression fit ($y = 0.00311x^{0.821}$ for all spp.; $y = 0.00307x^{0.824}$ excluding *Allosaurus*).

VIII. Phylogenetic Trees

For our PIC regression analyses, phylogenetic trees were created from the literature for extinct dinosaurs and crocodilians, as these taxa lacked published trees for our species. As published branch lengths are unavailable, all lengths here are unscaled.

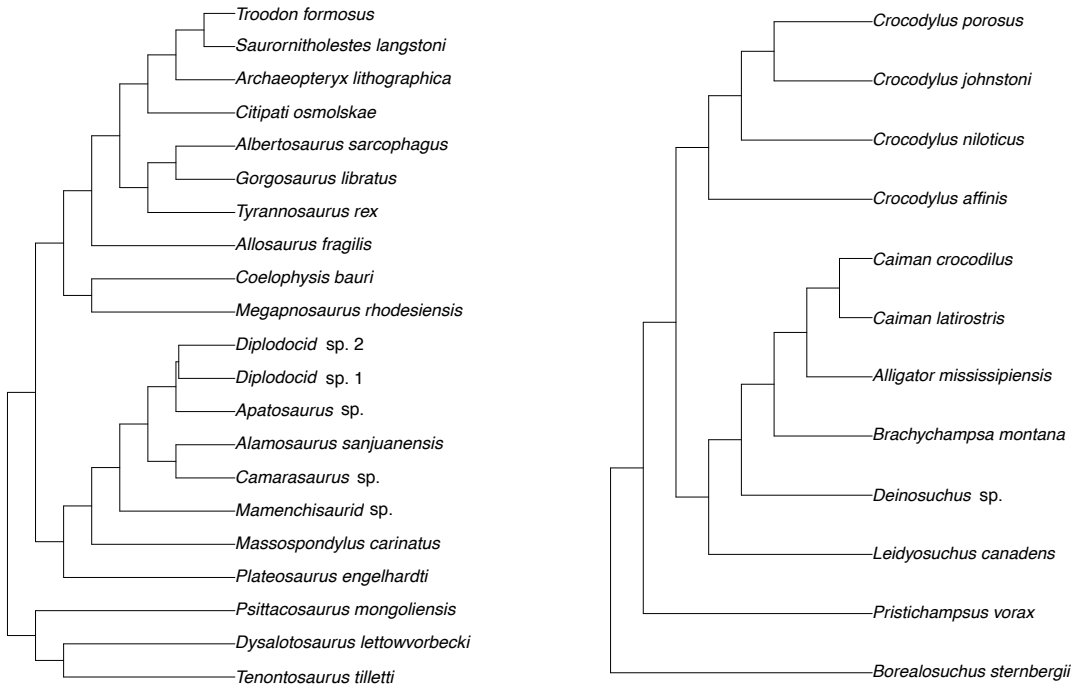

Phylogenetic Trees of Dinosaurs & Crocodilians

Fig. S15. Phylogenetic trees for PIC analyses. The left plot represents Mesozoic dinosaurs, the right extant and extinct crocodilians.

Table S1. A summary of species growth and metabolic rates. Metabolic mass and T_a refers to the mass of the organism and the ambient temperature at which standard metabolic rate was measured. Growth parameters and statistics shown here are based on the Gompertz equation. N refers to the number of mass by age values analyzed to determine maximum growth rate (G_{max}), and r^2 refers to the statistical fit of the growth curve. If multiple growth curves per species were analyzed, the average r^2 is reported. C refers to Curve, where no data was shown, only a growth curve, and EQ refers to Equation, where only a growth equation was provided. In the case of C or EQ, no r^2 values were calculated. Coldwater fish from polar regions include all species in the genera *Hippoglossoides*, *Notothenia*, and *Trematomus* (n = 6). *Troodon formosus M* was fitted by nonlinear regression of mass values, as the estimate based on length was unrealistically high. *Indicates an extant mesotherm, ϕ represents extinct species.

Table S1

Species	Metabolic Mass (g)	Metabolic Rate (W)	T_a (ºC)	Final growth Mass (g)	G_{max} (g d^{-1})	r^2	n
Crocodylia							
Alligator mississipiensis	1287	0.6701	25	125900	13.79		C
Caiman crocodilus	1684	0.1862	25	14820	4.044	0.96	16
Caiman latirostris				28090	3.651		C
Brachychampsa montana ϕ				632700	39.88	0.98	25
Deinosuchus sp. ϕ				4206000	202.6	0.98	103
Leidyosuchus canadens ϕ				306300	36.67	1	20
Crocodylus 'affinis' ϕ				1497000	91.48	0.99	18
Crocodylus johnstoni				46380	4.054		C
Crocodylus niloticus	215.3	0.06421	25	162700	10.06	0.97	53
Crocodylus porosus	389000	38.52	30	237500	21.72		C
Borealosuchus sternbergii ϕ				1839000	73.79	1	27
Pristichampsus vorax ϕ				461900	34.56	1	20
Mesozoic Dinosaurs ϕ							
Psittacosaurus mongoliensis ϕ				22720	13.8	0.97	8
Dysalotosaurus lettowvorbecki ϕ				148100	18.58	0.97	27
Tenontosaurus tilletti ϕ				1084000	194.5	0.88	13
Massospondylus carinatus ϕ				281000	75.95	0.94	10

Table S1

Species	Metabolic Mass (g)	Metabolic Rate (W)	T_a (ºC)	Final growth Mass (g)	G_{max} (g d^{-1})	r^2	n
Plateosaurus engelhardti ϕ				1587000	691	0.99	13
Alamosaurus sanjuanensis ϕ				32660000	3512	1	10
Apatosaurus sp. ϕ				19170000	4544	0.99	40
Camarasaurus sp. ϕ				14250000	4591	0.99	10
Diplodocid sp. 1 ϕ				4753000	1091	0.99	10
Diplodocid sp. 2 ϕ				18460000	2174	0.97	17
Mamenchisaurid sp. ϕ				25080000	4837	0.98	21
Allosaurus fragilis ϕ				1862000	311.9	0.85	100
Coelophysis bauri ϕ				33080	11.22	0.98	7
Megapnosaurus rhodesiensis ϕ				18780	20.29	0.97	7
Albertosaurus sarcophagus ϕ				1239000	472.2	0.99	6
Archaeopteryx lithographica ϕ				928	1.6	0.94	9
Citipati osmolskae ϕ				101700	34.66	0.98	25
Gorgosaurus libratus ϕ				1733000	225.8	0.97	6
Saurornitholestes langstoni ϕ				34240	14.12	0.98	10
Troodon formosus ϕ				52090	16.6	1	19
Tyrannosaurus rex ϕ				5654000	1293	0.96	9
Placental Mammals							
Acinonyx jubatus	38450	61.77		44010	33.06	0.98	15
Callorhinus ursinus				108700	20.31	1	43
Canis lupus	38900	49.02		32390	103.4	0.95	21
Caracal caracal				13650	60.48	1	28
Lynx rufus	9400	23.54		9977	30.91		C
Mustela nigripes				911.1	12.82	1	36
Mustela nivalis				70.81	1.222	1	29
Mustela putorius				1169	13.89	1	56

Table S1

Species	Metabolic Mass (g)	Metabolic Rate (W)	T_a (ºC)	Final growth Mass (g)	G_{max} (g d^{-1})	r^2	n
Panthera leo				153800	152	0.98	25
Panthera tigris	137900	133.9		171700	278.9	1	25
Puma concolor	37200	49.33		48970	125.7	0.91	110
Ursus arctos				176900	82.99	0.78	39
Vulpes lagopus				3346	24.92	0.71	286
Aepyceros melampus				49500	61.29	0.97	25
Alces alces	325000	286.8		366100	417.5	0.88	21
Bison bison				445700	546	0.94	21
Bison bonasus				518500	255.7	0.98	27
Cervus elaphus	67000	112.4		92550	109.4	0.95	34
Connochaetes gnou				146100	188.8	0.92	78
Eudorcas thomsonii				22670	63.2		C
Hippopotamus amphibius				1348000	270.2	0.97	39
Hippotragus niger				216100	165.2	0.9	73
Kobus ellipsipyrmnus	1.00E+05	148.9		214600	169.6	0.98	25
Kobus leche				93400	88.2	0.98	19
Odocoileus hemionus				43220	228.2	0.95	243
Odocoileus virginianus	61860	123.4		77820	86.74	0.91	240
Pudu puda				5402	49.78	0.99	49
Rangifer tarandus	85000	119.7		86240	72.19	0.75	130
Sus scrofa	135000	104.2		69350	118.9	0.98	52
Syncerus caffer				569900	382	0.98	18
Balaenoptera acutorostrata				8722000	3139		C
Balaenoptera borealis				17320000	5044		C
Balaenoptera edeni				13520000	3878	0.9	14
Balaenoptera musculus	1.22E+08	51320		104700000	43430		C

Table S1

Species	Metabolic Mass (g)	Metabolic Rate (W)	T_a (°C)	Final growth Mass (g)	G_{max} (g d^{-1})	r^2	n
Balaenoptera physalus	45830000	16530		56350000	22720		C
Eschrichtius robustus				22930000	6025	0.71	66
Megaptera novaeangliae				33090000	13390		C
Delphinapterus leucas				1044000	128	0.91	93
Delphinus delphis				86110	33.66	0.7	279
Globicephala melas				1482000	171.3	0.95	83
Monodon monoceros				1214000	140.2	0.89	50
Orcinus orca				5446000	610.9	0.51	112
Physeter catodon	11380000	4325		13110000	4349	0.68	84
Pontoporia blainvillei				25380	18.37	0.85	78
Pseudorca crassidens				1495000	162.9	0.83	124
Sousa chinensis				172400	46.92	0.93	33
Stenella attenuata				61260	35.31	0.8	232
Stenella longirostris				64430	30.63	0.83	356
Tursiops truncatus	157500	328.2		235100	41.78	0.82	99
Artibeus watsoni				16.37	0.161	0.99	16
Eptesicus fuscus	13.3	0.113		12.52	0.383	0.77	155
Hipposideros larvatus				14.48	0.475	0.96	56
Hipposideros terasensis				41.78	1.34	0.8	61
Hypsignathus monstrosus				570.4	0.805	0.96	26
Myotis blythii				28.74	0.351	0.42	71
Myotis lucifugus	5.8	0.051		6.34	0.355	0.97	30
Myotis macrodactylus				8.5	0.413	0.96	91
Phyllostomus hastatus	84.2	0.559		75.51	1.257	0.96	232
Pipistrellus subflavus				5.17	0.175	0.81	49
Plecotus auritus	10.25	0.082		8.45	0.196	0.96	69

Table S1

Species	Metabolic Mass (g)	Metabolic Rate (W)	T_a (°C)	Final growth Mass (g)	G_{max} (g d^{-1})	r^2	n
Pteropus conspicillatus				865	3.629	0.99	6
Pteropus poliocephalus	598	1.768		389.3	3.284	0.77	106
Rhinolophus cornutus				5.2	0.138	0.93	18
Rhinolophus hipposideros				4.47	0.168	0.77	153
Rousettus leschenaulti				36.85	0.341	0.93	103
Tolypeutes matacus				1192	15.93	0.99	24
Lepus americanus	3004	6.036		1543	16.61		C
Lepus californicus	2300	7.314		1790	13.66		C
Lepus othus				4650	51.42		C
Lepus townsendii	2523	7.698		2933	23.1	0.91	139
Oryctolagus cuniculus	2168	7.395		3944	36.16	1	22
Sylvilagus floridanus				1281	10.76	0.97	129
Cryptotis parva	6.3	0.164		4.21	0.228	0.96	91
Neomys fodiens	16	0.328		16.03	0.453	0.97	65
Sorex cinereus	5.2	0.238		3.79	0.301	0.99	8
Sorex palustris				14.63	0.705	0.98	115
Sorex unguiculatus				9.87	0.574	0.99	41
Suncus murinus	39.7	0.403		66.75	2.094	0.99	137
Macroscelides proboscideus	39	0.292		38.27	0.62	0.98	21
Ceratotherium simum				2130000	1411	0.91	29
Diceros bicornis				1058000	1046	1	39
Equus caballus	260000	362.9		531000	726.9	0.99	41
Equus quagga				315100	419.2	0.96	18
Rhinoceros unicornis				1750000	1967	0.94	67
Aotus trivirgatus	914.5	2.499		1013	1.476	0.61	465
Ateles geoffroyi				15580	10.39	0.87	116

Table S1

Species	Metabolic Mass (g)	Metabolic Rate (W)	T_a (ºC)	Final growth Mass (g)	G_{max} (g d^{-1})	r^2	n
Callicebus moloch				1330	1.669	0.86	185
Callimico goeldii				651.1	1.545	0.72	348
Callithrix jacchus	190	0.848		287.4	0.97	0.99	30
Cebuella pygmaea	110.7	0.599		150.3	0.37	0.74	125
Cebus apella				4759	2.126	0.82	151
Cercopithecus aethiops				2887	2.224	0.99	46
Cercopithecus mitis	8649	19.28		7735	3.301	0.79	199
Gorilla gorilla				142600	29.78	0.98	70
Homo sapiens	70000	82.78		63170	10.14	0.96	38
Leontopithecus rosalia				689.5	2.193	0.94	98
Lophocebus albigena				9896	3.891	0.98	56
Macaca fuscata				8266	3.076	0.85	26
Macaca mulatta	4900	17.01		10780	4.547	1	170
Macaca nemestrina				10640	5.191	0.77	210
Macaca silenus				8008	2.761	0.75	227
Pan troglodytes	45000	52.32		51060	13.85	0.95	136
Papio cynocephalus				19020	8.584	0.91	307
Saguinus imperator				526.6	0.868	0.66	49
Saimiri sciureus	836.7	4.429		697.6	1.333	0.99	24
Tarsius bancanus				118.8	0.567	0.96	40
Eulemur coronatus				1743	2.28	0.75	226
Eulemur macaco				2551	4.848	0.73	358
Eulemur mongoz				1740	2.648	0.69	355
Eulemur rubriventer				2024	5.198	0.92	120
Eulemur rufus	2374	4.239		2201	3.436	0.69	134
Galago senegalensis	171.5	0.764		148.2	1.234	0.99	13

Table S1

Species	Metabolic Mass (g)	Metabolic Rate (W)	T_a (ºC)	Final growth Mass (g)	G_{max} (g d^{-1})	r^2	n
Hapalemur griseus				993.2	2.003	0.67	230
Loris tardigradus	284	0.714		186.5	0.908	1	11
Microcebus murinus	115	0.594		51.14	1.317	0.94	33
Nycticebus coucang	1129	1.504		1398	7.136	1	14
Otolemur crassicaudatus	993.5	2.595		1130	8.14	1	14
Propithecus diadema				5729	7.817	0.94	35
Propithecus tattersalli				3460	6.18	0.85	44
Propithecus verreauxi	3350	3.738		3572	8.534	0.81	47
Varecia variegata				3577	5.437	0.77	227
Elephas maximus	3672000	2336		3311000	420.3	0.99	40
Loxodonta africana				3865000	374.4	0.91	205
Acomys cahirinus				35.89	0.761	1	17
Akodon lindberghi				20.8	0.241		EQ
Apodemus semotus				29.65	0.498	1	46
Arvicanthis niloticus				61.07	0.803	0.99	24
Ctenomys mendocinus				165.2	2.266	1	13
Dipodomys stephensi				47.91	1.467	0.99	29
Eligmodontia typus	17.5	0.167		15.56	0.499	0.99	8
Funisciurus congicus				104.7	0.923		C
Gerbillus perpallidus				49.53	0.832	1	34
Heterocephalus glaber	35.3	0.128		42.98	0.293	0.98	57
Hoplomys gymnurus				288.4	2.481	1	17
Mastomys coucha				36.66	0.407	0.99	64
Mastomys natalensis	41.5	0.183		42.88	0.503	0.99	50
Microtus cabrerae				35.89	0.797	0.91	209
Neotoma cinerea				287.2	4.012	0.97	40

Table S1

Species	Metabolic Mass (g)	Metabolic Rate (W)	T_a (ºC)	Final growth Mass (g)	G_{max} (g d^{-1})	r^2	n
Otomys unisulcatus	96	0.595		85.56	1.475		15
Paraxerus cepapi	223.6	0.811		223.8	2.43		C
Paraxerus palliatus	274.8	1.191		366	2.353		C
Peromyscus eremicus	21	0.173		24.02	0.376		C
Peromyscus interparietalis				15.86	0.281		C
Peromyscus leucopus	22.3	0.213		17.53	0.406		34
Peromyscus maniculatus	20.5	0.219		15.11	0.377	0.98	25
Proechimys semispinosus				291.2	2.43	1	34
Scotinomys teguina	12	0.174		15.23	0.351	0.99	11
Scotinomys xerampelinus	15.2	0.178		15.36	0.277	0.99	10
Spermophilus armatus	313.2	0.915		440.2	7.979	1	18
Spermophilus columbianus				370.6	9.208	0.96	47
Spermophilus elegans				486.4	7.95	0.99	18
Spermophilus richardsonii	266.3	0.788		325.5	7.562	0.99	15
Tupaia belangeri				167.8	2.751	0.99	13
Marsupials							
Antechinus flavipes	46.5	0.252		24.62	0.255	0.96	68
Antechinus stuartii	25	0.189		32.64	0.148	0.85	448
Didelphis virginiana	2847	5.299		2350	8.82	0.98	26
Bettongia lesueur				1233	8.465	0.99	135
Macropus giganteus				35850	43.05		C
Macropus parma				3331	11.48	1	50
Macropus robustus				30960	28.5		C
Macropus rufus	28500	31.35		44430	22.21		C
Petaurus breviceps	129.3	0.517		211.8	1.18	0.96	58
Petaurus norfolcensis				178.1	1.697	0.99	47

Table S1

Species	Metabolic Mass (g)	Metabolic Rate (W)	T_a (°C)	Final growth Mass (g)	G_{max} (g d^{-1})	r^2	n
Phascolarctos cinereus	4732	5.744		3211	7.85	0.92	380
Pseudocheirus peregrinus	859.3	2.27		850.9	5.136	0.97	164
Thylogale billardierii				4795	17.39	0.98	94
Trichosurus caninus				2646	4.761	0.96	34
Trichosurus vulpecula	1994	3.8		2241	10.16	0.99	33
Wallabia bicolor				17140	11		C
Isoodon macrourus	1551	3.202		1274	6.051	0.99	57
Isoodon obesulus				883.7	3.672	0.94	69
Perameles gunnii	837	2.343		847.4	3.896	0.89	90
Monotremeta							
Ornithorhynchus anatinus	1315	2.665		1650	5.441	0.94	33
*Tachyglossus aculeatus**	2909	2.327		4078	2.92	0.81	71
Neornithes (altricial)							
Aquila chrysaetos				3458	106	0.99	22
Haliaeetus leucocephalus				4501	124.7	0.99	119
Archilochus alexandri				4.46	0.427	0.97	58
Selasphorus rufus				3.57	0.345	0.97	21
Sternoclyta cyanopectus				8.51	0.541	0.81	93
Geococcyx californianus				342.5	12.09	1	11
Buteo jamaicensis				1138	37.16	1	14
Buteo swainsoni				686	33.65	0.98	11
Cathartes aura				2062	51.96	0.97	26
Coragyps atratus				2049	43.78	0.96	81
Falco mexicanus				566.5	27.41	0.99	8
Acrocephalus arundinaceus	21.9	0.257		29.22	3.87	0.89	78
Acrocephalus melanopogon				12.25	1.389	0.84	120

Table S1

Species	Metabolic Mass (g)	Metabolic Rate (W)	T_a (ºC)	Final growth Mass (g)	G_{max} (g d^{-1})	r^2	n
Acrocephalus palustris	10.8	0.203		12.81	1.523	0.92	45
Acrocephalus scirpaceus				12.16	1.473	0.78	106
Aimophila carpalis				13.6	1.689	1	11
Campylorhynchus brunneicapillus				34.8	2.31	0.91	49
Corvus brachyrhynchos	384.8	3.283		436.1	23.91	0.99	13
Corvus corax	1203	5.534		973.4	51.01	0.98	20
Corvus cryptoleucus				476.2	26.18		C
Parus caeruleus				12.62	1.16	0.99	15
Passer domesticus	25.5	0.334		26.13	3.898	0.96	30
Pica pica				197.5	13.33	0.98	25
Spizella passerina	11.9	0.194		11.42	1.744	0.98	16
Spizella pusilla	13	0.264		12.51	1.692	0.99	8
Sturnus vulgaris	75	0.877		76.63	8.889	0.98	22
Amazona aestiva				332.4	10.5	0.86	55
Amazona agilis				191.5	9.867	0.89	162
Ara macao				1017	28.35	0.91	1320
Cyanoliseus patagonus				289.1	21.36	0.46	294
Myiopsitta monachus				105	6.917	0.96	34
Nymphicus hollandicus				77.9	3.913	0.81	138
Poicephalus cryptoxanthus				125.7	5.29	0.99	65
Megascops asio				128	6.405	0.99	14
Tyto alba				626.7	20.85	1	10
Neornithes (Precocial)							
Aix galericulata				559.4	9.994	0.99	24
Anas rubripes				1115	26.44	1	9
Aythya affinis				564.1	16.95	0.99	9

Table S1

Species	Metabolic Mass (g)	Metabolic Rate (W)	T_a (ºC)	Final growth Mass (g)	G_{max} (g d^{-1})	r^2	n
Aythya americana				877.4	19.57	0.99	27
Aythya valisineria				1204	25.57	0.98	107
Branta hutchinsii				1269	36.06	0.96	54
Chen caerulescens				2383	55.16	0.9	133
Dendrocygna autumnalis				729.5	12.15	0.93	87
Alectoris chukar	475	1.961		528.8	8.174	1	10
Alectura lathami				1860	10.91	0.99	34
Coturnix chinensis				58.09	1.328	0.99	68
Coturnix coturnix	115	0.978		118.9	2.229	0.99	16
Dendragapus obscurus	1131	4.957		748.7	11.5	0.84	46
Gallus gallus	121.8	0.8919		904.8	7.854	0.99	96
Meleagris gallopavo	3700	8.91		6600	40.42	1	59
Numida meleagris				1669	17.69	1	46
Pavo cristatus				3439	10.38	0.96	162
Phasianus colchicus				1187	6.05	0.94	213
Tetrao tetrix				1172	14.07	0.98	12
Tetrao urogallus	4010	11.63		2442	34.94		C
Tympanuchus pallidicinctus				796.8	10.53	0.95	60
Apteryx mantelli	2380	4.029		2154	4.291	0.95	366
Casuarius bennetti	17600	24.99		17600	89.19	1	11
Casuarius casuarius				44000	146.3	1	11
Dromaius novaehollandiae	40700	33		46660	117.7	0.97	37
Rhea americana	21800	34.69		21740	113.6	0.93	246
Rhynchotus rufescens				672.8	5.895	1	236
Struthio camelus	1.00E+05	63.05		101600	287.8	0.99	7
Sharks							

Table S1

Species	Metabolic Mass (g)	Metabolic Rate (W)	T_a (ºC)	Final growth Mass (g)	G_{max} (g d^{-1})	r^2	n
Carcharhinus acronotus	650	0.6085	28	43450	16.59	1	35
Carcharhinus brevipinna				194600	27.03	0.95	21
Carcharhinus falciformis				144700	27.41	0.87	197
Carcharhinus leucas				136100	20.78	0.94	23
Carcharhinus limbatus				40600	11.22	0.86	61
Carcharhinus plumbeus	3279	1.153	24	54090	12.65	0.58	226
Carcharhinus signatus				98200	12.31	0.88	215
Carcharhinus sorrah				22030	14.99	0.73	176
Carcharhinus tilstoni				44060	8.723	0.84	335
Galeocerdo cuvier				331600	82.8	0.98	25
Negaprion brevirostris	1600	0.9588	25	183700	25.97	0.99	90
Prionace glauca				121400	31.18	0.87	13
Rhizoprionodon lalandii				1295	0.403	0.99	7
Rhizoprionodon porosus				4045	0.868	1	6
Rhizoprionodon taylori				717.3	0.864	0.9	135
Scoliodon laticaudus				2361	0.681	1	12
Sphyrna lewini	700	0.5182	24.5	49400	6.695	0.8	233
Sphyrna tiburo	1100	0.6721	25	1424	1.097	0.7	110
Isurus oxyrinchus *	6016	2.922	18.3	141300	20.89	0.95	56
Cretoxyrhina mantelli ϕ				3249000	327.4	1	16
Chiloscyllium plagiosum	880	0.1609	23	3840	0.793	0.73	312
Rhincodon typus				15640000	668.4	0.92	18
Squamata							
Agama impalearis				60	0.39	0.75	148
Basiliscus basiliscus				124.4	0.204	0.8	89
Ctenosaura pectinata				209	0.529	1	54

Table S1

Species	Metabolic Mass (g)	Metabolic Rate (W)	T_a (°C)	Final growth Mass (g)	G_{max} (g d^{-1})	r^2	n
Liolaemus lutzae				13.78	0.021		C
Sceloporus grammicus				9.7	0.019	0.98	59
Sceloporus mucronatus				32.82	0.014	0.91	192
Sceloporus scalaris				8.45	0.022	0.97	62
Microlophus occipitalis				9.37	0.025	0.8	194
Tropidurus itambere				21.61	0.039	0.97	33
Tropidurus torquatus				49.55	0.105		C
Uranoscodon superciliosus				120.2	0.086	0.99	23
Xenosaurus grandis				68.03	0.028	0.96	117
Acrochordus arafurae	1048	0.1579	27	1693	0.766	0.95	18
Acanthophis praelongus	105.5	0.03004	27	60.42	0.074	0.98	8
Eublepharis macularius	48.8	0.02207	26.5	50.48	0.058	0.8	131
Coleonyx brevis	2.1	0.00178	31.8	2.27	0.01	0.91	27
Coleonyx elegans	9.3	0.00384	23.8	14.28	0.012	0.82	75
Coleonyx mitratus	11.3	0.0036	25.7	10.6	0.012	0.88	142
Heloderma suspectum	463.9	0.1476	25	238.8	0.148	0.99	23
Liasis fuscus	1307	0.1299	27	2642	1.483	0.92	300
Morelia viridis				1230	0.469	0.97	84
Oligosoma suteri				4.8	0.01	0.99	7
Varanus indicus				1809	2.093	0.88	622
Varanus komodoensis				63350	6.146		C
Varanus niloticus	32.5	0.01736	25	14530	4.672	0.66	290
Varanus semiremex				279.3	0.639	1	18
Teleost Fish							
Tenualosa toli				7608	4.598	0.78	60
Labeo cylindricus				200.9	0.115	0.95	9

Table S1

Species	Metabolic Mass (g)	Metabolic Rate (W)	T_a (°C)	Final growth Mass (g)	G_{max} (g d^{-1})	r^2	n
Poecilia latipinna				2.4	0.012	0.99	25
Poecilia reticulata	0.53	0.00104	25	0.56	0.002	1	15
Xiphophorus maculatus	1.8	0.00129	25	0.65	0.002	0.97	18
Acanthurus lineatus				269.6	0.107	0.52	81
Acanthurus olivaceus				442.8	0.426	0.6	55
Ctenochaetus striatus				194.2	0.115	0.44	101
Naso brevirostris				871.2	0.166	0.85	79
Naso tuberosus				2015	1.507	0.84	55
Zebrasoma scopas				109.8	0.053	0.48	43
Salarias patzneri				2.44	0.01	0.51	101
Chaetodon larvatus				38.2	0.061	0.53	109
Cichla intermedia				1083	1.702	0.69	14
Cichla orinocensis				1620	0.997	0.64	36
Cichla temensis				5107	2.78	0.46	44
Oreochromis macrochir				177.8	0.1	0.97	12
Pharyngochromis darlingi				68.22	0.052	1	17
Pseudocrenilabrus philander				8.76	0.017	1	18
Amblygobius bynoensis				98.68	0.092	0.61	120
Amblygobius phalaena				23.27	0.043	0.83	99
Asterropteryx semipunctatus				7.3	0.01	0.91	67
Istigobius goldmanni				18.6	0.019	0.87	71
Valenciennea muralis				7.27	0.024	0.67	106
Cheilinus undulatus				12560	1.492	0.59	89
Lutjanus erythropterus				2770	1.609	0.91	84
Lutjanus malabaricus				5527	2.146	0.86	44
Lutjanus sebae				9996	2.309	0.71	65

Table S1

Species	Metabolic Mass (g)	Metabolic Rate (W)	T_a (ºC)	Final growth Mass (g)	G_{max} (g d^{-1})	r^2	n
Pristipomoides multidens				4387	1.099	0.99	14
Pristipomoides typus				2599	0.855	1	11
Notothenia neglecta	32.38	0.00267	0	1241	0.231	0.99	19
Notothenia rossi	761.1	0.045	3	9706	1.196	0.96	28
Trematomus bernacchii	178.1	0.0346	-1.5	168.4	0.094	0.96	14
Trematomus hansoni	547.8	0.02405	3	477.8	0.093		EQ
Trematomus loennbergii	158.1	0.02155	-1.5	292	0.054	0.99	24
Stegastes fuscus				35.42	0.008	0.64	162
Chlorurus gibbus				3952	1.084	0.67	64
Chlorurus sordidus				368	0.237	0.57	63
Scarus frenatus				685.2	0.431	0.63	76
Scarus niger				670.8	0.358	0.73	65
Scarus psittacus				228.7	0.211	0.72	31
Scarus rivulatus				3231	0.529	0.75	72
Scarus schlegeli				704.5	0.245	0.89	43
Euthynnus affinis *	1278	1.9	25	10000	6.798		EQ
Katsuwonus pelamis *	594	0.93	25	15610	8.498	1	9
Thunnus albacares *	1129	1.14	25	49250	23.65	1	8
Thunnus obesus *	2030	2.56	25	74670	31.95	0.97	15
Thunnus tongol *				26500	15.91		C
Epinephelus fuscoguttatus				8953	1.176	0.82	119
Epinephelus polyphekadion				3156	0.555	0.73	71
Epinephelus tukula				24710	2.979	0.69	59
Mycteroperca rosacea				22730	1.907	0.99	18
Plectropomus laevis				14730	3.63	0.62	21
Plectropomus leopardus				5062	0.559	0.6	155

Table S1

Species	Metabolic Mass (g)	Metabolic Rate (W)	T_a (°C)	Final growth Mass (g)	G_{max} (g d^{-1})	r^2	n
Variola louti				1555	0.818	0.52	91
Siganus sutor				2302	2.178	0.94	46
Diplodus sargus				1018	0.325	0.99	13
Rhabdosargus sarba				14670	2.911	0.87	109
Hippoglossoides platessoides	277	0.021	3	3388	0.242		EQ
Sorubim lima				719.7	0.871	0.38	90
Masturus lanceolatus				545400	50.91	0.96	133
Testudines							
Chelonia mydas	22000	4.18	25	70310	9.679	1	14
Dermochelys coriacea *	354000	141.6	23	310500	166.9	0.99	87

Table S2. Summary of Parameter Statistics. Taxa highlighted in bold were fitted with regression lines in Fig. 1. The geometric means for taxonomic values of mass-independent maximum growth rate G_0 are provided. Significant differences in G_0 from Tukey's HSD test are indicated by bolded letters (alpha = 0.05), where differences are significant if the given letter differs from the letter assigned to another taxa. Slope values for Fig. 1B are provided (G_{max} vs. M), calculated via ordinary least squares criterion (OLS), or standardized major axis (SMA), with and without phylogenetically independent contrasts (PIC). The intercept β and slope α reported describe the relationship: $G_{max} = \beta M^{\alpha}$, where M is final adult mass. r^2 and n values are equivalent for SMA and OLS methods. For Fig. 1A, the OLS regressions are – Endotherms: $0.112M^{0.59}$; Ectotherms: $0.0034M^{0.72}$; Dinosaurs: $0.0031M^{0.82}$

Table S2

Taxon	G_0 ($\times 10^3$) ($g^{1/4}\ d^{-1}$)		G_{max} OLS Interc. β	G_{max} Slope OLS (CI)	G_{max} Slope RMA (CI)	n	r^2	G_{max} PIC Slope OLS (CI, r^2, n)	G_{max} PIC Slope SMA (CI)
Neornithes			0.32	0.59 (0.52–0.66)	0.65 (0.58–0.73)	63	0.83	0.73 (0.65–0.81, 0.84, 63)	0.82 (0.73–0.92)
Altricial Birds	203	**a**	0.19	0.76 (0.71–0.81)	0.77 (0.72–0.83)	35	0.96	0.77 (0.68–0.85, 0.90, 35)	0.84 (0.73–0.96)
Passeriformes				0.79 (0.72–0.87)	0.80 (0.83–0.89)	15	0.97	0.89 (0.78–1.0, 0.95, 15)	0.94 (0.81–1.08)
Precocial Birds	65.4	**b**	0.13	0.66 (0.53–0.79)	0.74 (0.62–0.88)	28	0.80	0.74 (0.60–0.88, 0.81, 28)	0.83 (0.68–1.00)
Mammalia				0.64 (0.61–0.67)	0.67 (0.64–0.71)	174	0.91	0.62 (0.57–0.67, 0.75, 172)	0.72 (0.66–0.79)
Placentalia	22.5	**c**	0.056	0.64 (0.61–0.67)	0.67 (0.64–0.70)	153	0.91	0.63 (0.57–0.68, 0.77, 151)	0.72 (0.66–0.79)
Marsupials	20.2	**c**	0.040	0.66 (0.54–0.77)	0.69 (0.59–0.82)	19	0.90	0.49 (0.25–0.73, 0.50, 19)	0.73 (0.43–1.30)
Dinosaurs	7.93	**d**	0.0029	0.82 (0.74–0.90)	0.84 (0.76–0.92)	21	0.96	0.76 (0.64–0.88, 0.90, 21)	0.79 (0.67–0.93)
Dinosaurs excluding Sauropods				0.77 (0.64–0.90)	0.80 (0.68–0.95)	15	0.93	0.71 (0.56–0.86, 0.90, 13)	0.74 (0.59–0.93)
Theropoda				0.75 (0.63–0.88)	0.77 (0.65–0.91)	10	0.96	0.71 (0.54–0.88, 0.91, 10)	0.74 (0.56–0.96)
Tuna	6.93	**de**	0.0043	0.80 (0.63–0.97)	0.80 (0.65–0.99)	5	0.99	0.74 (0.54–0.94, 0.97; 5)	0.73 (0.48–1.10)
Squamata	3.53	**e**	0.0037	0.74 (0.63–0.85)	0.78 (0.68–0.90)	26	0.89	0.56 (0.42–0.70; 0.72; 26)	0.67 (0.52–0.88)
Sharks				0.77 (0.68–0.86)	0.80 (0.71–0.90)	22	0.94	0.74 (0.60–0.89, 0.85, 21)	0.81 (0.66–0.98)
Sharks (excluding mako)	3.52	**e**	0.0023	0.79 (0.66–0.90)	0.82 (0.72–0.94)	21	0.92	0.74 (0.59–0.89, 0.85, 20)	0.81 (0.66–0.99)
Fish				0.75 (0.70–0.81)	0.78 (0.72–0.84)	55	0.92	0.74 (0.61–0.87, 0.76, 45)	0.83 (0.70–0.99)
Fish (excluding tuna)	2.73	**e**	0.0033	0.71 (0.66–0.77)	0.74 (0.68–0.79)	50	0.93	0.73 (0.59–0.87, 0.74, 40)	0.83 (0.67–1.00)

Table S2

Taxon	G_0 ($\times 10^3$) ($g^{1/4}\ d^{-1}$)	G_{max} OLS Interc. β	G_{max} Slope OLS (CI)	G_{max} Slope RMA (CI)	n	r^2	G_{max} PIC Slope OLS (CI, r^2, n)	G_{max} PIC Slope SMA (CI)
Crocodylia	1.90 **e**	0.0020	0.75 (0.63–0.86)	0.76 (0.66–88)	12	0.96	0.73 (0.58–0.88; 0.91; 12)	0.82 (0.64–1.06)

Table S3. A summary of species characteristics and references. Abbreviations: *B*: basal or standard metabolic rate, m_0 is neonate mass, L: length, SVL: snout-vent length, FL: fork length, PCL: pre-caudal length, F: female, M: male, W is wild, C is captive, B is both. If the wild or captive status was not reported, then no code is given. In some cases, length-mass relations were calculated by the authors using data provided in the L-M reference. Growth in the leatherback turtle, *Dermochelys coriacea*, was based on captive turtles grown at 25 ºC, not wild turtle data provided in the reference, as many wild individuals forage and grow in cold, temperate waters.

Table S3

Species	Wild/ Captive	Gowth Ref.	*B* Ref.	Length–Mass Equation	L–M Ref	m_0 Ref
Crocodylia						
Alligator mississipiensis	W	(*77*)	(*12*)	kg = 2.84·TL(m)$^{3.342}$ (estuarine) kg = 1.86·TL(m)$^{3.593}$ (palustrine)	(*77*)	(*78*)
Caiman crocodilus	W	(*79, 80*)	(*81*)	g = 0.0049·TL(cm)^3 (calculated)	(*82*)	
Caiman latirostris	W	(*83*)		g = 0.0049·TL(cm)^3 (calculated, *C. crocodilus*)	(*82*)	(*78*)
Brachychampsa montana	W	(*84*)		g = 8.38E-6 · SVL(mm)$^{3.189}$ (*C. niloticus*)	(*85*)	(*69*)
Deinosuchus sp.	W	(*84*)		g = 8.38E-6 · SVL(mm)$^{3.189}$ (*C. niloticus*)	(*85*)	(*69*)
Leidyosuchus canadens	W	(*84*)		g = 8.38E-6 · SVL(mm)$^{3.189}$ (*C. niloticus*)	(*85*)	(*69*)
Crocodylus 'affinis'	W	(*84*)		g = 8.38E-6 · SVL(mm)$^{3.189}$ (*C. niloticus*)	(*85*)	(*69*)
Crocodylus johnstoni	W	(*86*)		g = 0.0049·TL(cm)^3 (calculated, *C. crocodilus*)	(*82*)	(*78*)
Crocodylus niloticus	W	(*87*)	(*88*)	g = 8.38E-6 · SVL(mm)$^{3.189}$ (*C. niloticus*)	(*85*)	(*78*)
Crocodylus porosus	W	(*89*)	(*90*)	g = 8.38E-6 · SVL(mm)$^{3.189}$ (*C. niloticus*)	(*85*)	(*78*)
Borealosuchus sternbergii	W	(*84*)		g = 8.38E-6 · SVL(mm)$^{3.189}$ (*C. niloticus*)	(*85*)	(*69*)
Pristichampsus vorax	W	(*84*)		g = 8.38E-6 · SVL(mm)$^{3.189}$ (*C. niloticus*)	(*85*)	(*69*)
Mesozoic Dinosaurs						
Psittacosaurus mongoliensis	W	(*7*)				(*66*)

Table S3

Species	Wild/ Captive	Gowth Ref.	*B* Ref.	Length–Mass Equation	L–M Ref	m_0 Ref
Dysalotosaurus lettowvorbecki	W	(*91*)				(*66*)
Tenontosaurus tilletti	W	(*8*)				(*66*)
Massospondylus carinatus	W	(*7*)				(*66*)
Plateosaurus engelhardti	W	(*92*)				(*66*)
Apatosaurus sp.	W	(*92*)				(*66*)
Camarosaurus sp.	W	(*92*)				(*66*)
Diplodocid sp. 1		(*92*)				(*66*)
Diplodocid sp. 2		(*92*)				(*66*)
Mamenchisaurid sp.		(*92*)				(*66*)
Alamosaurus sanjuanensis	W	(*75*)				(*66*)
Allosaurus fragilis	W	(*8*)				(*66*)
Coelophysis bauri	W	(*93*)		$kg = 10^{-6.288} \cdot \text{femur length}^{3.222}$	(*93*)	(*66*)
Megapnosaurus rhodesiensis	W	(*7*)				(*66*)
Albertosaurus sarcophagus	W	(*76*)				(*66*)
Archaeopteryx lithographica	W	(*17*)				(*66*)
Citipati osmolskae	W	(*94*)				(*65*)
Gorgosaurus libratus	W	(*76*)				(*66*)
Saurornitholestes langstoni	W	(*95*)				(*66*)
Troodon formosus	W	(*94*)				(*65*)
Tyrannosaurus rex	W	(*8, 76*)				(*66*)
Placental Mammals						
Acinonyx jubatus	W	(*96*)	(*97*)			(*98*)

Table S3

Species	Wild/ Captive	Gowth Ref.	*B* Ref.	Length–Mass Equation	L–M Ref	m_0 Ref
Callorhinus ursinus	W	(*99*)				(*98*)
Canis lupus	W	(*100*)				(*98*)
Caracal caracal	C	(*101*)				(*98*)
Puma concolor	W	(*102*)				(*98*)
Lynx rufus	W	(*103*)	(*97*)			(*98*)
Mustela nigripes	C	(*104*)				
Mustela nivalis	C	(*105*)				
Mustela putorius	C	(*106*)				(*98*)
Panthera leo	W	(*107*)				(*98*)
Panthera tigris	C	(*108*)	(*97*)			
Ursus arctos	W	(*109*)				(*98*)
Vulpes lagopus	W	(*110*)				(*98*)
Balaenoptera acutorostrata	W	(*111*)	(*112*)			
Balaenoptera borealis	W	(*111*)				(*98*)
Balaenoptera edeni	W	(*113*)		$\text{tonne} = 0.012 \cdot \text{TL(m)}^{2.74}$	(*114*)	(*98*)
Balaenoptera musculus	W	(*111*)	(*112*)			(*98*)
Balaenoptera physalus	W	(*111*)	(*112*)			(*98*)
Eschrichtius robustus	W	(*115*)		$\text{tonne} = 0.0051 \cdot \text{TL(m)}^{3.28}$	(*114*)	(*98*)
Megaptera novaeangliae	W	(*111*)				(*98*)
Delphinapterus leucas	W	(*116*)		$\text{kg} = 1.56\text{E-}4 \cdot \text{TL(cm)}^{2.605}$	(*117*)	(*98*)
Delphinus delphis	W	(*118*)		$\text{kg} = 5.6\text{E-}6 \cdot \text{TL(cm)}^{3.14}$ (calculated)	(*119*)	(*98*)
Globicephala melas	W	(*120*)				

Table S3

Species	Wild/ Captive	Gowth Ref.	*B* Ref.	Length–Mass Equation	L–M Ref	m_0 Ref
Monodon monoceros	W	(*121*)				(*98*)
Orcinus orca	W	(*122*)		$kg = 6E\text{-}6 \cdot TL(cm)^{3.2}$	(*123*)	(*98*)
Physeter catodon	W	(*124*)	(*112*)	$tonne = 0.0029 \cdot TL(m)^{3.55}$	(*114*)	(*98*)
Pontoporia blainvillei	W	(*125*)		$kg = 8.37E\text{-}4 \cdot TL(cm)^{2.1244}$	(*126*)	(*98*)
Pseudorca crassidens	W	(*127*)		$kg = 5.6E\text{-}6 \cdot TL(cm)^{3.14}$ (calculated)	(*119*)	
Sousa chinensis	W	(*119*)		$kg = 5.6E\text{-}6 \cdot TL(cm)^{3.14}$ (calculated)	(*119*)	
Stenella attenuata	W	(*128*)		$kg = 5.6E\text{-}6 \cdot TL(cm)^{3.14}$ (calculated)	(*119*)	
Stenella longirostris	W	(*129*)		$kg = 5.6E\text{-}6 \cdot TL(cm)^{3.14}$ (calculated)	(*119*)	
Tursiops truncatus	W	(*130*)	(*131*)			(*98*)
Aepyceros melampus		(*132*)				(*98*)
Alces alces	W	(*133*)	(*97*)			(*98*)
Bison bison	W	(*134*)				(*98*)
Bison bonasus	W	(*135*)				
Cervus elaphus		(*132*)	(*97*)			(*98*)
Connochaetes gnou	C	(*136*)				(*98*)
Eudorcas thomsonii	W	(*137*)				
Hippopotamus amphibius	W	(*138*)		$kg = 2.5E\text{-}4 \cdot L(cm)^{2.7}$	(*139*)	(*98*)
Hippotragus niger	W	(*140*)				
Kobus ellipsiprymnus		(*132*)				(*98*)
Kobus leche		(*132*)				(*98*)
Odocoileus hemionus	C	(*141*)				
Odocoileus virginianus	C	(*142*)	(*97*)			(*98*)

Table S3

Species	Wild/ Captive	Gowth Ref.	*B* Ref.	Length–Mass Equation	L–M Ref	m_0 Ref
Pudu puda	C	(*143*)				
Rangifer tarandus	W	(*144*)	(*97*)			
Sus scrofa	W	(*145*)	(*97*)			(*98*)
Syncerus caffer	W	(*146*)				(*98*)
Artibeus watsoni	W	(*147*)				
Eptesicus fuscus	W	(*148*)	(*97*)			
Hipposideros larvatus	W	(*149*)				
Hipposideros terasensis	W	(*150*)				
Hypsignathus monstrosus	C	(*151*)				
Myotis blythii	W	(*152*)				
Myotis lucifugus	W	(*153*)	(*97*)			
Myotis macrodactylus	W	(*154*)				
Phyllostomus hastatus	W	(*155*)	(*97*)			
Pipistrellus subflavus	W	(*156*)				
Plecotus auritus	C	(*157*)	(*97*)			
Pteropus conspicillatus	C	(*158*)				
Pteropus poliocephalus	C	(*159*)	(*97*)			(*160*)
Rhinolophus cornutus	C	(*161*)				
Rhinolophus hipposideros	W	(*162*)				
Rousettus leschenaulti	W	(*163*)				(*160*)
Tolypeutes matacus	C	(*164*)				
Lepus americanus		(*165*)	(*97*)			

Table S3

Species	Wild/ Captive	Gowth Ref.	*B* Ref.	Length–Mass Equation	L–M Ref	m_0 Ref
Lepus californicus	C	(*165*)	(*97*)			
Lepus othus	W	(*165*)				
Lepus townsendii	W	(*165*)				(*98*)
Oryctolagus cuniculus	C	(*166*)				(*166*)
Sylvilagus floridanus	C	(*167*)				(*98*)
Cryptotis parva	C	(*168*)	(*97*)			
Neomys fodiens	C	(*169*)	(*97*)			
Sorex cinereus	W	(*170*)	(*97*)			
Sorex palustris	C	(*171*)				
Sorex unguiculatus	C	(*172*)				
Suncus murinus	C	(*173*)	(*97*)			
Macroscelides proboscideus	C	(*174*)	(*97*)			
Ceratotherium simum	W	(*175*)				(*98*)
Diceros bicornis		(*176*)				(*98*)
Equus ferus	C	(*177*)	(*97*)			
Equus quagga	W	(*178*)				
Rhinoceros unicornis	C	(*179*)				
Aotus trivirgatus	C	(*180*)	(*97*)			
Ateles geoffroyi	C	(*180*)				
Callicebus moloch	C	(*181*)				(*98*)
Callimico goeldii	C	(*181*)				
Callithrix jacchus	C	(*181*)	(*97*)			

Table S3

Species	Wild/ Captive	Gowth Ref.	*B* Ref.	Length–Mass Equation	L–M Ref	m_0 Ref
Cebuella pygmaea	C	(*181*)	(*97*)			
Cebus apella	C	(*180*)				(*98*)
Cercopithecus aethiops	C	(*182*)				
Cercopithecus mitis	C	(*180*)	(*97*)			
Gorilla gorilla	C	(*183*)				(*98*)
Homo sapiens	W	(*166*)	(*97*)			
Leontopithecus rosalia	C	(*181*)				
Lophocebus albigena	C	(*184*)				
Macaca fuscata	B	(*185*)				
Macaca mulatta	C	(*186*)	(*187*)			
Macaca nemestrina	C	(*180*)				(*98*)
Macaca silenus	C	(*180*)				
Pan troglodytes	W	(*188*)	(*189*)			(*98*)
Papio cynocephalus	C	(*180*)				
Saguinus imperator	C	(*181*)				(*98*)
Saimiri sciureus	C	(*190*)	(*97*)			
Tarsius bancanus	C	(*191*)				
Eulemur coronatus	C	(*192*)				(*98*)
Eulemur macaco	C	(*192*)				
Eulemur mongoz	C	(*192*)				
Eulemur rubriventer	C	(*192*)				
Eulemur rufus	C	(*192*)				

Table S3

Species	Wild/ Captive	Gowth Ref.	*B* Ref.	Length–Mass Equation	L–M Ref	m_0 Ref
Galago senegalensis	C	(*193*)	(*97*)			(*98*)
Hapalemur griseus	C	(*192*)				
Loris tardigradus	C	(*193*)	(*97*)			(*98*)
Microcebus murinus	C	(*194*)	(*195*)			
Nycticebus coucang	C	(*193*)	(*97*)			(*98*)
Otolemur crassicaudatus	C	(*193*)	(*97*)			(*98*)
Propithecus diadema	C	(*196*)				(*196*)
Propithecus tattersalli	C	(*196*)				(*98, 196*)
Propithecus verreauxi	C	(*196*)	(*97*)			(*98*)
Varecia variegata	C	(*192*)				
Elephas maximus	C	(*197*)	(*97*)			
Loxodonta africana	W	(*198*)				
Acomys cahirinus	C	(*199*)				
Akodon lindberghi	C	(*200*)				
Apodemus semotus	C	(*201*)				
Arvicanthis niloticus	W	(*202*)				
Ctenomys mendocinus	C	(*203*)				
Dipodomys stephensi	C	(*204*)				(*98*)
Eligmodontia typus	C	(*205*)	(*97*)			
Funisciurus congicus	C	(*206*)				
Gerbillus perpallidus	C	(*199*)				
Hoplomys gymnurus	C	(*207*)				(*98*)

Table S3

Species	Wild/ Captive	Gowth Ref.	*B* Ref.	Length–Mass Equation	L–M Ref	m_0 Ref
Mastomys coucha	C	(*208*)				
Mastomys natalensis	C	(*208*)	(*97*)			
Microtus cabrerae	C	(*209*)				
Neotoma cinerea	W	(*210*)				(*98*)
Otomys unisulcatus	C	(*211*)	(*97*)			
Paraxerus cepapi	C	(*206*)	(*97*)			
Paraxerus palliatus	C	(*206*)	(*97*)			
Peromyscus eremicus	C	(*212*)	(*97*)			
Peromyscus interparietalis	C	(*212*)				
Peromyscus leucopus	C	(*213*)	(*97*)			(*98*)
Peromyscus maniculatus	C	(*214*)	(*97*)			
Proechimys semispinosus	C	(*207*)				(*98*)
Scotinomys teguina	C	(*215*)	(*97*)			
Scotinomys xerampelinus	C	(*215*)	(*97*)			(*98*)
Spermophilus armatus	C	(*216*)	(*97*)			
Spermophilus columbianus	C	(*216*)				
Spermophilus elegans	C	(*216*)				
Spermophilus richardsonii	C	(*216*)	(*97*)			
Tupaia belangeri	C	(*217*)				(*98*)
Marsupials						
Antechinus flavipes	C	(*218*)	(*97*)			(*219*)
Antechinus stuartii	C	(*220*)	(*97*)			(*219*)

Table S3

Species	Wild/ Captive	Gowth Ref.	*B* Ref.	Length–Mass Equation	L–M Ref	m_0 Ref
Didelphis virginiana	W	(*221*)	(*97*)			(*219*)
Bettongia lesueur	C	(*222*)				(*219*)
Macropus giganteus		(*132*)				(*219*)
Macropus parma	C	(*223*)				(*219*)
Macropus robustus		(*132*)				(*224*)
Macropus rufus		(*132*)	(*97*)			(*219*)
Petaurus breviceps	C	(*225*)	(*97*)			
Petaurus norfolcensis	C	(*225*)				(*219*)
Phascolarctos cinereus	C	(*226*)	(*97*)			(*219*)
Pseudocheirus peregrinus	C	(*227*)	(*97*)			(*219*)
Thylogale billardierii	C	(*228*)				(*219*)
Trichosurus caninus	C	(*229*)				(*219*)
Trichosurus vulpecula		(*230*)	(*97*)			(*219*)
Wallabia bicolor		(*132*)				(*219*)
Isoodon macrourus	C	(*231*)	(*97*)			(*219*)
Isoodon obesulus	B	(*232*)				(*219*)
Perameles gunnii	B	(*232*)	(*97*)			(*219*)
Monotremes						
Ornithorhynchus anatinus	C	(*233, 234*)	(*97*)			(*224*)
Tachyglossus aculeatus	W	(*235*)	(*97*)			
Precocial Birds						
Aix galericulata	W	(*236*)				

Table S3

Species	Wild/ Captive	Gowth Ref.	*B* Ref.	Length–Mass Equation	L–M Ref	m_0 Ref
Anas rubripes	C	(*237*)				
Aythya affinis	C	(*238*)				
Aythya valisineria	W	(*238*)				
Branta hutchinsii	W	(*239*)				
Chen caerulescens	C	(*240*)				
Dendrocygna autumnalis	W	(*241*)				
Alectoris chukar	C	(*242*)	(*243*)			
Alectura lathami	C	(*244*)				
Coturnix chinensis	C	(*245*)				
Coturnix coturnix	C	(*243, 245*)	(*243*)			
Dendragapus obscurus	C	(*246*)	(*243*)			
Gallus gallus	W	(*247*)	(*243*)			
Tetrao tetrix	C	(*248*)				
Meleagris gallopavo	C	(*249*)	(*243*)			
Numida meleagris	W	(*250*)				
Pavo cristatus	C	(*244*)				(*251*)
Phasianus colchicus	C	(*244*)				
Tetrao urogallus	C	(*252*)				
Tympanuchus pallidicinctus	W	(*253*)				
Apteryx mantelli	W	(*254*)	(*243*)			
Casuarius bennetti	C	(*255, 256*)				
Casuarius casuarius	C	(*255, 256*)				

Table S3

Species	Wild/ Captive	Gowth Ref.	*B* Ref.	Length–Mass Equation	L–M Ref	m_0 Ref
Dromaius novaehollandiae	C	(*257*)	(*243*)			
Rhea americana	C	(*258*)	(*259*)			
Rhynchotus rufescens	C	(*260*)				
Struthio camelus	C	(*261*)	(*243*)			
Altricial Birds						
Aquila chrysaetos	W	(*262*)				
Haliaeetus leucocephalus	W	(*263*)				
Archilochus alexandri	W	(*264*)				
Selasphorus rufus	W	(*265*)				
Sternoclyta cyanopectus	W	(*266*)				
Geococcyx californianus	C	(*267*)				
Buteo jamaicensis	W	(*268*)				
Buteo swainsoni	W	(*269*)				
Cathartes aura	W	(*270*)				
Coragyps atratus	W	(*270*)				
Falco mexicanus	W	(*271*)				
Acrocephalus arundinaceus	W	(*272*)	(*243*)			
Acrocephalus melanopogon	W	(*272*)				
Acrocephalus palustris	W	(*272*)	(*243*)			
Acrocephalus scirpaceus	W	(*272*)				
Aimophila carpalis	W	(*273*)				
Campylorhynchus brunneicapillus	W	(*274*)				

Table S3

Species	Wild/ Captive	Gowth Ref.	*B* Ref.	Length–Mass Equation	L–M Ref	m_0 Ref
Corvus brachyrhynchos	W	(*275*)				
Corvus corax	W	(*275*)	(*276*)			
Corvus cryptoleucus	W	(*277*)				
Parus caeruleus	W	(*278*)				
Passer domesticus	W	(*279*)	(*243*)			
Pica pica	W	(*275*)				
Spizella passerina	W	(*280*)				
Spizella pusilla	W	(*281*)	(*282*)			
Sturnus vulgaris	W	(*283*)	(*243*)			
Amazona aestiva	W	(*284*)				
Amazona agilis	W	(*285*)				
Ara macao	W	(*286*)				
Cyanoliseus patagonus	W	(*287*)				
Myiopsitta monachus	W	(*288*)				
Nymphicus hollandicus	C	(*289*)				
Poicephalus cryptoxanthus	C	(*290*)				
Megascops asio	W	(*281*)				
Tyto alba	W	(*281*)				
Sharks						
Carcharhinus acronotus	W	(*291*)	(*292*)	$g = 0.0127 \cdot TL(cm)^3$; TL = 1.215·FL	(*293*)	
Carcharhinus brevipinna	W	(*294*)		$kg = 3E\text{-}06 \cdot TL(cm)^{3.145}$	(*294*)	
Carcharhinus falciformis	W	(*295*)		$kg = 2.73E\text{-}5 \cdot PCL(cm)^{2.86}$	(*295*)	

Table S3

Species	Wild/ Captive	Gowth Ref.	*B* Ref.	Length–Mass Equation	L–M Ref	m_0 Ref
Carcharhinus leucas	W	(*296*)		kg = 2.71E-5·TL·(cm)$^{3.30}$	(*296*)	
Carcharhinus limbatus	W	(*297*)		g = 0.0144·TL(cm)$^{2.870}$	(*293*)	
Carcharhinus plumbeus	W	(*298*)	(*299*)	g = 0.0254·PCL(cm)$^{2.691}$	(*298*)	
Carcharhinus signatus	W	(*300*)		g = 0.0091·TL(cm)$^{2.886}$	(*293*)	
Carcharhinus sorrah	W	(*301*)		g = 7.2E-4·TL(cm)$^{3.656}$	(*293*)	(*293*)
Carcharhinus tilstoni	W	(*301*)		g = 0.0144·TL(cm)$^{2.870}$ (*C. limbatus*)	(*293*)	
Galeocerdo cuvier	W	(*302*)		kg = 1.41E-6·TL(cm)$^{3.24}$	(*302*)	
Negaprion brevirostris	W	(*293, 303*)	(*304*) *266*)	g = 0.0053·SL(cm)$^{3.16}$	(*293*)	(*305*)
Prionace glauca	W	(*306*) (*293*)		g = 0.00318·FL(cm)$^{3.131}$; FL = 0.822·TL	(*293*)	
Rhizoprionodon lalandii	W	(*307*)		g = 0.0012·TL(cm)$^{3.14}$ (*R. porosus*)	(*293*)	
Rhizoprionodon porosus	W	(*307*)		g = 0.0012·TL(cm)$^{3.14}$	(*293*)	
Rhizoprionodon taylori	W	(*308*)		g = 0.0012·TL(cm)$^{3.14}$ (*R. porosus*)	(*293*)	(*293*)
Scoliodon laticaudus	W	(*309*)		g = 0.0086·FL(cm)$^{2.784}$ (female) g = 0.0044·FL(cm)$^{2.935}$ (male)	(*293*)	
Sphyrna lewini	W	(*310*)	(*292*)	g = 0.0077·FL(cm)$^{3.067}$	(*293*)	
Sphyrna tiburo	W	(*311*)	(*292*)	g = 0.0016·FL(cm)$^{3.16}$ FL = 0.797·TL	(*293*)	
Cretoxyrhina mantelli	W	(*312*)		kg = 16.26·PCL(m)$^{2.9851}$ PCL (cm) = 0.8535·TL(cm) - 0.09195	(*313*)	
Isurus oxyrinchus	W	(*314*)	(*315*)	g = 0.0167·FL(cm)$^{2.847}$; FL = 0.927·TL	(*293*)	
Chiloscyllium plagiosum	W	(*316*)	(*276*)	g = 0.00509TL·(cm)$^{2.87}$	(*316*)	(*293*)
Rhincodon typus	W	(*317*)		g = 0.0043·TL(cm)^{3} TL(cm) = 20.309 + 1.252·PCL (cm)	(*293*)	
Squamates						
Agama impalearis	W	(*318*)				
Basiliscus basiliscus	W	(*319*)		g = 9.08E-6·SVL(mm)$^{3.257}$	(*319*)	(*320*)

Table S3

Species	Wild/ Captive	Gowth Ref.	*B* Ref.	Length–Mass Equation	L–M Ref	m_0 Ref
Ctenosaura pectinata	W	(*321*)				
Liolaemus lutzae	W	(*322*)		$g = 0.031 \cdot SVL(cm)^{2.98}$	(*323*)	
Sceloporus grammicus	W	(*324*)		$g = 1.95E\text{-}4 \cdot SVL(cm)^{2.62}$	(*323*)	
Sceloporus mucronatus	W	(*325*)		$g = 1.95E\text{-}4 \cdot SVL(cm)^{2.62}$	(*323*)	(*320*)
Sceloporus scalaris	W	(*326*)		$g = 1.95E\text{-}4 \cdot SVL(cm)^{2.62}$	(*323*)	
Microlophus occipitalis	W	(*327*)		$g = 0.031 \cdot SVL(cm)^{2.98}$	(*323*)	
Tropidurus itambere	W	(*328*)		$g = 0.031 \cdot SVL(cm)^{2.98}$	(*323*)	
Tropidurus torquatus	W	(*329*)		$g = 0.031 \cdot SVL(cm)^{2.98}$	(*323*)	
Uranoscodon superciliosus	W	(*330*)		$g = 0.031 \cdot SVL(cm)^{2.98}$	(*323*)	
Xenosaurus grandis	W	(*331*)		$g = 0.031 \cdot SVL(cm)^{2.98}$	(*323*)	(*320*)
Eublepharis macularius	C	(*332*)	(*333*)			
Coleonyx brevis	C	(*332*)	(*333*)			
Coleonyx elegans	C	(*332*)	(*333*)			
Coleonyx mitratus	C	(*332*)	(*333*)			
Acrochordus arafurae	W	(*334*)	(*12*)	$g = 3.2E\text{-}4 \cdot SVL(cm)^{3.14}$	(*335*)	(*320*)
Acanthophis praelongus	W	(*336*)	(*12*)	$g = 3.2E\text{-}4 \cdot SVL(cm)^{3.14}$	(*335*)	
Liasis fuscus	W	(*337*)	(*12*)	$g = 3.2E\text{-}4 \cdot SVL(cm)^{3.14}$	(*335*)	(*320*)
Morelia viridis	W	(*338*)		$g = 3.2E\text{-}4 \cdot SVL(cm)^{3.14}$	(*335*)	(*320*)
Heloderma suspectum	W	(*339*)	(*340*)	$g = 9.09E\text{-}6 \cdot SVL(mm)^{3.47}$	(*341*)	
Oligosoma suteri	C	(*342*)		$g = 0.031 \cdot SVL(cm)^{2.98}$	(*323*)	
Varanus indicus	C	(*343*)				
Varanus komodoensis	W	(*344*)		$g = 0.016 \cdot SVL(cm)^{3.07}$ (calculated)	(*345, 346*)	(*347*)

Table S3

Species	Wild/ Captive	Gowth Ref.	*B* Ref.	Length–Mass Equation	L–M Ref	m_0 Ref
Varanus niloticus	W	(*348*)	(*88*)	kg = 9.65E-6·SVL (cm)$^{3.161}$	(*348*)	
Varanus semiremex	C	(*349*)		log(g) = 2.70·log(SVL(mm)) - 4.09	(*323*)	
Teleost Fish						
Tenualosa toli	W	(*350*)		g = 0.0119·FL(cm)$^{3.087}$; FL = 1.08SL	(*293*)	(*68*)
Danio rerio	C	(*351*)				
Labeo cylindricus	W	(*352*)		g = 0.0105·FL(cm)$^{3.010}$	(*352*)	(*68*)
Poecilia latipinna	C	(*353*)		g = 0.0084·TL(cm)$^{3.0447}$ (*P. reticulata*)	(*354*)	(*68*)
Poecilia reticulata	W	(*354*)	(*355*)	g = 0.0084·TL(cm)$^{3.0447}$	(*354*)	(*68*)
Xiphophorus maculatus		(*356*)	(*357*)	g = 0.0236·SL(cm)^{3}	(*293*)	(*68*)
Acanthurus lineatus	C	(*358*)		g = 2.219E-5·SL(mm)$^{2.691}$	(*358*)	(*68*)
Acanthurus olivaceus	W	(*358*)		g = 3.385E-5·SL(mm)$^{3.055}$	(*358*)	(*68*)
Ctenochaetus striatus	W	(*358*)		g = 3.517E-5·SL(mm)$^{3.066}$	(*358*)	(*68*)
Naso brevirostris	W	(*358*)		g = 1.088E-4·SL(mm)$^{2.743}$	(*358*)	(*68*)
Naso tuberosus	W	(*358*)		g = 1.088E-4·SL(mm)$^{2.743}$	(*358*)	(*68*)
Zebrasompa scopas	W	(*358*)		g = 6.302E-5·SL(mm)$^{2.948}$	(*358*)	(*68*)
Salarias patzneri	W	(*359*)		g = 0.0176·SL(cm)^{3} (*Salarias fasciatus*)	(*293*)	(*68*)
Chaetodon larvatus	W	(*360*)		g = 0.0257·TL(cm)$^{3.1}$	(*293*)	(*68*)
Cichla intermedia	W	(*361*)		g = 0.0327·TL(cm)$^{2.771}$; TL = 1.19·SL	(*293*)	(*68*)
Cichla orinocensis	W	(*361*)		g = 0.0063·TL(cm)$^{3.241}$; TL = 1.202·SL	(*293*)	(*68*)
Cichla temensis	W	(*361*)		g = 0.0327·TL(cm)$^{2.771}$ TL = 1.19·SL (*C. intermedia*)	(*293*)	(*68*)
Oreochromis macrochir	W	(*362*)		g = 0.014·TL(cm)$^{3.106}$	(*293*)	(*68*)
Pharyngochromis darlingi	W	(*363*)		g = 1.55E-5·TL(mm)$^{3.01}$	(*363*)	(*68*)

Table S3

Species	Wild/ Captive	Gowth Ref.	*B* Ref.	Length–Mass Equation	L–M Ref	m_0 Ref
Pseudocrenilabrus philander	W	(*363*)		$g = 1.3E\text{-}5 \cdot TL(mm)^{3.03}$	(*363*)	(*68*)
Amblygobius bynoensis	W	(*364*)		$g = 9.6E\text{-}6 \cdot TL(mm)^{3.01}$	(*364*)	(*68*)
Amblygobius phalaena	W	(*364*)		$g = 1.33E\text{-}5 \cdot TL(mm)^{2.96}$	(*364*)	(*68*)
Asterropteryx semipunctatus	W	(*364*)		$g = 9.5E\text{-}6 \cdot TL(mm)^{3.1}$	(*364*)	(*68*)
Istigobius goldmanni	W	(*364*)		$g = 1.07E\text{-}5 \cdot TL(mm)^{2.99}$	(*364*)	(*68*)
Valenciennea muralis	W	(*364*)		$g = 1.32E\text{-}5 \cdot TL(mm)^{2.84}$	(*364*)	(*68*)
Cheilinus undulatus	W	(*365*)		$g = 0.0113 \cdot FL(cm)^{3.136}$	(*293*)	(*68*)
Lutjanus erythropterus	W	(*366*)		$g = 0.0244 \cdot TL(cm)^{2.870}$	(*293*)	(*68*)
Lutjanus malabaricus	W	(*366*)		$g = 0.0208 \cdot FL(cm)^{2.919}$	(*293*)	(*68*)
Lutjanus sebae	W	(*366*)		$g = 0.0176 \cdot FL(cm)^{3.06}$	(*293*)	(*68*)
Pristipomoides multidens	W	(*367*)		$g = 0.032 \cdot SL(cm)^{2.897}$	(*293*)	(*68*)
Pristipomoides typus	W	(*367*)		$g = 0.038 \cdot SL(cm)^{2.822}$	(*293*)	(*68*)
Notothenia neglecta	W	(*368*)	(*369*)	$g = 0.0085 \cdot TL(cm)^{3.1602}$	(*368*)	(*68*)
Notothenia rossi	W	(*370*)	(*371*)	$g = 0.0112 \cdot (cm)^3$	(*293*)	(*68*)
Trematomus bernacchii	W	(*370*)	(*372*)	$g = 1.6E\text{-}6 \cdot TL(mm)^3$ (F) (calc.) $g = 1.5E\text{-}6 \cdot TL(mm)^3$ (M) (calc.)	(*370*)	(*68*)
Trematomus hansoni	W	(*373*)	(*371*)	$g = 0.0014 \cdot TL(cm)^{3.632}$	(*293*)	(*68*)
Trematomus lonnbergi	W	(*373*)	(*372*)	$g = 1.16E\text{-}6 \cdot TL(mm)^{3.2916}$ (F) $g = 3.55E\text{-}6 \cdot TL(mm)^{3.2759}$ (M)		(*68*)
Stegastes fuscus	W	(*374*)		$g = 0.02 \cdot FL(cm)^{3.12}$	(*374*)	(*68*)
Chlorurus gibbus	W	(*375*)		$g = 9.25E\text{-}5 \cdot SL(mm)^{2.85}$	(*375*)	(*68*)
Chlorurus sordidus	W	(*375*)		$g = 1.82E\text{-}5 \cdot SL(mm)^{3.15}$	(*375*)	(*68*)
Scarus frenatus	W	(*375*)		$g = 2.79E\text{-}5 \cdot SL(mm)^{3.06}$	(*375*)	(*68*)
Scarus niger	W	(*375*)		$g = 2.57E\text{-}5 \cdot SL(mm)^{3.09}$	(*375*)	(*68*)

Table S3

Species	Wild/ Captive	Gowth Ref.	*B* Ref.	Length–Mass Equation	L–M Ref	m_0 Ref
Scarus psittacus	W	(*375*)		$g = 6.08E\text{-}5 \cdot SL(mm)^{2.90}$	(*375*)	(*68*)
Scarus rivulatus	W	(*375*)		$g = 1.73E\text{-}5 \cdot SL(mm)^{3.14}$	(*375*)	(*68*)
Scarus schlegeli	W	(*375*)		$g = 1.86E\text{-}5 \cdot SL(mm)^{3.12}$	(*375*)	(*68*)
Euthynnus affinis	W	(*376*)	(*377*)	$g = 0.0254 \cdot FL(cm)^{2.889}$	(*378*)	(*68*)
Katsuwonus pelamis	W	(*379*)	(*377*)	$g = 0.0069 \cdot FL(cm)^{3.287}$	(*293*)	(*68*)
Thunnus albacares	W	(*379*)	(*377*)	$g = 0.0214 \cdot FL(cm)^{2.974}$	(*293*)	(*68*)
Thunnus obesus	W	(*380*)	(*381*)	$g = 0.0119 \cdot FL(cm)^{3.09}$	(*293*)	(*68*)
Thunnus tongol	W	(*382*)		$g = 0.0143 \cdot FL(cm)^{3}$	(*293*)	(*68*)
Epinephelus fuscoguttatus	W	(*383*)		$g = 0.0134 \cdot FL(cm)^{3.057}$	(*293*)	(*68*)
Epinephelus polyphekadion	W	(*384*)		$kg = 1E\text{-}5 \cdot TL(cm)^{3.11}$	(*384*)	(*68*)
Epinephelus tukula	W	(*384*)		$kg = 1E\text{-}5 \cdot TL(cm)^{3.07}$	(*384*)	(*68*)
Mycteroperca rosacea	W	(*385*)		$g = 0.0133 \cdot TL(cm)^{2.97}$	(*293*)	(*68*)
Plectropomus laevis	W	(*384*)		$kg = 6E\text{-}6 \cdot FL(cm)^{3.20}$	(*384*)	(*68*)
Plectropomus leopardus	W	(*386*)		$g = 0.0079 \cdot FL(cm)^{3.157}$	(*386*)	(*68*)
Variola louti	W	(*384*)		$kg = 3E\text{-}6 \cdot FL(cm)^{3.35}$	(*384*)	(*68*)
Siganus sutor	W	(*387*)		$g = 0.0597 \cdot TL(cm)^{2.754}$; $SL = 0.846 \cdot TL$	(*387*)	(*68*)
Diplodus sargus	W	(*388*)		$g = 0.0097 \cdot TL(cm)^{3.123}$	(*293*)	(*68*)
Rhabdosargus sarba	W	(*389*)		$g = 0.0277 \cdot SL(cm)^{3.085}$; $FL = 0.868 \cdot SL$	(*293*)	(*68*)
Hippoglossoides platessoides	W	(*390*)	(*390*)	$g = 0.0049 \cdot L(cm)^{3.10}$ (calculated)	(*390*)	(*68*)
Sorubim lima	W	(*391*)		$g = 0.0109 \cdot SL(cm)^{2.94}$; $SL = 0.98 \cdot FL$	(*293*)	(*68*)
Masturus lanceolatus	W	(*392*)		$kg = 9.98E\text{-}4 \cdot SL(cm)^{2.4488}$	(*392*)	(*68*)
Testudines						

Table S3

Species	Wild/ Captive	Gowth Ref.	*B* Ref.	Length–Mass Equation	L–M Ref	m_0 Ref
Chelonia mydas	W	(*393*)	(*394*)			
Dermochelys coriacea	C	(*395*)	(*396*)			

Table S4. A summary of AICc statistics calculated for 3 ontogenetic growth models.

Table S4

Taxa	Average	AICc Gompertz	AICc von Bertalanffy	AICc logistic
Dinosaurs	Median	264.1	274.1	260.7
Dinosaurs	Mean	408.2	418.4	408.9
All Species	Median	355.4	355.3	358.6
All Species	Mean	754.9	754.8	761.7

References and Notes

1. K. Padian, A. J. de Ricqlès, J. R. Horner, Dinosaurian growth rates and bird origins. *Nature* **412**, 405–408 (2001). doi:10.1038/35086500 Medline

2. P. M. Sander, A. Christian, M. Clauss, R. Fechner, C. T. Gee, E. M. Griebeler, H. C. Gunga, J. Hummel, H. Mallison, S. F. Perry, H. Preuschoft, O. W. Rauhut, K. Remes, T. Tütken, O. Wings, U. Witzel, Biology of the sauropod dinosaurs: The evolution of gigantism. *Biol. Rev. Camb. Philos. Soc.* **86**, 117–155 (2011). doi:10.1111/j.1469-185X.2010.00137.x Medline

3. R. A. Eagle, T. Tütken, T. S. Martin, A. K. Tripati, H. C. Fricke, M. Connely, R. L. Cifelli, J. M. Eiler, Dinosaur body temperatures determined from isotopic (C- ^{8}O) ordering in fossil biominerals. *Science* **333**, 443–445 (2011). doi:10.1126/science.1206196 Medline

4. J. H. Brown, J. F. Gillooly, A. P. Allen, V. M. Savage, G. B. West, Toward a metabolic theory of ecology. *Ecology* **85**, 1771–1789 (2004). doi:10.1890/03-9000

5. P. Else, A. Hulbert, *Am. J. Physiol. Regul. Integr. Comp. Physiol.* **240**, R3–R9 (1981).

6. J. F. Gillooly, J. H. Brown, G. B. West, V. M. Savage, E. L. Charnov, Effects of size and temperature on metabolic rate. *Science* **293**, 2248–2251 (2001). doi:10.1126/science.1061967 Medline

7. G. M. Erickson, K. C. Rogers, S. A. Yerby, Dinosaurian growth patterns and rapid avian growth rates. *Nature* **412**, 429–433 (2001). doi:10.1038/35086558 Medline

8. A. H. Lee, S. Werning, Sexual maturity in growing dinosaurs does not fit reptilian growth models. *Proc. Natl. Acad. Sci. U.S.A.* **105**, 582–587 (2008). doi:10.1073/pnas.0708903105 Medline

9. See the supplementary materials.

10. F. Seebacher, Dinosaur body temperatures: The occurrence of endothermy and ectothermy. *Paleobiology* **29**, 105–122 (2003). doi:10.1666/0094-8373(2003)029<0105:DBTTOO>2.0.CO;2

11. R. H. Peters, *The Ecological Implications of Body Size* (Cambridge Univ. Press, Cambridge, MA, 1983).

12. C. R. White, N. F. Phillips, R. S. Seymour, The scaling and temperature dependence of vertebrate metabolism. *Biol. Lett.* **2**, 125–127 (2006). doi:10.1098/rsbl.2005.0378 Medline

13. T. J. Case, On the evolution and adaptive significance of postnatal growth rates in the terrestrial vertebrates. *Q. Rev. Biol.* **53**, 243–282 (1978). doi:10.1086/410622 Medline

14. G. B. West, J. H. Brown, B. J. Enquist, A general model for ontogenetic growth. *Nature* **413**, 628–631 (2001). doi:10.1038/35098076 Medline

15. C. Hou, W. Zuo, M. E. Moses, W. H. Woodruff, J. H. Brown, G. B. West, Energy uptake and allocation during ontogeny. *Science* **322**, 736–739 (2008). doi:10.1126/science.1162302 Medline

16. D. Bernal, K. A. Dickson, R. E. Shadwick, J. B. Graham, Review: Analysis of the evolutionary convergence for high performance swimming in lamnid sharks and tunas. *Comp. Biochem. Physiol. A Mol. Integr. Physiol.* **129**, 695–726 (2001). doi:10.1016/S1095-6433(01)00333-6 Medline

17. G. M. Erickson, O. W. Rauhut, Z. Zhou, A. H. Turner, B. D. Inouye, D. Hu, M. A. Norell, Was dinosaurian physiology inherited by birds? Reconciling slow growth in archaeopteryx. *PLOS ONE* **4**, e7390 (2009). doi:10.1371/journal.pone.0007390 Medline

18. A. Chinsamy, *Mesozoic Birds: Above the Heads of Dinosaurs* (Univ. of California Press, Berkeley, CA, 2002), pp. 421–431.

19. E. L. Charnov, D. Berrigan, *Evol. Anthropol.* **1**, 191–194 (1993).

20. K. Isler, C. P. van Schaik, The Expensive Brain: A framework for explaining evolutionary changes in brain size. *J. Hum. Evol.* **57**, 392–400 (2009). doi:10.1016/j.jhevol.2009.04.009 Medline

21. R. Reid, in *The Complete Dinosaur,* M. K. Brett-Surman, T. R. Holtz, J. O. Farlow, Eds. (Indiana Univ. Press, Bloomington, IN, 2012), pp. 873–24.

22. F. V. Paladino, M. P. O'Connor, J. R. Spotila, Metabolism of leatherback turtles, gigantothermy, and thermoregulation of dinosaurs. *Nature* **344**, 858–860 (1990). doi:10.1038/344858a0

23. F. Seebacher, G. C. Grigg, L. A. Beard, Crocodiles as dinosaurs: Behavioural thermoregulation in very large ectotherms leads to high and stable body temperatures. *J. Exp. Biol.* **202**, 77–86 (1999). Medline

24. P. Brice, G. C. Grigg, L. A. Beard, J. A. Donovan, Patterns of activity and inactivity in echidnas (*Tachyglossus aculeatus*) free-ranging in a hot dry climate: Correlates with ambient temperature, time of day and season. *Aust. J. Zool.* **50**, 461–475 (2002). doi:10.1071/ZO01080

25. R. Refinetti, M. Menaker, The circadian rhythm of body temperature. *Physiol. Behav.* **51**, 613–637 (1992). doi:10.1016/0031-9384(92)90188-8 Medline

26. T. Kubo, W. Sakamoto, O. Murata, H. Kumai, Whole-body heat transfer coefficient and body temperature change of juvenile Pacific bluefin tuna *Thunnus orientalis* according to growth. *Fish. Sci.* **74**, 995–1004 (2008). doi:10.1111/j.1444-2906.2008.01617.x

27. P. H. Brice, Thermoregulation in monotremes: Riddles in a mosaic. *Aust. J. Zool.* **57**, 255–263 (2009). doi:10.1071/ZO09039

28. H. J. Harlow, D. Purwandana, T. S. Jessop, J. A. Phillips, Body temperature and thermoregulation of Komodo dragons in the field. *J. Therm. Biol.* **35**, 338–347 (2010). doi:10.1016/j.jtherbio.2010.07.002

29. B. K. McNab, W. Auffenberg, The effect of large body size on the temperature regulation of the Komodo dragon, *Varanus komodoensis*. *Comp. Biochem. Physiol. A Comp. Physiol.* **55**, 345–350 (1976). doi:10.1016/0300-9629(76)90058-X Medline

30. S. H. Emery, Hematological comparisons of endothermic vs ectothermic elasmobranch fishes. *Copeia* **1986**, 700–705 (1986). doi:10.2307/1444952

31. M. Thums, M. Meekan, J. Stevens, S. Wilson, J. Polovina, Evidence for behavioural thermoregulation by the world's largest fish. *J. R. Soc. Interface* **10**, 20120477 (2012). doi:10.1098/rsif.2012.0477 Medline

32. Arizona-Software, GraphClick 3.0 (Arizona-Software, 2008).

33. R. Andrews, in *Biology of the Reptilia* C. Gans, F. H. Pough, Eds. (Academic Press, New York, 1982), vol. 13, chap. Patterns of Growth in Reptiles, pp. 273–320.

34. R. C. Team, R 3.1.0 (http://cran.r-project.org) (R Foundation for Statistical Computing, Vienna, Austria, 2012).

35. S. I. Inc., JMP 9.0.1 (SAS Institute, Cary, NC, 1989–2007).

36. C. Lockyer, in *Mammals in the Seas*, J. Clark, Ed. (Food and Agriculture Organization, Rome, 1981), vol. 3, pp. 379–487.

37. S. A. L. M. Kooijman, *Dynamic Energy Budget Theory for Metabolic Organisation* (Cambridge Univ. Press, Cambridge, 2010), chap. 1.

38. C. R. White, P. B. Frappell, S. L. Chown, An information-theoretic approach to evaluating the size and temperature dependence of metabolic rate. *Proc. Biol. Sci.* **279**, 3616–3621 (2012). doi:10.1098/rspb.2012.0884 Medline

39. T. V. Elzhov, K. M. Mullen, A.-N. Spiess, B. Bolker, minpack.lm: R interface to the Levenberg-Marquardt nonlinear least-squares algotithm found in MINPACK, plus support for bounds; http://CRAN.R-project.org/package=minpack.lm (2013).

40. C. Ritz, A.-N. Spiess, qpcR: An R package for sigmoidal model selection in quantitative real-time polymerase chain reaction analysis. *Bioinformatics* **24**, 1549–1551 (2008). doi:10.1093/bioinformatics/btn227 Medline

41. E. Paradis, J. Claude, K. Strimmer, APE: Analyses of phylogenetics and evolution in R language. *Bioinformatics* **20**, 289–290 (2004). doi:10.1093/bioinformatics/btg412 Medline

42. O. R. Bininda-Emonds, M. Cardillo, K. E. Jones, R. D. MacPhee, R. M. Beck, R. Grenyer, S. A. Price, R. A. Vos, J. L. Gittleman, A. Purvis, The delayed rise of present-day mammals. *Nature* **446**, 507–512 (2007). doi:10.1038/nature05634 Medline

43. W. Jetz, G. H. Thomas, J. B. Joy, K. Hartmann, A. O. Mooers, The global diversity of birds in space and time. *Nature* **491**, 444–448 (2012). doi:10.1038/nature11631 Medline

44. R. A. Pyron, F. T. Burbrink, J. J. Wiens, A phylogeny and revised classification of Squamata, including 4161 species of lizards and snakes. *BMC Evol. Biol.* **13**, 93 (2013). doi:10.1186/1471-2148-13-93 Medline

45. T. J. Near, R. I. Eytan, A. Dornburg, K. L. Kuhn, J. A. Moore, M. P. Davis, P. C. Wainwright, M. Friedman, W. L. Smith, Resolution of ray-finned fish phylogeny and timing of diversification. *Proc. Natl. Acad. Sci. U.S.A.* **109**, 13698–13703 (2012). doi:10.1073/pnas.1206625109 Medline

46. X. Vélez-Zuazo, I. Agnarsson, Shark tales: A molecular species-level phylogeny of sharks (Selachimorpha, Chondrichthyes). *Mol. Phylogenet. Evol.* **58**, 207–217 (2011). doi:10.1016/j.ympev.2010.11.018 Medline

47. R. M. Sibly, C. C. Witt, N. A. Wright, C. Venditti, W. Jetz, J. H. Brown, Energetics, lifestyle, and reproduction in birds. *Proc. Natl. Acad. Sci. U.S.A.* **109**, 10937–10941 (2012). doi:10.1073/pnas.1206512109 Medline

48. P. Senter, A new look at the phylogeny of coelurosauria (Dlnosauria: Theropoda). *J. Syst. Palaeontology* **5**, 429–463 (2007). doi:10.1017/S1477201907002143

49. P. Upchurch, C. A. Hunn, D. B. Norman, An analysis of dinosaurian biogeography: Evidence for the existence of vicariance and dispersal patterns caused by geological events. *Proc. R. Soc. London Ser. B* **269**, 613–621 (2002). doi:10.1098/rspb.2001.1921 Medline

50. M. A. Loewen, R. B. Irmis, J. J. Sertich, P. J. Currie, S. D. Sampson, Tyrant dinosaur evolution tracks the rise and fall of Late Cretaceous oceans. *PLOS ONE* **8**, e79420 (2013). doi:10.1371/journal.pone.0079420 Medline

51. J. Gatesy, R. H. Baker, C. Hayashi, Inconsistencies in arguments for the supertree approach: Supermatrices versus supertrees of Crocodylia. *Syst. Biol.* **53**, 342–355 (2004). doi:10.1080/10635150490423971 Medline

52. A. Yates, in *The Complete Dinosaur*, M. K. Brett-Surman, T. R. Holtz, J. O. Farlow, Eds. (Indiana Univ. Press, Bloomington, IN, 2012).

53. P. Upchurch, P. M. Barrett, P. Dodson, in *The Dinosauria,* D. Weishampel, P. Dodson, H. Osmolska, Eds. (Univ. of California Press, Berkeley, CA, 2004), pp. 259–324.

54. A. M. Yates, The first complete skull of the Triassic dinosaur *Melanorosaurus* Haughton (Sauropodomorpha: Anchisauria). *Spec. Pap. Paleontology: Evol. Palaeobiol. of Early Sauropodomorph Dinosaurs* **77**, 9–55 (2007).

55. M. E. Moses, C. Hou, W. H. Woodruff, G. B. West, J. C. Nekola, W. Zuo, J. H. Brown, Revisiting a model of ontogenetic growth: Estimating model parameters from theory and data. *Am. Nat.* **171**, 632–645 (2008). doi:10.1086/587073 Medline

56. W. A. Calder, *Size, Function, and Life History* (Harvard Univ. Press, Cambridge, MA, 1984).

57. D. S. Glazier, Beyond the '3/4-power law': Variation in the intra- and interspecific scaling of metabolic rate in animals. *Biol. Rev. Camb. Philos. Soc.* **80**, 611–662 (2005). doi:10.1017/S1464793105006834 Medline

58. G. B. West, J. H. Brown, B. J. Enquist, The fourth dimension of life: Fractal geometry and allometric scaling of organisms. *Science* **284**, 1677–1679 (1999). doi:10.1126/science.284.5420.1677 Medline

59. J. R. Banavar, M. E. Moses, J. H. Brown, J. Damuth, A. Rinaldo, R. M. Sibly, A. Maritan, A general basis for quarter-power scaling in animals. *Proc. Natl. Acad. Sci. U.S.A.* **107**, 15816–15820 (2010). doi:10.1073/pnas.1009974107 Medline

60. C. R. White, P. Cassey, T. M. Blackburn, Allometric exponents do not support a universal metabolic allometry. *Ecology* **88**, 315–323 (2007). doi:10.1890/05-1883 Medline

61. J. Spotila, P. Lommen, G. Bakken, D. Gates, A mathematical model for body temperatures of large reptiles: Implications for dinosaur ecology. *Am. Nat.* **107**, 391–404 (1973). doi:10.1086/282842

62. G. Seber, C. Wild, *Nonlinear Regression* (Wiley-Interscience, Hoboken, NJ, 2003), pp. 325–326.

63. W. Ricker, in *Fish Physiology*, W. Hoar, D. Randall, J. Brett, Eds. (Academic Press, New York, 1979), vol. 8, pp. 677–743.

64. R. Alexander, A. Jayes, G. Maloiy, E. Wathuta, Allometry of the limb bones of mammals from shrews (*Sorex*) to elephant (*Loxodonta*). *J. Zool.* **189**, 305–314 (1979). doi:10.1111/j.1469-7998.1979.tb03964.x

65. D. J. Varricchio, J. R. Moore, G. M. Erickson, M. A. Norell, F. D. Jackson, J. J. Borkowski, Avian paternal care had dinosaur origin. *Science* **322**, 1826–1828 (2008). doi:10.1126/science.1163245 Medline

66. V. R. Dol'nik, [Allometry of egg mass, clutch size and total clutch mass in dinosaurs: comparison with modern reptiles and birds]. *Zhurnal Obshchei Biologii* **62**, 275–285 (2001). Medline

67. D. Deeming, G. Birchard, Allometry of egg and hatchling mass in birds and reptiles: Roles of developmental maturity, eggshell structure and phylogeny. *J. Zool. (London)* **271**, 78–87 (2007). doi:10.1111/j.1469-7998.2006.00219.x

68. C. M. Duarte, M. Alcaraz, To produce many small or few large eggs: A size-independent reproductive tactic of fish. *Oecologia* **80**, 401–404 (1989). doi:10.1007/BF00379043

69. J. B. Thorbjarnarson, Reproductive characteristics of the order Crocodylia. *Herpetologica* **52**, 8–24 (1996).

70. N. P. Myhrvold, Revisiting the estimation of dinosaur growth rates. *PLOS ONE* **8**, e81917 (2013). doi:10.1371/journal.pone.0081917 Medline

71. G. Erickson, T. Tumanova, Growth curve of *Psittacosaurus mongoliensis* Osborn (Ceratopsia: Psittacosauridae) inferred from long bone histology. *Zool. J. Linn. Soc.* **130**, 551–566 (2000). doi:10.1111/j.1096-3642.2000.tb02201.x

72. J. F. Anderson, A. Hall-Martin, D. Russell, Long-bone circumference and weight in mammals, birds and dinosaurs. *J. Zool.* **207**, 53–61 (1985). doi:10.1111/j.1469-7998.1985.tb04915.x

73. D. I. Warton, I. J. Wright, D. S. Falster, M. Westoby, Bivariate line-fitting methods for allometry. *Biol. Rev. Camb. Philos. Soc.* **81**, 259–291 (2006). doi:10.1017/S1464793106007007 Medline

74. K. P. Sebens, The ecology of indeterminate growth in animals. *Annu. Rev. Ecol. Syst.* **18**, 371–407 (1987). doi:10.1146/annurev.es.18.110187.002103

75. T. Lehman, H. Woodward, Modeling growth rates for sauropod dinosaurs. *Paleobiology* **34**, 264–281 (2008). doi:10.1666/0094-8373(2008)034[0264:MGRFSD]2.0.CO;2

76. G. M. Erickson, P. J. Makovicky, P. J. Currie, M. A. Norell, S. A. Yerby, C. A. Brochu, Gigantism and comparative life-history parameters of tyrannosaurid dinosaurs. *Nature* **430**, 772–775 (2004). doi:10.1038/nature02699 Medline

77. W. Rootes, R. Chabreck, V. Wright, B. Brown, T. Hess, Growth rates of American alligators in estuarine and palustrine wetlands in Louisiana. *Estuaries Coasts* **14**, 489–494 (1991). doi:10.2307/1352272

78. M. W. Ferguson, in *Biology of the Reptilia: Development A*, C. Gans, F. Billett, P. Maderson, Eds. (Wiley, Hoboken, NJ, 1985), vol. 14, chap. 5, pp. 329–491.

79. S. Gorzula, An ecological study of *Caiman crocodilus crocodilus* inhabiting savanna lagoons in the Venezuelan Guayana. *Oecologia* **35**, 21–34 (1978). doi:10.1007/BF00345539

80. W. Magnusson, T. M. Sanaiotti, Growth of *Caiman crocodilus crocodilus* in central Amazonia, Brazil. *Copeia* **1995**, 498–501 (1995). doi:10.2307/1446922

81. R. E. Gatten Jr., Metabolic rates of fasting and recently fed spectacled caimans (*Caiman crocodilus*). *Herpetologica* **36**, 361–364 (1980).

82. C. Diefenbach, Thermal preferences and thermoregulation in *Caiman crocodilus*. *Copeia* **1975**, 530–540 (1975). doi:10.2307/1443654

83. T. Moulton, W. Magnusson, M. Melo, Growth of *Caiman latirostris* inhabiting a coastal environment in Brazil. *J. Herpetol.* **33**, 479–484 (1999). doi:10.2307/1565647

84. G. Erickson, C. Brochu, How the terror crocodile grew so big. *Nature* **398**, 205–206 (1999). doi:10.1038/18343

85. J. Hutton, Morphometrics and field estimation of the size of the Nile crocodile. *Afr. J. Ecol.* **25**, 225–230 (1987). doi:10.1111/j.1365-2028.1987.tb01113.x

86. A. D. Tucker, C. J. Limpus, K. R. McDonald, H. I. McCallum, Growth dynamics of freshwater crocodiles (*Crocodylus johnstoni*) in the Lynd River, Queensland. *Aust. J. Zool.* **54**, 409–415 (2007). doi:10.1071/ZO06099

87. J. Hutton, Growth and feeding ecology of the Nile crocodile *Crocodylus niloticus* at Ngezi, Zimbabwe. *J. Anim. Ecol.* **56**, 25–38 (1987). doi:10.2307/4797

88. L. Montes, N. Le Roy, M. Perret, V. De Buffrenil, J. Castanet, J. Cubo, Relationships between bone growth rate, body mass and resting metabolic rate in growing amniotes: A phylogenetic approach. *Biol. J. Linn. Soc. Lond.* **92**, 63–76 (2007). doi:10.1111/j.1095-8312.2007.00881.x

89. G. Webb, H. Messel, J. Crawford, M. Yerbury, Growth rates of *Crocodylus Porosus* (Reptilia: Crocodilia) from Arnhem Land, Northern Australia. *Wildl. Res.* **5**, 385–399 (1978). doi:10.1071/WR9780385

90. G. C. Grigg, Metabolic rate, Q_{10} and respiratory quotient (RQ) in *Crocodylus porosus*, and some generalizations about low RQ in reptiles. *Physiol. Zool.* **51**, 354–360 (1978).

91. T. R. Hübner, Bone histology in *Dysalotosaurus lettowvorbecki* (Ornithischia: Iguanodontia)—variation, growth, and implications. *PLOS ONE* **7**, e29958 (2012). doi:10.1371/journal.pone.0029958 Medline

92. E. M. Griebeler, N. Klein, P. M. Sander, Aging, maturation and growth of Sauropodomorph dinosaurs as deduced from growth curves using long bone histological data: An assessment of methodological constraints and solutions. *PLOS ONE* **8**, e67012 (2013). doi:10.1371/journal.pone.0067012 Medline

93. L. Rinehart, S. Lucas, J. Heckert, M. Celeskey, Growth, allometry and population dynamics. *N. M. Museum Nat. Hist. Sci. Bull.* **45**, 100–116 (2009).

94. G. M. Erickson, K. Curry Rogers, D. J. Varricchio, M. A. Norell, X. Xu, Growth patterns in brooding dinosaurs reveals the timing of sexual maturity in non-avian dinosaurs and genesis of the avian condition. *Biol. Lett.* **3**, 558–561 (2007). doi:10.1098/rsbl.2007.0254 Medline

95. T. Lehman, in *Horns and Beaks: Ceratopsian and Ornithopod Dinosaurs*, K. Carpenter, Ed. (Indiana Univ. Press, Bloomington, IN, 2006), pp. 259–317.

96. L. L. Marker, A. J. Dickman, Morphology, physical condition, and growth of the cheetah (*Acinonyx jubatus jubatus*). *J. Mammal.* **84**, 840–850 (2003). doi:10.1644/BRB-036

97. V. M. Savage, J. Gillooly, W. Woodruff, G. West, A. Allen, B. Enquist, J. Brown, The predominance of quarter-power scaling in biology. *Funct. Ecol.* **18**, 257–282 (2004). doi:10.1111/j.0269-8463.2004.00856.x

98. S. K. M. Ernest, Life history characteristics of placental nonvolant mammals. *Ecology* **84**, 3402–3402 (2003). doi:10.1890/02-9002

99. A. Trites, M. Bigg, Physical growth of northern fur seals (*Callorhinus ursinus*): Seasonal fluctuations and migratory influences. *J. Zool. (London)* **238**, 459–482 (1996). doi:10.1111/j.1469-7998.1996.tb05406.x

100. L. D. Mech, Age-related body mass and reproductive measurements of gray wolves in Minnesota. *J. Mammal.* **87**, 80–84 (2006). doi:10.1644/05-MAMM-F-212R1.1

101. J. Grobler, Growth of a male caracal kitten *Felis caracal* in the Mountain Zebra National Park. *Koedoe-African Protected Area Conservation and Science* **25**, 117–119 (1982). doi:10.4102/koedoe.v25i1.611

102. J. W. Laundre, L. Hernandez, Growth curve models and age estimation of young cougars in the northern Great Basin. *J. Wildl. Manage.* **66**, 849–858 (2002). doi:10.2307/3803149

103. D. M. Crowe, Aspects of aging, growth, and reproduciton of bobcats from Wyoming. *J. Mammal.* **56**, 177–198 (1975). doi:10.2307/1379615 Medline

104. A. Vargas, S. H. Anderson, Growth and physical development of captive-raised black-footed ferrets (*Mustela nigripes*). *Am. Midl. Nat.* **135**, 43–52 (1996). doi:10.2307/2426870

105. G. A. Heidt, M. K. Petersen, G. L. Kirkland Jr., Mating behavior and development of least weasels (*Mustela nivalis*) in captivity. *J. Mammal.* **49**, 413–419 (1968). doi:10.2307/1378199 Medline

106. J. Fox, *Biology and Diseases of the Ferret* (Wiley-Blackwell, Hoboken, NJ, 1998).

107. G. Smuts, G. Robinson, I. Whyte, Comparative growth of wild male and female lions (*Panthera leo*). *J. Zool.* **190**, 365–373 (1980). doi:10.1111/j.1469-7998.1980.tb01433.x

108. V. Mazák, *Der Tiger: Panthera tigris* (A. Ziemsen Verlag, Wittenberg Lutherstadt, Germany, 1979).

109. J. E. Swenson, M. Adamic, D. Huber, S. Stokke, Brown bear body mass and growth in northern and southern Europe. *Oecologia* **153**, 37–47 (2007). doi:10.1007/s00442-007-0715-1 Medline

110. P. Prestrud, K. Nilssen, P. Prestrud, Growth, size, and sexual dimorphism in arctic foxes. *J. Mammal.* **76**, 522–530 (1995). doi:10.2307/1382360

111. S. Brown, C. Lockyer, in *Antarctic Ecology,* R. Laws, Ed. (Academic Press, New York, 1984), pp. 717–781.

112. I. Boyd, in *Marine Mammal Biology: An Evolutionary Approach*, A. Hoelzel, Ed. (Blackwell Science, Malden, MA, 2002), pp. 247–277.

113. H. Omura, Further information on Bryde's whale from the coast of Japan. *Sci. Rep. Whales Res. Inst.* **16**, 7–18 (1962).

114. C. Lockyer, Body weights of some species of large whales. *ICES J. Mar. Sci.* **36**, 259–273 (1976). doi:10.1093/icesjms/36.3.259

115. J. L. Sumich, Growth in young gray whales (*Eschrichtius robustus*). *Mar. Mamm. Sci.* **2**, 145–152 (1986). doi:10.1111/j.1748-7692.1986.tb00035.x

116. P. Brodie, A reconsideration of aspects of growth, reproduction, and behavior of the white whale (*Delphinapterus leucas*), with reference to the Cumberland Sound, Baffin Island, population. *J. Fisheries Board Can.* **28**, 1309–1318 (1971). doi:10.1139/f71-198

117. D. Sergeant, P. Brodie, Body size in white whales, *Delphinapterus leucas*. *J. Fisheries Board Can.* **26**, 2561–2580 (1969). doi:10.1139/f69-251

118. K. Danil, S. Chivers, Growth and reproduction of female short-beaked common dolphins, *Delphinus delphis*, in the eastern tropical Pacific. *Can. J. Zool.* **85**, 108–121 (2007). doi:10.1139/z06-188

119. T. A. Jefferson, Population biology of the Indo-Pacific hump-backed dolphin in Hong Kong waters. *Wildl. Monogr.* **144**, 1–65 (2000).

120. D. Bloch, C. Lockyer, M. Zachariassen, Age and growth parameters of the long-finned pilot whale off the Faroe Islands. *Rep. Int. Whal. Comm. Spec. Issue* **14**, 163–207 (1993).

121. E. Garde, M. Heide-Jorgensen, S. Hansen, G. Nachman, M. Forchhammer, Age-specific growth and remarkable longevity in narwhals (*Monodon monoceros*) from West Greenland as estimated by aspartic acid racemization. *J. Mammal.* **88**, 49–58 (2007). doi:10.1644/06-MAMM-A-056R.1

122. I. Christensen, W. Perrin, R. Brownell, I. Demaster, Growth and reproduction of killer whales, *Orcinus orca*, in Norwegian coastal waters. *Rep. Int. Whal. Comm. Spec. Issue* **6**, 253–258 (1984).

123. S. T. Clark, D. K. Odell, C. T. Lacinak, Aspects of growth in captive killer whales (*Orcinus orca*). *Mar. Mamm. Sci.* **16**, 110–123 (2000). doi:10.1111/j.1748-7692.2000.tb00907.x

124. K. Evans, M. Hindell, The age structure and growth of female sperm whales (*Physeter macrocephalus*) in southern Australian waters. *J. Zool. (London)* **263**, 237–250 (2004). doi:10.1017/S0952836904005096

125. R. Ramos, A. Di Beneditto, N. Lima, Growth parameters of *Pontoporia blainvillei* and *Sotalia fluviatilis* (Cetacea) in northern Rio de Janeiro, Brazil. *Aquat. Mamm.* **26**, 65–75 (2000).

126. S. Botta, M. M. C. Muelbert, E. R. Secchi, Morphometric relationships of franciscana dolphin, *Pontoporia blainvillei* (Cetacea), off Rio Grande do Sul coast, southern Brazil. *Lat. Am. J. Aquat. Mamm. (LAJAM)* **5**, 117–123 (2006). doi:10.5597/lajam00102

127. I. Ferreira, thesis, Univ. of Pretoria, Pretoria, South Africa (2008).

128. A. A. Hohn, P. Hammond, Early postnatal growth of the spotted dolphin, *Stenella attenuata*, in the offshore eastern tropical Pacific. *Fish Bull.* **83**, 553–566 (1884).

129. W. Perrin, D. Holts, R. Miller, Growth and reproduction of the eastern spinner dolphin, a geographical form of *Stenella longirostris* in the eastern tropical Pacific. *Fish Bull.* **75**, 725–750 (1977).

130. A. Read, R. Wells, A. Hohn, M. Scott, Patterns of growth in wild bottlenose dolphins, *Tursiops truncatus*. *J. Zool. (London)* **231**, 107–123 (1993). doi:10.1111/j.1469-7998.1993.tb05356.x

131. A. E. Vinogradov, Nucleotypic effect in homeotherms: body-mass-corrected basal metabolic rate of mammals is related to genome size. *Evolution* **49**, 1249–1259 (1995). doi:10.2307/2410449

132. P. Jarman, Mating system and sexual dimorphism in large, terrestrial, mammalian herbivores. *Biol. Rev. Camb. Philos. Soc.* **58**, 485–520 (1983). doi:10.1111/j.1469-185X.1983.tb00398.x

133. A. W. Franzmann, R. E. LeResche, R. A. Rausch, J. L. Oldemeyer, Alaskan moose measurements and weights and measurement-weight relationships. *Can. J. Zool.* **56**, 298–306 (1978). doi:10.1139/z78-040

134. W. C. Green, A. Rothstein, Trade-offs between growth and reproduction in female bison. *Oecologia* **86**, 521–527 (1991). doi:10.1007/BF00318318

135. M. Krasińska, Z. Krasiński, Body mass and measurements of the European bison during postnatal development. *Acta Theriol. (Warsz.)* **47**, 85–106 (2002). doi:10.1007/BF03193569

136. L. Dobroruka, J. Vahala, J. Ded, Breeding and development of White-tailed gnu: *Connochaetes gnou* at Dvur Kralove Zoo. *Int. Zoo Yearb.* **29**, 197–201 (1990). doi:10.1111/j.1748-1090.1990.tb03352.x

137. W. Robinette, A. Archer, Notes on ageing criteria and reproduction of Thomson's gazelle. *Afr. J. Ecol.* **9**, 83–98 (1971). doi:10.1111/j.1365-2028.1971.tb00222.x

138. R. Laws, Dentition and ageing of the hippopotamus. *Afr. J. Ecol.* **6**, 19–52 (1968). doi:10.1111/j.1365-2028.1968.tb00899.x

139. R. B. Martin, *Transboundary Mammal Project: Background Study, Hippopotamus* (Ministry of Environment and Tourism, Namibia, Africa; faciliated by the Namibia Nature Foundation, 2005); www.nnf.org.na/RARESPECIES/rare_library/documents/Hippo.pdf.

140. J. Grobler, Body growth and age determination of the Sable *Hippotragus niger niger* (Harris, 1838). *Koedoe* **23**, 131–156 (1980). doi:10.4102/koedoe.v23i1.641

141. W. L. Robinette, C. H. Baer, R. E. Pillmore, C. E. Knittle, Effects of nutritional change on captive mule deer. *J. Wildl. Manage.* **37**, 312–326 (1973). doi:10.2307/3800121

142. K. L. Monteith, L. E. Schmitz, J. A. Jenks, J. A. Delger, R. T. Bowyer, Growth of male white-tailed deer: Consequences of maternal effects. *J. Mammal.* **90**, 651–660 (2009). doi:10.1644/08-MAMM-A-191R1.1

143. S. Czernay, Zur Haltung und Zucht von Südpudus (*Pudu pudu* Molina 1782) im Thüringer Zoopark Erfurt. *Zool. Garten N.F. Jena* **47**, 226–240 (1977).

144. N. Leader-Williams, C. Ricketts, Seasonal and sexual patterns of growth and condition of reindeer introduced into South Georgia. *Oikos* **38**, 27–39 (1982). doi:10.2307/3544564

145. F. Spitz, G. Valet, I. L. Brisbin Jr., Variation in body mass of wild boars from southern France. *J. Mammal.* **79**, 251–259 (1998). doi:10.2307/1382861

146. U. Pienaar, Observations on developmental biology, growth and some aspects of the population ecology of African buffalo (*Syncerus caffer caffer* Sparrman) in the Kruger National Park. *Koedoe* **12**, 29–52 (1969). doi:10.4102/koedoe.v12i1.745

147. G. Chaverri, T. H. Kunz, Reproductive biology and postnatal development in the tent-making bat *Artibeus watsoni* (Chiroptera: Phyllostomidae). *J. Zool. (London)* **270**, 650–656 (2006). doi:10.1111/j.1469-7998.2006.00171.x

148. W. R. Hood, J. Bloss, T. H. Kunz, Intrinsic and extrinsic sources of variation in size at birth and rates of postnatal growth in the big brown bat *Eptesicus fuscus* (Chiroptera: Vespertilionidae). *J. Zool. (London)* **258**, 355–363 (2002). doi:10.1017/S0952836902001504

149. A.-Q. Lin, L.-R. Jin, Y. Liu, K.-P. Sun, J. Feng, Postnatal growth and age estimation in Horsfield's leaf-nosed bat *Hipposideros larvatus*. *Zool. Stud.* **49**, 789–796 (2010).

150. H. Cheng, L. Lee, Postnatal growth, age estimation, and sexual maturity in the Formosan leaf-nosed bat (*Hipposideros terasensis*). *J. Mammal.* **83**, 785–793 (2002). doi:10.1644/1545-1542(2002)083<0785:PGAEAS>2.0.CO;2

151. J. W. Bradbury, Lek mating behavior in the hammer-headed bat. *Z. Tierpsychol.* **45**, 225–255 (1977). doi:10.1111/j.1439-0310.1977.tb02120.x

152. M. Sharifi, Postnatal growth in *Myotis blythii* (Chiroptera, Vespertilionidae). *Mammalia* **68**, 283–290 (2004). doi:10.1515/mamm.2004.027

153. T. L. Baptista, C. S. Richardson, T. H. Kunz, Postnatal growth and age estimation in free-ranging bats: A comparison of longitudinal and cross-sectional sampling methods. *J. Mammal.* **81**, 709–718 (2000). doi:10.1644/1545-1542(2000)081<0709:PGAAEI>2.3.CO;2

154. Y. Liu, L.-R. Jin, W. Metzner, J. Feng, Postnatal growth and age estimation in big-footed myotis, *Myotis macrodactylus*. *Acta Chiropt.* **11**, 105–111 (2009). doi:10.3161/150811009X465721

155. A. A. Stern, T. H. Kunz, Intraspecific variation in postnatal growth in the greater spear-nosed bat. *J. Mammal.* **79**, 755–763 (1998). doi:10.2307/1383086

156. K. Hoying, T. Kunz, Variation in size at birth and post-natal growth in the insectivorous bat *Pipistrellus subflavus* (Chiroptera: Vespertilionidae). *J. Zool. (London)* **245**, 15–27 (1998). doi:10.1111/j.1469-7998.1998.tb00067.x

157. J. McLean, J. Speakman, Morphological changes during postnatal growth and reproduction in the brown long-eared bat *Plecotus auritus*: Implications for wing loading and predicted flight performance. *J. Nat. Hist.* **34**, 773–791 (2000). doi:10.1080/002229300299417

158. E. N. Smith, *Husbandry Manual for SFfox* Pteropus conspicillatus *(Mammalia: Pteropodidae)* (Western Sydney Institute of TAFE, Richmond College, Richmond, Australia, 2006).

159. M. Griffith, *Husbandry Manual for Grey-HFflying Fox* Pteropus poliocephalus *(Mammlia: Pteropodidae)* (Sydney Institute of TAFE, Ultimo, Australia, 2004).

160. T. H. Kunz, A. Kurta, *Symp. Zool. Soc. London* **57**, 79–106 (1987).

161. K. Funakoshi, E. Nomura, M. Matsukubo, Y. Wakita, Postnatal growth and vocalization development of the lesser horseshoe bat, *Rhinolophus cornutus*, in the Kyushu district, Japan. *Mammal Study* **35**, 65–78 (2010). doi:10.3106/041.035.0105

162. G. Reiter, Postnatal growth and reproductive biology of *Rhinolophus hipposideros* (Chiroptera: Rhinolophidae). *J. Zool. (London)* **262**, 231–241 (2004). doi:10.1017/S0952836903004588

163. V. Elangovan, H. Raghuram, E. Y. Satya Priya, G. Marimuthu, Postnatal growth, age estimation and development of foraging behaviour in the fulvous fruit bat *Rousettus leschenaulti*. *J. Biosci. (Bangalore)* **27**, 695–702 (2002). doi:10.1007/BF02708378 Medline

164. M. Roberts, L. Newman, G. Peterson, The management and reproduction of the large hairy armadillo at the National Zoological Park. *Int. Zoo Yearb.* **22**, 185–194 (1982). doi:10.1111/j.1748-1090.1982.tb02032.x

165. H. L. Anderson, P. C. Lent, Reproduction and growth of the tundra hare (*Lepus othus*). *J. Mammal.* **58**, 53–57 (1977). doi:10.2307/1379727 Medline

166. P. L. Altman, D. D. Katz, *Growth Including Reproduction and Morphological Development* (Biological Handbooks, Federation of American Societies for Experimental Biology, Washington, DC, 1962).

167. O. J. Rongstad, A cottontail rabbit lens-growth curve from Southern Wisconsin. *J. Wildl. Manage.* **30**, 114–121 (1966). doi:10.2307/3797890

168. C. Conaway, Maintenance, reproduction and growth of the least shrew in captivity. *J. Mammal.* **39**, 507–512 (1958). doi:10.2307/1376787

169. I. Michalak, Keeping and breeding the Eurasian water shrew *Neomys fodiens* under laboratory conditions. *Int. Zoo Yearb.* **26**, 223–228 (1987). doi:10.1111/j.1748-1090.1987.tb03163.x

170. D. J. Forsyth, A field study of growth and development of nestling masked shrews (*Sorex cinereus*). *J. Mammal.* **57**, 708–721 (1976). doi:10.2307/1379441 Medline

171. R. Gusztak, K. Campbell, Growth, development and maintenance of American water shrews (*Sorex palustris*) in captivity. *Mammal Study* **29**, 65–72 (2004). doi:10.3106/mammalstudy.29.65

172. V. Nesterenko, S. D. Ohdachi, Postnatal growth and development in *Sorex unguiculatus*. *Mammal Study* **26**, 145–148 (2001). doi:10.3106/mammalstudy.26.145

173. A. Ishikawa, T. Namikawa, Postnatal growth and development in laboratory strains of large and small musk shrews (*Suncus murinus*). *J. Mammal.* **68**, 766–774 (1987). doi:10.2307/1381553

174. G. Olbricht, thesis, Univ. of Duisburg-Essen, Duisburg-Essen, Germany (2009).

175. A. Hillman-Smith, N. Owen-Smith, J. Anderson, A. Hall-Martin, J. Selaladi, Age estimation of the white rhinoceros (*Ceratotherium simum*). *J. Zool.* **210**, 355–377 (1986). doi:10.1111/j.1469-7998.1986.tb03639.x

176. D. Purchase, Using spoor to determine the age and weight of subadult black rhinoceroses (*Diceros bicornis* L.). *S. Afr. J. Wildl. Res* **37**, 96–100 (2007). doi:10.3957/0379-4369-37.1.96

177. W. R. Allen, S. Wilsher, C. Tiplady, R. M. Butterfield, The influence of maternal size on pre- and postnatal growth in the horse: III Postnatal growth. *Reproduction* **127**, 67–77 (2004). doi:10.1530/rep.1.00024 Medline

178. G. Smuts, Pre-and postnatal growth phenomena of Burchell's Zebra *Equus burchelli antiquorum*. *Koedoe* **18**, 69–102 (1975). doi:10.4102/koedoe.v18i1.915

179. S. Zschokke, B. Baur, Inbreeding, outbreeding, infant growth, and size dimorphism in captive Indian rhinoceros (*Rhinoceros unicornis*). *Can. J. Zool.* **80**, 2014–2023 (2002). doi:10.1139/z02-183

180. S. R. Leigh, Patterns of variation in the ontogeny of primate body size dimorphism. *J. Hum. Evol.* **23**, 27–50 (1992). doi:10.1016/0047-2484(92)90042-8

181. P. A. Garber, S. R. Leigh, Ontogenetic variation in small-bodied New World primates: Implications for patterns of reproduction and infant care. *Folia Primatol. (Basel)* **68**, 1–22 (1997). doi:10.1159/000157226 Medline

182. A. Hiyaoka, T. Yoshida, F. Cho, N. Goto, [Growth curves of body weight changes in laboratory-bred female African green monkeys (C*ercopithecus aethiops*)]. *Exp. Anim.* **38**, 239–244 (1989). Medline

183. A. Gijzen, J. Tijskens, Growth in weight of the lowland gorilla and of the mountain gorilla. *Int. Zoo Yearb.* **11**, 183–193 (1971). doi:10.1111/j.1748-1090.1971.tb01899.x

184. B. L. Deputte, Life history of captive gray-cheeked mangabeys: Physical and sexual development. *Int. J. Primatol.* **13**, 509–531 (1992). doi:10.1007/BF02547830

185. A. Mori, Analysis of population changes by measurement of body weight in the Koshima troop of Japanese monkeys. *Primates* **20**, 371–397 (1979). doi:10.1007/BF02373390

186. G. van Wagenen, H. R. Catchpole, Physical growth of the Rhesus monkey (*Macaca mulatta*). *Am. J. Phys. Anthropol.* **14**, 245–273 (1956). doi:10.1002/ajpa.1330140219 Medline

187. R. Chaffee, J. Allen, Effects of ambient temperature on the resting metabolic rate of cold- and heat- acclimated *Macaca mulutta*. *Comp. Biochem. Physiol.* **44A**, 1215–1225 (1973). doi:10.1016/0300-9629(73)90260-0

188. Y. Hamada, T. Udono, M. Teramoto, T. Sugawara, The growth pattern of chimpanzees: Somatic growth and reproductive maturation in *Pan troglodytes*. *Primates* **37**, 279–295 (1996). doi:10.1007/BF02381860

189. K. E. Jones, J. Bielby, M. Cardillo, S. A. Fritz, J. O'Dell, C. D. L. Orme, K. Safi, W. Sechrest, E. H. Boakes, C. Carbone, PanTHERIA: A species-level database of life history, ecology, and geography of extant and recently extinct mammals: Ecological Archives E090-184. *Ecology* **90**, 2648–2648 (2009).

190. L. M. Ausman, K. M. Rasmussen, D. L. Gallina, Spontaneous obesity in maturing squirrel monkeys fed semipurified diets. *Am. J. Physiol.* **241**, R316–R321 (1981). Medline

191. M. Roberts, Growth, development, and parental care in the western tarsier (*Tarsius bancanus*) in captivity: Evidence for a "slow" life-history and nonmonogamous mating system. *Int. J. Primatol.* **15**, 1–28 (1994). doi:10.1007/BF02735232

192. S. R. Leigh, C. J. Terranova, Comparative perspectives on bimaturism, ontogeny, and dimorphism in lemurid primates. *Int. J. Primatol.* **19**, 723–749 (1998). doi:10.1023/A:1020381026848

193. D. T. Rasmussen, M. K. Izard, Scaling of growth and life history traits relative to body size, brain size, and metabolic rate in lorises and galagos (Lorisidae, primates). *Am. J. Phys. Anthropol.* **75**, 357–367 (1988). doi:10.1002/ajpa.1330750307 Medline

194. A. R. Glatston, The husbandry, breeding and hand-rearing of the lesser mouse lemur at Rotterdam Zoo. *Int. Zoo Yearb.* **21**, 131–137 (1981). doi:10.1111/j.1748-1090.1981.tb01966.x

195. M. Perret, Energetic advantage of nest-sharing in a solitary primate, the lesser mouse lemur (*Microcebus murinus*). *J. Mammal.* **79**, 1093–1102 (1998). doi:10.2307/1383001

196. M. J. Ravosa, D. M. Meyers, K. E. Glander, Relative growth of the limbs and trunk in sifakas: Heterochronic, ecological, and functional considerations. *Am. J. Phys. Anthropol.* **92**, 499–520 (1993). doi:10.1002/ajpa.1330920408 Medline

197. R. Sukumar, *The Asian Elephant: Ecology and Management* (Cambridge Univ. Press, Cambridge, 1993).

198. J. Hanks, Growth of the African elephant (*Loxodonta africana*). *Afr. J. Ecol.* **10**, 251–272 (1972). doi:10.1111/j.1365-2028.1972.tb00870.x

199. A. Waldschmidt, E. F. Müller, A comparison of postnatal thermal physiology and energetics in an altricial (*Gerbillus perpallidus*) and a precocial (*Acomys cahirinus*) rodent species. *Comp. Biochem. Physiol. A Comp. Physiol.* **90**, 169–181 (1988). doi:10.1016/0300-9629(88)91024-9 Medline

200. V. De Conto, R. Cerqueira, Reproduction, development and growth of *Akodon lindberghi* (Hershkovitz, 1990) (Rodentia, Muridae, Sigmodontinae) raised in captivity. *Braz. J. Biol.* **67**, 707–713 (2007). doi:10.1590/S1519-69842007000400017 Medline

201. L.-K. Lin, T. Nishino, S. Shiraishi, Postnatal growth and development of the Formosan wood mouse *Apodemus semotus*. *J. Mammal. Soc. Jpn.* **18**, 1–18 (1993).

202. M. Delany, R. Monro, Growth and development of wild and captive Nile rats, *Arvicanthis niloticus* (Rodentia: Muridae). *Afr. J. Ecol.* **23**, 121–131 (1985). doi:10.1111/j.1365-2028.1985.tb00720.x

203. S. Camín, Gestation, maternal behaviour, growth and development in the subterranean caviomorph rodent *Ctenomys mendocinus* (Rodentia, Hystricognathi, Ctenomyidae). *Anim. Biol.* **60**, 79–95 (2010). doi:10.1163/157075610X12610595764255

204. J. A. Lackey, Growth and development of *Dipodomys stephensi*. *J. Mammal.* **48**, 624–632 (1967). doi:10.2307/1377586 Medline

205. M. A. Mares, Reproduction, growth, and development in Argentine gerbil mice, *Eligmodontia typus*. *J. Mammal.* **69**, 852–854 (1988). doi:10.2307/1381647

206. S. Viljoen, S. Du Toit, Postnatal development and growth of southern African tree squirrels in the genera *Funisciurus* and *Paraxerus*. *J. Mammal.* **66**, 119–127 (1985). doi:10.2307/1380963

207. R. B. Tesh, Notes on the reproduction, growth, and development of echimyid rodents in Panama. *J. Mammal.* **51**, 199–202 (1970). doi:10.2307/1378568

208. T. P. Jackson, R. J. van Aarde, Sex-and species-specific growth patterns in cryptic African rodents, *Mastomys natalensis* and *M. coucha*. *J. Mammal.* **84**, 851–860 (2003). doi:10.1644/BPR-001

209. R. Fernández-Salvador, R. García-Perea, J. Ventura, Reproduction and postnatal growth of the Cabrera vole, *Microtus cabrerae*, in captivity. *Can. J. Zool.* **79**, 2080–2085 (2001). doi:10.1139/z01-175

210. R. J. Martin, Growth curves for bushy-tailed woodrats based upon animals raised in the wild. *J. Mammal.* **54**, 517–518 (1973). doi:10.2307/1379144 Medline

211. N. Pillay, Reproduction and postnatal development in the bush Karoo rat *Otomys unisulcatus* (Muridae, Otomyinae). *J. Zool. (London)* **254**, 515–520 (2001). doi:10.1017/S0952836901001017

212. L. R. Brand, R. E. Ryckman, Laboratory life histories of *Peromyscus eremicus* and *Peromyscus interparietalis*. *J. Mammal.* **49**, 495–501 (1968). doi:10.2307/1378208 Medline

213. E. M. Derrickson, Patterns of postnatal growth in a laboratory colony of *Peromyscus leucopus*. *J. Mammal.* **69**, 57–66 (1988). doi:10.2307/1381747

214. A. Svihla, Development and growth of the prairie deermouse, *Peromyscus maniculatus bairdii*. *J. Mammal.* **16**, 109–115 (1935). doi:10.2307/1374355

215. E. T. Hooper, M. D. Carleton, Reproduction, growth and development in two contiguously allopatric rodent species, genus *Scotinomys*. *Miscell. Publ., Mus. Zool.Univ. Mich.* **151**, 35–43 (1976).

216. J. Koeppl, R. Hoffmann, Comparative postnatal growth of four ground squirrel species. *J. Mammal.* **62**, 41–57 (1981). doi:10.2307/1380476

217. P. M. Collins, W. N. Tsang, Growth and reproductive development in the male tree shrew (*Tupaia belangeri*) from birth to sexual maturity. *Biol. Reprod.* **37**, 261–267 (1987). doi:10.1095/biolreprod37.2.261 Medline

218. B. Marlow, Reproductive behaviour of the marsupial mouse, *Antechinus flavipes* (Waterhouse) (Marsupialia) and the development of the pouch young. *Aust. J. Zool.* **9**, 203–218 (1961). doi:10.1071/ZO9610203

219. E. M. Russell, Patterns of parental care and parental investment in marsupials. *Biol. Rev. Camb. Philos. Soc.* **57**, 423–486 (1982). doi:10.1111/j.1469-185X.1982.tb00704.x Medline

220. W. Westman, G. Körtner, F. Geiser, Developmental thermoenergetics of the dasyurid marsupial, *Antechinus stuartii*. *J. Mammal.* **83**, 81–90 (2002). doi:10.1644/1545-1542(2002)083<0081:DTOTDM>2.0.CO;2

221. G. A. Petrides, Sex and age determination in the opossum. *J. Mammal.* **30**, 364–378, illust (1949). doi:10.2307/1375212 Medline

222. C. Tyndale-Biscoe, Reproduction and post-natal development in the marsupial *Bettongia lesueur* (Quoy & Gaimard). *Aust. J. Zool.* **16**, 577–602 (1968). doi:10.1071/ZO9680577

223. G. Maynes, Growth of the parma wallaby, *Macropus parma* Waterhouse. *Aust. J. Zool.* **24**, 217–236 (1976). doi:10.1071/ZO9760217

224. M. J. Hamilton, A. D. Davidson, R. M. Sibly, J. H. Brown, Universal scaling of production rates across mammalian lineages. *Proc. Biol. Sci.* **278**, 560–566 (2011). doi:10.1098/rspb.2010.1056 Medline

225. M. Smith, Observations on growth of *Petaurus breviceps* and *P. norfolcensis* (Petauridae: Marsupialia) in captivity. *Aust. Wildl. Res.* **6**, 141–150 (1979). doi:10.1071/WR9790141

226. J. Tobey, C. Andrus, L. Doyle, V. Thompson, F. Bercovitch, Maternal effort and joey growth in koalas (*Phascolarctos cinereus*). *J. Zool. (London)* **268**, 423–431 (2006). doi:10.1111/j.1469-7998.2005.00041.x

227. S. A. Munks, B. Green, Milk consumption and growth in a marsupial arboreal folivore, the common ringtail possum, *Pseudocheirus peregrinus*. *Physiol. Zool.* **70**, 691–700 (1997). doi:10.1086/515871 Medline

228. R. Rose, D. McCatney, Growth of the red-bellied pademelon *Thylogale billardierii*, and age estimation of pouch young. *Aust. Wildl. Res.* **9**, 33–38 (1982). doi:10.1071/WR9820033

229. R. How, Reproduction, growth and survival of young in the mountain possum, *Trichosurus caninus* (Marsupialia). *Aust. J. Zool.* **24**, 189–199 (1976). doi:10.1071/ZO9760189

230. A. G. Lyne, A. M. Verhagen, Growth of the marsupial *Trichosurus vulpecula* and a comparison with some higher mammals. *Growth* **21**, 167–195 (1957). Medline

231. M. Mackerras, R. Smith, Breeding the short-nosed marsupial bandicoot *Isoodon macrouras* (Gould), in captivity. *Aust. J. Zool.* **8**, 371–382 (1960). doi:10.1071/ZO9600371

232. G. E. Heinsohn, Ecology and reproduction of the Tasmanian bandicoots (*Perameles gunnii* and *Isoodon obesulus*). *Univ. Calif. Publ. Zool.* **80**, 1–96 (1966).

233. E. Furlan, J. Griffiths, N. Gust, R. Armistead, P. Mitrovski, K. Handasyde, M. Serena, A. Hoffmann, A. Weeks, Is body size variation in the platypus (*Ornithorhynchus anatinus*) associated with environmental variables? *Aust. J. Zool.* **59**, 201–215 (2012). doi:10.1071/ZO11056

234. S. Jackson, L. Fisk, N. Holland, M. Serena, D. Middleton, Platypus (*Ornithorhnychus anatinus*): Captive husbandry guidelines; www.australasianzookeeping.org (2004–2011).

235. S. Nicol, N. Andersen, The life history of an egg-laying mammal, the echidna (*Tachyglossus aculeatus*). *Ecoscience* **14**, 275–285 (2007). doi:10.2980/1195-6860(2007)14[275:TLHOAE]2.0.CO;2

236. R. L. Bruggers, W. B. Jackson, Morphological and behavioral development of the mandarin duck. *Auk* **94**, 608–612 (1977).

237. K. J. Reinecke, Feeding ecology and development of juvenile black ducks in Maine. *Auk* **96**, 737–745 (1979).

238. J. P. Lightbody, C. D. Ankney, Seasonal influence on the strategies of growth and development of Canvasback and Lesser Scaup ducklings. *Auk* **101**, 121–133 (1984).

239. J. S. Sedinger, Growth and development of Canada goose goslings. *Condor* **88**, 169–180 (1986). doi:10.2307/1368912

240. A. Aubin, E. Dunn, C. MacInnes, Growth of Lesser Snow Geese on Arctic breeding grounds. *Condor* **88**, 365–370 (1986). doi:10.2307/1368884

241. B. W. Cain, Energetics of growth for Black-bellied Tree Ducks. *Condor* **78**, 124–128 (1976). doi:10.2307/1366940

242. T. Pis, Energy metabolism and thermoregulation in hand-reared chukars (*Alectoris chukar*). *Comp. Biochem. Physiol. A Mol. Integr. Physiol.* **136**, 757–770 (2003). doi:10.1016/S1095-6433(03)00245-9 Medline

243. A. E. McKechnie, B. O. Wolf, The allometry of avian basal metabolic rate: Good predictions need good data. *Physiol. Biochem. Zool.* **77**, 502–521 (2004). doi:10.1086/383511 Medline

244. J. M. Starck, E. Sutter, Patterns of growth and heterochrony in moundbuilders (Megapodiidae) and fowl (Phasianidae). *J. Avian Biol.* **31**, 527–547 (2000). doi:10.1034/j.1600-048X.2000.310413.x

245. T. Pis, D. Luśnia, Growth rate and thermoregulation in reared king quails (*Coturnix chinensis*). *Comp. Biochem. Physiol. A Mol. Integr. Physiol.* **140**, 101–109 (2005). doi:10.1016/j.cbpb.2004.11.008 Medline

246. L. Wing, J. Beer, W. Tidyman, Brood habits and growth of 'Blue Grouse'. *Auk* **61**, 426–440 (1944). doi:10.2307/4079516

247. S. Jackson, J. Diamond, Ontogenetic development of gut function, growth, and metabolism in a wild bird, the Red Jungle Fowl. *Am. J. Physiol.* **269**, R1163–R1173 (1995). Medline

248. O. Heinroth, M. Heinroth, *Die Vögel Mitteleuropas in Allen Lebens- und Entwicklungsstufen Photographisch Aufgenommen und in Ihrem Seelenleben bei der Aufzucht vom ei ab Beobachtet* (H. Bermuhler, Berlin, Germany, 1967), vol. 6.

249. W. Healy, E. Nenno, in *4th National Wild Turkey Symposium* (National Wild Turkey Federation, Little Rock, AK, 1980), pp. 168–185.

250. S. N. Nahashon, S. E. Aggrey, N. A. Adefope, A. Amenyenu, D. Wright, Growth characteristics of pearl gray guinea fowl as predicted by the Richards, Gompertz, and logistic models. *Poult. Sci.* **85**, 359–363 (2006). doi:10.1093/ps/85.2.359 Medline

251. V. D. Hayssen, A. Van Tienhoven, A. Van Tienhoven, *Asdell's Patterns of Mammalian Reproduction: A Compendium of Species-Specific Data* (Cornell Univ. Press, Ithaca, NY, 1993).

252. H. Lindén, Growth rates and early energy requirements of captive juvenile capercaillie, *Tetrao urogallus*. *Finnish Game Res.* **39**, 53–67 (1981).

253. L. A. Bell, J. C. Pitman, M. A. Patten, D. H. Wolfe, S. K. Sherrod, S. D. Fuhlendorf, Juvenile Lesser Prairie-chicken growth and development in southeastern New Mexico. *Wilson J. Ornithol.* **119**, 386–391 (2007). doi:10.1676/05-125.1

254. J. McLennan, L. Dew, J. Miles, N. Gillingham, R. Waiwai, Size matters: Predation risk and juvenile growth in North Island Brown Kiwi (*Apteryx mantelli*). *N. Z. J. Ecol.* **28**, 241–250 (2004).

255. B. Reid, Food intake and growth rate of Cassowary chicks *Casuarius* spp reared at Mendi, Southern Highland Papua New Guinea. *Int. Zoo Yearb.* **26**, 189–198 (1987). doi:10.1111/j.1748-1090.1987.tb03157.x

256. J. B. Dunning, *CRC Handbook of Avian Body Masses* (CRC Press, Boca Raton, FL, 1993).

257. K. Williams, D. Blache, I. Malecki, P. Sharp, T. Trigg, R. Rigby, G. Martin, in *Ratites in a Competitive World - Proceedings of the 2nd International Ratite Congress*, F. Huchzermeyer *et al*., Eds. (Oudtshoorn, South Africa, 1998), pp. 75–80.

258. J. Navarro, P. Vignolo, M. R. Demaría, N. Maceira, M. Martella, Growth curves of farmed Greater Rheas (*Rhea americana albescens*) from central Argentina. *Arch. Geflugelkd.* **69**, 90–93 (2005).

259. M. W. Bundle, H. Hoppeler, R. Vock, J. M. Tester, P. G. Weyand, High metabolic rates in running birds. *Nature* **397**, 31–32 (1999). doi:10.1038/16173

260. P. Tholon, S. Queiroz, Models for the analysis of growth curves for rearing tinamous (*Rhynchotus rufescens*) in captivity. *Braz. J. Poutry Sci.* **9**, 23–31 (2007).

261. Y. Elhashmi, O. Arabi, T. Taha, O. Eidam, Growth and development of muscles, bones and fat of red-necked ostrich (*Struthio camelus camelus*). *Online J. Anim. Feed Res.* **1**, 417–422 (2011) (OJAFR).

262. E. Sumner Jr., Notes on the growth and behavior of young Golden Eagles. *Auk* **46**, 161–169 (1929). doi:10.2307/4075690

263. G. R. Bortolotti, Physical development of nestling bald eagles with emphasis on the timing of growth events. *Wilson Bull.* **96**, 524–542 (1984).

264. H. F. Greeney, E. R. Hough, C. E. Hamilton, S. M. Wethington, Nestling growth and plumage development of the Black-chinned Hummingbird (*Archilochus alexandri*) in southeastern Arizona. *Huitzil Rev. Ornitología Mexicana* **9**, 35–42 (2008).

265. G. D. Constantz, Growth of nestling Rufous Hummingbirds. *Auk* **97**, 622–624 (1980).

266. K. Fierro-Calderón, T. E. Martin, Reproductive biology of the Violet-chested Hummingbird in Venezuela and comparisons with other tropical and temperate hummingbirds. *Condor* **109**, 680–685 (2007). doi:10.1650/8305.1

267. K. A. Muller, Physical and behavioral development of a roadrunner raised at the National Zoological Park. *Wilson Bull.* **83**, 186–193 (1971).

268. M. A. Springer, D. R. Osborne, Analysis of growth of the red-tailed hawk. *Ohio J. Sci.* **83**, 13–19 (1983).

269. J. W. Parker, Growth of the Swainson's Hawk. *Condor* **78**, 557–558 (1976). doi:10.2307/1367108

270. J. Coleman, J. Fraser, Age estimation and growth of black and turkey vultures. *J. Field Ornithol.* **60**, 197–208 (1989).

271. F. Fowler, Studies of food and growth of the Prairie Falcon. *Condor* **33**, 193–201 (1931). doi:10.2307/1363715

272. S. Kleindorfer, H. Hoi, R. Ille, Nestling growth patterns and antipredator responses: A comparison between four *Acrocephalus* warblers. *Biologia* **52**, 677–685 (1997).

273. G. T. Austin, R. E. Ricklefs, Growth and development of the Rufous-winged Sparrow (*Aimophila carpalis*). *Condor* **79**, 37–50 (1977). doi:10.2307/1367528

274. R. E. Ricklefs, Patterns of growth in birds. III. Growth and development of the Cactus Wren. *Condor* **77**, 34–45 (1975). doi:10.2307/1366757

275. K. D. Whitmore, J. M. Marzluff, Hand-rearing corvids for reintroduction: Importance of feeding regime, nestling growth, and dominance. *J. Wildl. Manage.* **62**, 1460–1479 (1998). doi:10.2307/3802013

276. A. M. Makarieva, V. G. Gorshkov, B.-L. Li, S. L. Chown, P. B. Reich, V. M. Gavrilov, Mean mass-specific metabolic rates are strikingly similar across life's major domains: Evidence for life's metabolic optimum. *Proc. Natl. Acad. Sci. U.S.A.* **105**, 16994–16999 (2008). doi:10.1073/pnas.0802148105 Medline

277. J. Haydock, J. D. Ligon, Brood reduction in the Chihuahuan Raven: An experimental study. *Ecology* **67**, 1194–1205 (1986). doi:10.2307/1938675

278. C. Kunz, J. Ekman, Genetic and environmental components of growth in nestling blue tits (*Parus caeruleus*). *J. Evol. Biol.* **13**, 199–212 (2000). doi:10.1046/j.1420-9101.2000.00158.x

279. R. J. O'Connor, Initial size and subsequent growth in passerine nestlings. *Bird-banding* **46**, 329–340 (1975). doi:10.2307/4512164

280. R. Weaver, Measurement of growth in the Eastern Chipping Sparrow. *Auk* **54**, 103–104 (1937). doi:10.2307/4078340

281. R. Ricklefs, Patterns of growth in birds. *Ibis* **110**, 419–451 (1968). doi:10.1111/j.1474-919X.1968.tb00058.x

282. M. S. Dutenhoffer, D. L. Swanson, Relationship of basal to summit metabolic rate in passerine birds and the aerobic capacity model for the evolution of endothermy. *Physiol. Zool.* **69**, 1232–1254 (1996).

283. B. Kessel, A study of the breeding biology of the European starling (*Sturnus vulgaris* L.) in North America. *Am. Midl. Nat.* **58**, 257–331 (1957). doi:10.2307/2422615

284. G. H. F. Seixas, G. Mourão, Growth of nestlings of the Blue-fronted Amazon (*Amazona aestiva*) raised in the wild or in captivity. *Ornitol. Neotrop.* **14**, 295–305 (2003).

285. S. E. Koenig, The breeding biology of Black-billed Parrot *Amazona agilis* and Yellow-billed Parrot *Amazona collaria* in cockpit country, Jamaica. *Bird Conserv. Int.* **11**, 205–225 (2001). doi:10.1017/S0959270901000284

286. G. Vigo, M. Williams, D. J. Brightsmith, Growth of Scarlet Macaw (*Ara macao*) chicks in southeastern Peru. *Ornitol. Neotrop.* **22**, 143–153 (2011).

287. J. F. Masello, P. Quillfeldt, Chick growth and breeding success of the Burrowing Parrot. *Condor* **104**, 574–586 (2002). doi:10.1650/0010-5422(2002)104[0574:CGABSO]2.0.CO;2

288. J. L. Navarro, E. H. Bucher, Growth of Monk parakeets. *Wilson Bull.* **102**, 520–525 (1990).

289. J. T. Pearson, Development of thermoregulation and posthatching growth in the altricial cockatiel *Nymphicus hollandicus*. *Physiol. Zool.* **71**, 237–244 (1998). Medline

290. S. Taylor, M. R. Perrin, Application of Richards's growth model to Brown-headed Parrot *Poicephalus cryptoxanthus* nestlings. *Ostrich J. Afr. Ornithol.* **79**, 79–82 (2008). doi:10.2989/OSTRICH.2008.79.1.10.377

291. J. K. Carlson, E. Cortés, A. G. Johnson, E. Cortes, Age and growth of the blacknose shark, *Carcharhinus acronotus*, in the eastern Gulf of Mexico. *Copeia* **1999**, 684–691 (1999). doi:10.2307/1447600

292. J. K. Carlson, K. J. Goldman, C. G. Lowe, in *Biology of Sharks and their Relatives*, J. Carrier, J. Musick, M. Heithaus, Eds. (CRC Press, Boca Raton, FL, 2004), pp. 203–224.

293. R. Froese, D. Pauly, Eds., Fishbase: World Wide Web electronic publication, www.fishbase.org (2011); accessed April 2014.

294. S.-J. Joung, Y.-Y. Liao, K.-M. Liu, C.-T. Chen, L.-C. Leu, Age, growth, and reproduction of the spinner shark, *Carcharhinus brevipinna*, in the northeastern waters of Taiwan. *Zool. Stud.* **44**, 102–110 (2005).

295. S. Oshitani, H. Nakano, S. Tanaka, Age and growth of the silky shark *Carcharhinus falciformis* from the Pacific Ocean. *Fish. Sci.* **69**, 456–464 (2003). doi:10.1046/j.1444-2906.2003.00645.x

296. A. Cruz-Martinez, X. Chiappa-Carrara, V. Arenas-Fuentes, Age and growth of the bull shark, *Carcharhinus leucas,* from southern Gulf of Mexico. *J. Northwest Atl. Fish. Sci.* **35**, 367–374 (2005).

297. K. A. Killam, G. R. Parsons, Age and growth of the blacktip shark, *Carcharhinus limbatus*, near Tampa Bay, Florida. *Fish Bull.* **87**, 845–857 (1989).

298. S.-J. Joung, Y.-Y. Liao, C.-T. Chen, Age and growth of sandbar shark *Carcharhinus plumbeus* in northeastern Taiwan waters. *Fish. Res.* **70**, 83–96 (2004). doi:10.1016/j.fishres.2004.06.018

299. W. W. Dowd, R. W. Brill, P. G. Bushnell, J. A. Musick, Standard and routine metabolic rates of juvenile sandbar sharks (*Carcharhinus plumbeus*), including the effects of body mass and acute temperature change. *Fish Bull.* **104**, 323–331 (2006).

300. F. Santana, R. Lessa, Age determination and growth of the night shark (*Carcharhinus signatus*) off the northeastern Brazilian coast. *Fish Bull.* **102**, 156–167 (2004).

301. S. Davenport, J. Stevens, Age and growth of two commercially imported sharks (*Carcharhinus tilstoni* and *C. sorrah*) from Northern Australia. *Mar. Freshw. Res.* **39**, 417–433 (1988). doi:10.1071/MF9880417

302. S. Branstetter, J. Musick, J. Colvocoresses, A comparison of the age and growth of the tiger shark, *Galeocerdo cuvieri*, from off Virginia and from the northwestern Gulf of Mexico. *Fish Bull.* **85**, 269–279 (1987).

303. C. A. Brown, S. H. Gruber, Age assessment of the lemon shark, *Negaprion brevirostris*, using tetracycline validated vertebral centra. *Copeia* **1988**, 747–753 (1988). doi:10.2307/1445397

304. P. G. Bushnell, P. L. Lutz, S. H. Gruber, The metabolic rate of an active, tropical elasmobranch, the lemon shark (*Negaprion brevirostris*). *Exp. Biol.* **48**, 279–283 (1989). Medline

305. R. Freitas, R. Rosa, S. Gruber, B. Wetherbee, Early growth and juvenile population structure of lemon sharks *Negaprion brevirostris* in the Atol das Rocas Biological Reserve, off northeast Brazil. *J. Fish Biol.* **68**, 1319–1332 (2006). doi:10.1111/j.0022-1112.2006.00999.x

306. R. Lessa, F. Santana, F. Hazin, Age and growth of the blue shark *Prionace glauca* (Linnaeus, 1758) off northeastern Brazil. *Fish. Res.* **66**, 19–30 (2004). doi:10.1016/S0165-7836(03)00193-0

307. F. S. Motta, O. B. Gadig, R. C. Namora, F. Braga, Size and sex compositions, length-weight relationship, and occurrence of the Brazilian sharpnose shark, *Rhizoprionodon lalandii*, caught by artisanal fishery from southeastern Brazil. *Fish. Res.* **74**, 116–126 (2005). doi:10.1016/j.fishres.2005.03.010

308. C. A. Simpfendorfer, Age and growth of the Australian sharpnose shark, *Rhizoprionodon taylori*, from north Queensland, Australia. *Environ. Biol. Fishes* **36**, 233–241 (1993). doi:10.1007/BF00001718

309. K. Nair, Age and growth of the yellow dog shark *Scoliodon laticaudus* Muller and Henle from Bombay waters. *J. Mar. Biol. Assoc. India* **18**, 531–539 (1976).

310. A. N. Piercy, J. K. Carlson, J. A. Sulikowski, G. H. Burgess, Age and growth of the scalloped hammerhead shark, *Sphyrna lewini*, in the north-west Atlantic Ocean and Gulf of Mexico. *Mar. Freshw. Res.* **58**, 34–40 (2007). doi:10.1071/MF05195

311. G. Parsons, Age determination and growth of the bonnethead shark *Sphyrna tiburo*: A comparison of two populations. *Mar. Biol.* **117**, 23–31 (1993). doi:10.1007/BF00346422

312. K. Shimada, Ontogenetic parameters and life history strategies of the Late Cretaceous lamniform shark, *Cretoxyrhina mantelli*, based on vertebral growth increments. *J. Vertebr. Paleontol.* **28**, 21–33 (2008). doi:10.1671/0272-4634(2008)28[21:OPALHS]2.0.CO;2

313. H. F. Mollet, G. M. Cailliet, in *Great White Sharks: The Biology of Charharadon carcharias*, A. P. Klimley, D. G. Ainley, Eds. (Academic Press, New York, 1996), pp. 81–89.

314. M. Ribot-Carballal, F. Galván-Magaña, C. Quiñónez-Velázquez, Age and growth of the shortfin mako shark *Isurus oxyrinchus* from the western coast of Baja California Sur, Mexico. *Fish. Res.* **76**, 14–21 (2005). doi:10.1016/j.fishres.2005.05.004

315. C. Sepulveda, J. Graham, D. Bernal, Aerobic metabolic rates of swimming juvenile mako sharks, *Isurus oxyrinchus*. *Mar. Biol.* **152**, 1087–1094 (2007). doi:10.1007/s00227-007-0757-2

316. W.-K. Chen, P.-C. Chen, K.-M. Liu, S.-B. Wang, Age and growth estimates of the whitespotted bamboo shark, *Chiloscyllium plagiosum*, in the northern waters of Taiwan. *Zool. Stud.* **46**, 92 (2007).

317. S. P. Wintner, Preliminary study of vertebral growth rings in the whale shark, *Rhincodon typus*, from the east coast of South Africa. *Environ. Biol. Fishes* **59**, 441–451 (2000). doi:10.1023/A:1026564707027

318. E. El Mouden, M. Znari, R. Brown, Skeletochronology and mark-recapture assessments of growth in the North African agamid lizard (*Agama impalearis*). *J. Zool. (London)* **249**, 455–461 (2001).

319. R. van Devender, Growth ecology of a tropical lizard, *Basiliscus basiliscus*. *Ecology* **59**, 1031–1038 (1978). doi:10.2307/1938555

320. L. Blueweiss, H. Fox, V. Kudzma, D. Nakashima, R. Peters, S. Sams, Relationships between body size and some life history parameters. *Oecologia* **37**, 257–272 (1978). doi:10.1007/BF00344996

321. J. Arcos-García, M. Peralta, V. Rosales, G. Martínez, M. Cerrilla, F. Sánchez, Growth characterization of black iguana (*Ctenosaura pectinata*) in captivity. *Veterinaria (Mexico)* **33**, 409–420 (2002).

322. C. Duarte Rocha, Growth of the tropical sand lizard *Liolaemus lutzae* in Southeastern Brazil. *Amphib.-Reptil.* **16**, 257–264 (1995). doi:10.1163/156853895X00055

323. R. Blob, Interspecific scaling of the hindlimb skeleton in lizards, crocodilians, felids and canids: Does limb bone shape correlate with limb posture? *J. Zool. (London)* **250**, 507–531 (2000). doi:10.1111/j.1469-7998.2000.tb00793.x

324. A. Ortega-Rubio, G. Halffter, R. Barbault, A. Castellanos, F. Salinas, Growth of S*celoporus grammicus* in La Michilia Biosphere Reserve, Mexico. *J. Herpetol.* **33**, 123–126 (1999). doi:10.2307/1565551

325. A. Ortega-León, E. Smith, J. Zúñiga-Vega, F. Méndez–de la Cruz, Growth and demography of one population of the lizard *Sceloporus mucronatus mucronatus*. *West. N. Am. Nat.* **67**, 492–502 (2007). doi:10.3398/1527-0904(2007)67[492:GADOOP]2.0.CO;2

326. A. Ortega-Rubio, R. Barbault, G. Halffter, A. Castellanos, F. Salinas, Growth effort of *Sceloporus scalaris* (Sauria: Phrynosomatidae) at La Michilía Biosphere Reserve, Mexico. *Rev. Biol. Trop.* **46**, 145–155 (1998).

327. G. G. Watkins, Proximate causes of sexual size dimorphism in the iguanian lizard *Microlophus occipitalis*. *Ecology* **77**, 1473–1482 (1996). doi:10.2307/2265544

328. M. Van Sluys, Growth and body condition of the saxicolous lizard *Tropidurus itambere* in southeastern Brazil. *J. Herpetol.* **32**, 359–365 (1998). doi:10.2307/1565450

329. A. Pinto, H. C. Wiederhecker, G. R. Colli, Sexual dimorphism in the Neotropical lizard, *Tropidurus torquatus* (Squamata, Tropiduridae). *Amphib.Rreptil.* **26**, 127–137 (2005). doi:10.1163/1568538054253384

330. T. R. Gasnier, W. E. Magnusson, A. V. Waichman, Growth curve shape and growth variation of the tropical lizard *Uranoscodon superciliosus* (Sauria: Tropiduridae). *Ecotropica* **3**, 101–107 (1997).

331. J. Zúñiga-Vega, R. Rojas-González, J. Lemos-Espinal, M. Pérez-Trejo, Growth ecology of the lizard *Xenosaurus grandis* in Veracruz, Mexico. *J. Herpetol.* **39**, 433–443 (2005). doi:10.1670/202-04A.1

332. L. Kratochvíl, D. Frynta, Production-growth model applied in eublepharid lizards (Eublepharidae, Squamata): Accordance between growth and metabolic rates. *Folia Zool. (Brno)* **52**, 317–322 (2003).

333. B. E. Dial, L. L. Grismer, A phylogenetic analysis of physiological-ecological character evolution in the lizard genus *Coleonyx* and its implications for historical biogeographic reconstruction. *Syst. Biol.* **41**, 178–195 (1992). doi:10.1093/sysbio/41.2.178

334. T. Madsen, R. Shine, Conflicting conclusions from long-term versus short-term studies on growth and reproduction of a tropical snake. *Herpetologica* **57**, 147–156 (2001).

335. G. A. Kaufman, J. W. Gibbons, Weight-length relationships in thirteen species of snakes in the southeastern United States. *Herpetologica* **6**, 31–37 (1975).

336. J. K. Webb, K. A. Christian, P. Fisher, Fast growth and early maturation in a viviparous sit-and-wait predator, the northern death adder (*Acanthophis praelongus*), from tropical Australia. *J. Herpetol.* **36**, 505–509 (2002). doi:10.1670/0022-1511(2002)036[0505:FGAEMI]2.0.CO;2

337. T. Madsen, R. Shine, Silver spoons and snake body sizes: Prey availability early in life influences long-term growth rates of free-ranging pythons. *J. Anim. Ecol.* **69**, 952–958 (2000). doi:10.1046/j.1365-2656.2000.00477.x

338. D. Wilson, R. Heinsohn, J. Wood, Life-history traits and ontogenetic colour change in an arboreal tropical python, *Morelia viridis*. *J. Zool. (London)* **270**, 399–407 (2006). doi:10.1111/j.1469-7998.2006.00190.x

339. J. J. Smith, M. Amarello, M. Goode, Seasonal growth of free-ranging Gila Monsters (*Heloderma suspectum*) in a southern Arizona population. *J. Herpetol.* **44**, 484–488 (2010). doi:10.1670/09-104.1

340. D. D. Beck, *Biology of Gila Monsters and Beaded Lizards* (Univ of California Press, Berkely, CA, 2009), vol. 9.

341. D. D. Beck, C. H. Lowe, Ecology of the beaded lizard, *Heloderma horridum*, in a tropical dry forest in Jalisco, Mexico. *J. Herpetol.* **25**, 395–406 (1991). doi:10.2307/1564760

342. K. M. Hare, C. G. Longson, S. Pledger, C. H. Daugherty, Size, growth, and survival are reduced at cool incubation temperatures in the temperate lizard *Oligosoma suteri* (Lacertilia: Scincidae). *Copeia* **2004**, 383–390 (2004).

343. D. Frynta, P. Frýdlová, J. Hnízdo, O. Simková, V. Cikánová, P. Velenský, Ontogeny of sexual size dimorphism in monitor lizards: Males grow for a longer period, but not at a faster rate. *Zoolog. Sci.* **27**, 917–923 (2010). doi:10.2108/zsj.27.917 Medline

344. R. J. Laver, D. Purwandana, A. Ariefiandy, J. Imansyah, D. Forsyth, C. Ciofi, T. S. Jessop, Life-history and spatial determinants of somatic growth dynamics in Komodo dragon populations. *PLOS ONE* **7**, e45398 (2012). doi:10.1371/journal.pone.0045398 Medline

345. J. M. Lemm, M. S. Edwards, T. D. Grant, A. C. Alberts, Comparison of growth and nutritional status of juvenile Komodo monitors (*Varanus komodoensis*) maintained on rodent or poultry-based diets. *Zoo Biol.* **23**, 239–252 (2004). doi:10.1002/zoo.20000

346. T. S. Jessop, T. Madsen, J. Sumner, H. Rudiharto, J. A. Phillips, C. Ciofi, Maximum body size among insular Komodo dragon populations covaries with large prey density. *Oikos* **112**, 422–429 (2006). doi:10.1111/j.0030-1299.2006.14371.x

347. E. R. Pianka, D. R. King, R. A. King, *Varanoid Lizards of the World* (Indiana Univ. Press, Bloomington, IN, 2004).

348. V. de Buffrénil, G. Hémery, Variation in longevity, growth, and morphology in exploited Nile Monitors (*Varanus niloticus*) from Sahelian Africa. *J. Herpetol.* **36**, 419–426 (2002). doi:10.1670/0022-1511(2002)036[0419:VILGAM]2.0.CO;2

349. R. Jackson, The poorly known rusty monitor *Varanus semiremex*: History, natural history, captive breeding and husbandry. *Herpetafauna* **35**, 15–24 (2005).

350. S. J. Blaber, D. A. Milton, J. Pang, P. Wong, O. Boon-Teck, L. Nyigo, D. Lubim, The life history of the tropical shad *Tenualosa toli* from Sarawak: First evidence of protandry in the Clupeiformes? *Environ. Biol. Fishes* **46**, 225–242 (1996). doi:10.1007/BF00004998

351. R. Eaton, R. Farley, Growth and the reduction of depensation of zebrafish, *Brachydanio rerio*, reared in the laboratory. *Copeia* **1974**, 204–209 (1974). doi:10.2307/1443024

352. O. L. Weyl, A. J. Booth, On the life history of a cyprinid fish, *Labeo cylindricus*. *Environ. Biol. Fishes* **55**, 215–225 (1999). doi:10.1023/A:1007543319416

353. J. Travis, J. A. Farr, M. McManus, J. C. Trexler, Environmental effects on adult growth patterns in the male sailfin molly, *Poecilia latipinna* (Poeciliidae). *Environ. Biol. Fishes* **26**, 119–127 (1989). doi:10.1007/BF00001028

354. C. García, W. Troncoso, S. Sánchez, L. Perdomo, Contribution to vital statistics of a guppy *Poecilia reticulata* Peters (Pisces: Cyprinodontiformes: Poecillidae) pond population in Santa Marta, Colombia. *Pan-American Journal of Aquatic Sciences* **3**, 335–339 (2008).

355. L.-H. Teo, T.-W. Chen, A study of metabolic rates of *Poecilia reticulata* Peters under different conditions. *Aquacult. Res.* **24**, 109–117 (1993). doi:10.1111/j.1365-2109.1993.tb00833.x

356. F. E. Felin, Growth characteristics of the poeciliid fish *Platypoecilus maculatus*. *Copeia* **1951**, 15–28 (1951). doi:10.2307/1438045

357. F. Guo, L. Teo, T. Chen, Effects of anaesthetics on the oxygen consumption rates of platyfish *Xiphophorus maculatus* (Günther). *Aquacult. Res.* **26**, 887–894 (1995). doi:10.1111/j.1365-2109.1995.tb00883.x

358. J. Choat, L. Axe, Growth and longevity in acanthurid fishes; an analysis of otolith increments. *Mar. Ecol. Prog. Ser.* **134**, 15–26 (1996). doi:10.3354/meps134015

359. S. K. Wilson, Growth, mortality and turnover rates of a small detritivorous fish. *Mar. Ecol. Prog. Ser.* **284**, 253–259 (2004). doi:10.3354/meps284253

360. Z. Zekeria, S. Weertman, B. Samuel, T. Kale-Ab, J. Videler, Growth of *Chaetodon larvatus* (Chaetodontidae: Pisces) in the southern Red Sea. *Mar. Biol.* **148**, 1113–1122 (2006). doi:10.1007/s00227-005-0146-7

361. D. Jepsen, K. Winemiller, D. Taphorn, D. R. Olarte, Age structure and growth of peacock cichlids from rivers and reservoirs of Venezuela. *J. Fish Biol.* **55**, 433–450 (1999). doi:10.1111/j.1095-8649.1999.tb00689.x

362. A. J. Booth, G. S. Merron, C. D. Buxton, The growth of *Oreochromis andersonii* (Pisces: Cichlidae) from the Okavango Delta, Botswana, and a comparison of the scale and otolith methods of ageing. *Environ. Biol. Fishes* **43**, 171–178 (1995). doi:10.1007/BF00002488

363. K. Hustler, B. Marshall, Population dynamics of two small cichlid fish species in a tropical man-made lake (Lake Kariba). *Hydrobiologia* **190**, 253–262 (1990). doi:10.1007/BF00008193

364. V. Hernaman, P. Munday, Life-history characteristics of coral reef gobies. I. Growth and life-span. *Mar. Ecol. Prog. Ser.* **290**, 207–221 (2005). doi:10.3354/meps290207

365. J. Choat, C. Davies, J. Ackerman, B. Mapstone, Age structure and growth in a large teleost, *Cheilinus undulatus*, with a review of size distribution in labrid fishes. *Mar. Ecol. Prog. Ser.* **318**, 237–246 (2006). doi:10.3354/meps318237

366. S. J. Newman, M. Cappo, D. M. Williams, Age, growth, mortality rates and corresponding yield estimates using otoliths of the tropical red snappers, *Lutjanus erythropterus, L. malabaricus* and *L. sebae*, from the central Great Barrier Reef. *Fish. Res.* **48**, 1–14 (2000). doi:10.1016/S0165-7836(00)00115-6

367. R. Edwards, Growth rates of Lutjanidae (snappers) in tropical Australian waters. *J. Fish Biol.* **26**, 1–4 (1985). doi:10.1111/j.1095-8649.1985.tb04233.x

368. T. B. Linkowski, C. Żukowski, Observations on the growth of *Notothenia coriiceps neglecta* Nybelin and *Notothenia rossii marmorata* Fischer in Admiralty Bay (King George Island, South Shetland Islands). *Polish Polar Res.* **1**, 155–162 (1980).

369. I. Johnston, A. Clarke, P. Ward, Temperature and metabolic rate in sedentary fish from the Antarctic, North Sea and Indo-West Pacific Ocean. *Mar. Biol.* **109**, 191–195 (1991). doi:10.1007/BF01319386

370. D. E. Wohlschlag, Growth of an Antarctic fish at freezing temperatures. *Copeia* **1961**, 11–18 (1961). doi:10.2307/1440165

371. D. Morris, A. North, Oxygen consumption of five species of fish from South Georgia. *J. Exp. Mar. Biol. Ecol.* **78**, 75–86 (1984). doi:10.1016/0022-0981(84)90070-4

372. R. M. Wells, Respiration of antarctic fish from McMurdo Sound. *Comp. Biochem. Physiol. A Comp. Physiol.* **88**, 417–424 (1987). doi:10.1016/0300-9629(87)90056-9 Medline

373. M. L. Mesa, M. Vacchi, Age and growth of high Antarctic notothenioid fish. *Antarct. Sci.* **13**, 227–235 (2001). doi:10.1017/S0954102001000335

374. S. Schwamborn, B. Ferreira, Age structure and growth of the dusky damselfish, *Stegastes fuscus*, from Tamandare reefs, Pernambuco, Brazil. *Environ. Biol. Fishes* **63**, 79–88 (2002). doi:10.1023/A:1013851532298

375. J. Choat, L. Axe, D. Lou, Growth and longevity in fishes of the family Scaridae. *Mar. Ecol. Prog. Ser.* **145**, 33–41 (1996). doi:10.3354/meps145033

376. S. Taghavi Motlagh, S. Hashemi, P. Kochanian, Population biology and assessment of Kawakawa (*Euthynnus affinis*) in Coastal Waters of the Persian Gulf and Sea of Oman (Hormozgan Province) *Iran*. *J. Fish. Sci.* **9**, 315–326 (2010).

377. R. Brill, On the standard metabolic rates of tropical tunas, including the effect of body size and acute temperature change. *Fish Bull.* **85**, 25–35 (1987).

378. P. Rohit, A. Chellappan, E. Abdussamad, K. Joshi, K. Koya, M. Sivadas, S. Ghosh, A. Margaret Muthu Rathinam, S. Kemparaju, H. Dhokia, Fishery and bionomics of the little tuna, *Euthynnus affinis* (Cantor, 1849) exploited from Indian waters. *Indian J. Fish.* **59**, 37–46 (2012).

379. M. Mohan, K. Kunhikoya, Age and growth of *Katsuwonus pelamis* (Linnaeus) and *Thunnus albacares* (Bonnaterre) from Minicoy waters. *Central Marine Fisheries Res. Bull.* **36**, 143–148 (1985).

380. J. H. Farley, N. P. Clear, B. Leroy, T. L. Davis, G. McPherson, Age, growth and preliminary estimates of maturity of bigeye tuna, *Thunnus obesus*, in the Australian region. *Mar. Freshw. Res.* **57**, 713–724 (2006). doi:10.1071/MF05255

381. P. G. Bushnell, R. W. Brill, R. E. Bourke, Cardiorespiratory responses of skipjack tuna (*Katsuwonus pelamis*), yellowfin tuna (*Thunnus albacares*), and bigeye tuna (*Thunnus obesus*) to acute reductions of ambient oxygen. *Can. J. Zool.* **68**, 1857–1865 (1990). doi:10.1139/z90-265

382. E. Abdussamad, Fishery, biology and population characteristics of longtail tuna, *Thunnus tonggol* (Bleeker, 1851) caught along the Indian coast. *Indian J. Fish.* **59**, 7–16 (2012).

383. R. J. Pears, J. H. Choat, B. D. Mapstone, G. A. Begg, Demography of a large grouper, *Epinephelus fuscoguttatus*, from Australia's Great Barrier Reef: Implications for fishery management. *Mar. Ecol. Prog. Ser.* **307**, 259–272 (2006). doi:10.3354/meps307259

384. E. Grandcourt, Demographic characteristics of selected epinepheline groupers (family Serranidae, subfamily Epinephelinae) from Aldabra Atoll, Seychelles. *Atoll Res. Bull.* **593**, 200–216 (2005).

385. J. G. Díaz-Uribe, J. F. Elorduy-Garay, M. González-Valdovinos, Age and growth of the leopard grouper, *Mycteroperca rosacea*, in the southern Gulf of California, México. *Pac. Sci.* **55**, 171–182 (2001). doi:10.1353/psc.2001.0012

386. B. Ferreira, G. Russ, Age validation and estimation of growth rate of the coral trout, *Plectropomus leopardus* (Lacepede 1802) from Lizard Island, Northern Great Barrier Reef. *Fish Bull.* **92**, 46–57 (1994).

387. M. Ntiba, V. Jaccarini, Age and growth parameters of *Siganus sutor* in Kenyan marine inshore water, derived from numbers of otolith microbands and fish lengths. *J. Fish Biol.* **33**, 465–470 (1988). doi:10.1111/j.1095-8649.1988.tb05487.x

388. J. G. Pajuelo, J. M. Lorenzo, Growth and age estimation of *Diplodus sargus cadenati* (Sparidae) off the Canary Islands. *Fish. Res.* **59**, 93–100 (2002). doi:10.1016/S0165-7836(01)00421-0

389. P. Radebe, B. Mann, L. Beckley, A. Govender, Age and growth of *Rhabdosargus sarba* (Pisces: Sparidae), from KwaZulu-Natal, South Africa. *Fish. Res.* **58**, 193–201 (2002). doi:10.1016/S0165-7836(01)00383-6

390. J. MacKinnon, Metabolism and its relationship with growth rate of American plaice, *Hippoglossoides platessoides* Fabr. *J. Exp. Mar. Biol. Ecol.* **11**, 297–310 (1973). doi:10.1016/0022-0981(73)90029-4

391. J. M. Penha, L. A. Mateus, G. Barbieri, Age and growth of the duckbill catfish (*Sorubim* cf. *lima)* in the Pantanal. *Braz. J. Biol.* **64**, 125–134 (2004). doi:10.1590/S1519-69842004000100014 Medline

392. K.-M. Liu, M.-L. Lee, S.-J. Joung, Y.-C. Chang, Age and growth estimates of the sharptail mola, *Masturus lanceolatus*, in waters of eastern Taiwan. *Fish. Res.* **95**, 154–160 (2009). doi:10.1016/j.fishres.2008.08.013

393. K. A. Bjorndal, A. B. Bolten, M. Y. Chaloupka, Green turtle somatic growth model: Evidence for density dependence. *Ecol. Appl.* **10**, 269–282 (2000).

394. B. Wallace, T. Jones, What makes marine turtles go: A review of metabolic rates and their consequences. *J. Exp. Mar. Biol. Ecol.* **356**, 8–24 (2008). doi:10.1016/j.jembe.2007.12.023

395. T. T. Jones, M. D. Hastings, B. L. Bostrom, D. Pauly, D. R. Jones, Growth of captive leatherback turtles, *Dermochelys coriacea*, with inferences on growth in the wild: Implications for population decline and recovery. *J. Exp. Mar. Biol. Ecol.* **399**, 84–92 (2011). doi:10.1016/j.jembe.2011.01.007

396. F. Paladino, J. Spotila, M. O'Connor, R. Gatten Jr., Respiratory physiology of adult leatherback turtles (*Dermochelys coriacea*) while nesting on land. *Chelonian Conserv. Biol.* **2**, 223–229 (1996).

Chapter III

‘Metabolic theory predicts whole-ecosystem properties’

Carbon comprises the molecular backbone of all living things. Organic carbon is created during photosynthesis and the bond energy between carbon and hydrogen forms the source of chemical energy that permits metabolism and sustains life. Interest in the abundance and flux of carbon has surged along with interest in climate change and increasingly sophisticated models have been developed to track and predict its movement. Measurement and manipulation of carbon dioxide is at an all-time high. Nonetheless, simple, even elegant insights into the movement of carbon are still possible.

In this chapter, colleagues and I explore the transit of carbon as mediated by organismal respiration. Body mass scales predictably with respiration, a fact that we use to theoretically quantify the time in which carbon is assimilated by organisms, incorporated into tissues, and respired back into the environment. We derive theory linking body size, production and biomass to carbon flux rates. We compile ecosystem data from grasslands, forests, lakes and oceans to test theory and find support for predictions of carbon cycling times. The framework developed will be useful in forging mechanistic linkages between individuals and basic ecosystem rates.

Metabolic theory predicts whole-ecosystem properties

John R. Schramski[a,1], Anthony I. Dell[b,c], John M. Grady[d], Richard M. Sibly[e], and James H. Brown[d,1]

[a]College of Engineering, University of Georgia, Athens, GA 30602; [b]Systemic Conservation Biology, Department of Biology, Georg August University, Göttingen 37073, Germany; [c]National Great Rivers Research and Education Center, Alton, IL 62024; [d]Department of Biology, University of New Mexico, Albuquerque, NM 87131; and [e]School of Biological Sciences, University of Reading, Reading RG6 6AS, United Kingdom

Contributed by James H. Brown, December 18, 2014 (sent for review September 11, 2014; reviewed by Just Cebrian)

Understanding the effects of individual organisms on material cycles and energy fluxes within ecosystems is central to predicting the impacts of human-caused changes on climate, land use, and biodiversity. Here we present a theory that integrates metabolic (organism-based bottom-up) and systems (ecosystem-based top-down) approaches to characterize how the metabolism of individuals affects the flows and stores of materials and energy in ecosystems. The theory predicts how the average residence time of carbon molecules, total system throughflow (TST), and amount of recycling vary with the body size and temperature of the organisms and with trophic organization. We evaluate the theory by comparing theoretical predictions with outputs of numerical models designed to simulate diverse ecosystem types and with empirical data for real ecosystems. Although residence times within different ecosystems vary by orders of magnitude—from weeks in warm pelagic oceans with minute phytoplankton producers to centuries in cold forests with large tree producers—as predicted, all ecosystems fall along a single line: residence time increases linearly with slope = 1.0 with the ratio of whole-ecosystem biomass to primary productivity (*B/P*). TST was affected predominantly by primary productivity and recycling by the transfer of energy from microbial decomposers to animal consumers. The theory provides a robust basis for estimating the flux and storage of energy, carbon, and other materials in terrestrial, marine, and freshwater ecosystems and for quantifying the roles of different kinds of organisms and environments at scales from local ecosystems to the biosphere.

metabolic theory | systems ecology | total system throughflow | residence time | cycling

In most ecosystems, energy and materials flow through trophic networks comprised of plant primary producers, animal consumers, and microbial decomposers (Fig. 1). The individual organisms that make up these networks control the storage and flux of energy, carbon, and other materials. Consequently, a theoretical framework that can account for how different kinds of organisms and ecosystems affect fluxes and stores of energy and materials in ecosystems is central to understanding the carbon cycle of the biosphere and to predicting the impacts of human-caused changes in climate, land use, and biodiversity (1–3). Although it has long been recognized that different kinds of organisms play important roles in the processing of energy and materials in ecosystems, existing treatments are incomplete. Most studies have focused on particular trophic levels, such as primary producers or herbivores, specific ecosystem types, such as tropical forest or pelagic marine, or single species, such as top predators or ecosystem engineers (4–14). Still missing is a simple mechanistic theory that can make precise, quantitative predictions based on the mechanistic relationships between traits of the organisms in the different trophic levels and whole-ecosystem properties, such as carbon flux or recycling.

Two main theoretical frameworks have been used to quantify and synthesize information on energy and material cycling in ecosystems. Systems theory (15, 16) is a top-down approach that quantifies the fluxes and stores of energy or materials among functional compartments and derives emergent whole-ecosystem properties, including average residence times of carbon and other molecules, total system throughflow (TST; the sum of all flows in the system), and the Finn cycling index (FCI; the percentage of organic carbon that is recycled through the decomposer loop). Metabolic theory (17, 18) is a bottom-up approach that quantifies the fluxes and stores of energy and materials within organisms and uses the scaling of metabolic rate with body size and body temperature to predict structural and functional characteristics at multiple levels of organization from individual organisms to ecosystems (6, 19–24). Both approaches are grounded in universal physical laws and established biological principles.

In this paper, we synthesize these two frameworks to show how the traits of individual organisms give rise to ecosystem properties. Our analytical mathematical and numerical simulation models show how residence times of carbon in ecosystems vary with the body size and temperature of the constituent organisms and how TST and FCI are determined by primary production and carbon flows between organisms. We use data on carbon fluxes in organisms and ecosystems to test the assumptions and predictions of the theory. The approach can be expanded straightforwardly to analyze many aspects of the flux and storage of energy and materials in the biosphere.

Theory

The carbon cycle in the biosphere, and in the organisms, populations, food webs, and ecosystems that comprise the biosphere, is controlled by biological metabolism. Individual organisms take up carbon compounds from the environment, transform and retain them within their bodies, and ultimately release them back into the environment (Fig. 1). Carbon and energy budgets are intimately related. Carbon dioxide, water, and solar energy are

Significance

A theory is presented which shows how the metabolism of individual organisms controls the flow of carbon through ecosystems. The theory synthesizes top-down, ecosystem-level and bottom-up, organism-level approaches to ecological energetics and material cycles. The theory predicts a very simple straight-line relationship between residence time of carbon molecules and the ratio of whole-ecosystem biomass to primary productivity. This and additional predictions for total throughfow and recycling are supported by numerical models and data from real ecosystems. The theory provides a powerful way to understand the roles of organisms in ecosystem processes at scales from local habitats to the biosphere. Such an understanding is important for addressing the impacts of human-caused changes in climate, land use, and biodiversity.

Author contributions: J.R.S., A.I.D., J.M.G., R.M.S., and J.H.B. designed research; J.R.S., A.I.D., J.M.G., R.M.S., and J.H.B. performed research; R.M.S. and J.H.B. contributed new reagents/analytic tools; J.R.S., A.I.D., J.M.G., R.M.S., and J.H.B. analyzed data; R.M.S. provided the mathematical analyses; and J.R.S., A.I.D., J.M.G., R.M.S., and J.H.B. wrote the paper.

Reviewers included: J.C., Dauphin Island Sea Lab.

The authors declare no conflict of interest.

See Commentary on page 2303.

[1]To whom correspondence may be addressed. Email: jschrams@uga.edu or jhbrown@unm.edu.

This article contains supporting information online at www.pnas.org/lookup/suppl/doi:10.1073/pnas.1423502112/-/DCSupplemental.

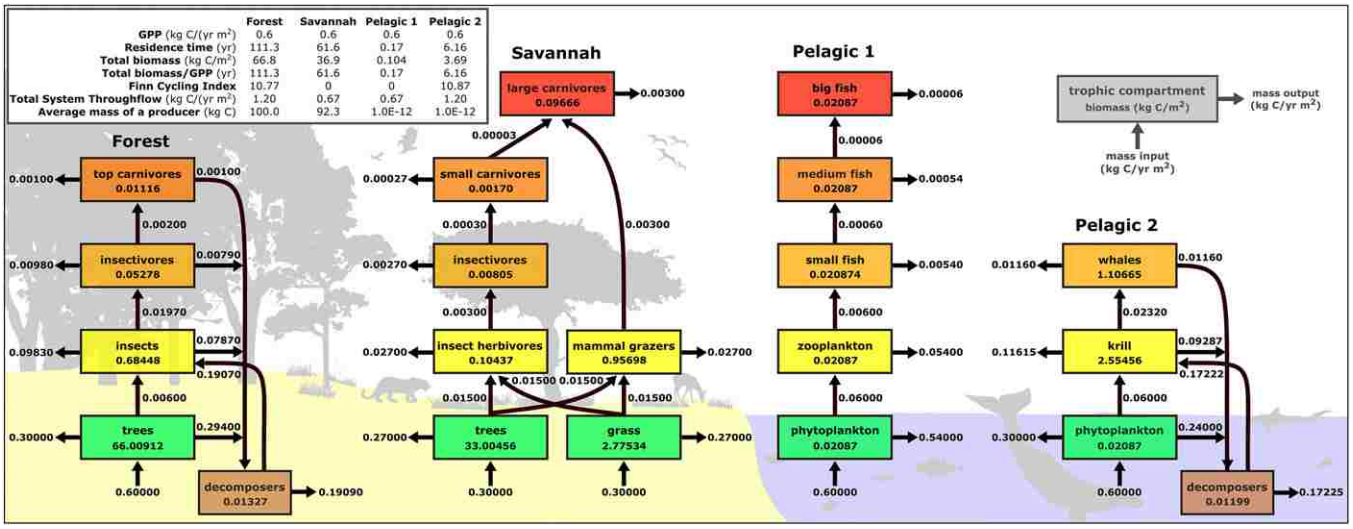

Fig. 1. Examples of four idealized trophic networks used for numerical analysis showing pathways of carbon flow from primary producers through successive trophic levels of animal consumers to top predators; Forest and Pelagic 2 networks also have cycling via a decomposer loop. Numbers in each box give total biomass in the trophic compartment (kg C/m^2), and the arrows in and out of each box give the flux of biomass (kg C/y·m^2) in and out of the compartment, respectively. Details of model construction and simulation are in *Materials and Methods*, with additional parameter values in *SI Appendix*, Table S1 and Fig. S1: Forest (model 2a); Savannah (model 7a), Pelagic 1 (model 3), and Pelagic 2 (model 6a).

incorporated into the high-energy bonds of organic compounds of plant producers during photosynthesis. When the organic bonds are broken during respiration, plants, animal consumers, and microbial decomposers obtain usable energy in the form of ATP.

In any organism, population, trophic compartment, or ecosystem where the flux of carbon is in steady state, the rate of uptake equals the rate of loss and the total number of molecules within the system remains constant. At steady state, the loss rate equals the uptake rate, so the average residence time of carbon molecules in the system ($\hat{t}$) is then equal to total biomass (B, in carbon units) divided by the uptake rate (P)

$$\hat{t} = B/P. \quad [1]$$

This follows straightforwardly from mass balance (*SI Appendix*; we use the $\hat{t}$ notation to indicate average residence time at steady state). Rate of carbon uptake is the rate of gross primary production in autotrophic cyanobacteria, algae, and higher plants, which obtain energy from sunlight, and the rate of gross assimilation in heterotrophic bacteria, fungi, and animals, which obtain energy by consuming living or dead biomass. These uptake rates scale similarly to the metabolic rates of the organisms (17, 25), which are usually measured in units of power but can equally well be expressed in units of carbon. Following Eq. **1**, the average residence time ($\hat{t}_{ind}$) of a carbon molecule in an individual organism with uptake rate (P_{ind}) and body mass (M_{ind}) is

$$\hat{t}_{ind} = M_{ind}/P_{ind}. \quad [2]$$

Residence time of carbon varies among organisms by orders of magnitude, from minutes in some microbes to centuries in some plants (17, 26). Most of this variation can be understood using metabolic scaling theory and allometry, where the metabolic rates of individuals characteristically scale as a power function of body mass and an exponential function of temperature

$$P_{ind} = P_0 M_{ind}^{\beta} e^{-E/kT}, \quad [3]$$

where P_0 is a normalization constant that varies between taxa and environments, β is the mass scaling exponent, E is an activation energy that gives the temperature dependence, k is Boltzmann's constant; and T is temperature in kelvin (17, 27, 28). Average residence time of carbon molecules within an individual is obtained by substituting Eq. **3** into Eq. **2**, giving

$$\hat{t}_{ind} = M_{ind}/P_{ind} = M_{ind} \Big/ \left(P_0 M_{ind}^{\beta} e^{-(E/kT)}\right) = P_0^{-1} M_{ind}^{1-\beta} e^{E/kT}. \quad [4]$$

Metabolic theory and available data suggest β is ~3/4 (17), so Eq. **4** predicts that whole-organism rates of carbon uptake increase ~15 orders of magnitude with the ~20 orders of magnitude increase in body size from microbes to trees and whales. Consequently, carbon residence times should scale as $\alpha = 1 - \beta$ or ~1/4, increasing by about five orders of magnitude over the same size interval (Fig. 2*A*). Theory and available data suggest that E is ~0.65 eV (i.e., rates increase about 2.5 times with every 10°C) (17, 27–29), meaning that uptake rates increase and residence times decrease exponentially with temperature, varying by about 40-fold over the range 0–40 °C (Fig. 2*D*).

Many ecosystems are composed of organisms of different kinds, organized into networks of trophic compartments that flux carbon, other materials, and energy from photosynthetic primary producers to heterotrophic consumers (Fig. 1). Initially, for purposes of illustration, we develop the theory in terms of such autotrophy-based ecosystems. The uptake rate of any compartment is simply the sum of the uptake of all individuals. Similarly, the total biomass of any compartment is the sum of the masses of all individuals. Following Eq. **1**, the average residence time of carbon within any compartment is equal to the total biomass divided by the total uptake rate. The expression for residence time in an entire ecosystem is slightly different, however, because the relevant uptake rate is of carbon entering the system, so in autotrophy-based ecosystems (Fig. 1), it is the rate of gross primary production (GPP). Ecosystem biomass is the sum of the body masses of all individual organisms in all trophic compartments. From Eq. **1** it follows that $\hat{t}_{eco} = B_{eco}/P_{pro}$, where the subscript *eco* indicates the entire ecosystem and the subscript *pro* indicates that production rate is summed only for the primary producers. Therefore, in a plot of $\hat{t}_{eco}$ as a function of B_{eco}/P_{pro}, all ecosystems fall along a single line through the origin with slope = 1.0, as in Fig. 2*B*. The positions of ecosystems along this line vary widely, however, depending on the body size and body temperature of

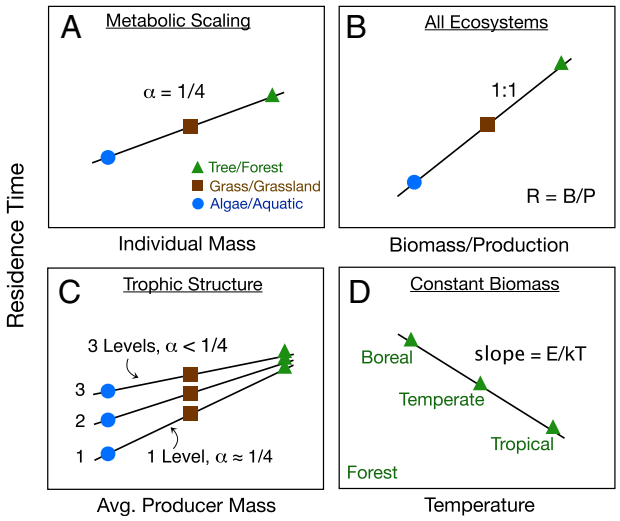

Fig. 2. Schematic presentations of model predictions for residence time plotted on logarithmic axes with α giving the scaling exponent. (*A*) Residence time or half-life of carbon ($\hat{t}_{ind}$) within an individual organism increases with increasing body mass as a power function with $\alpha = 1/4$. (*B*) Residence time of carbon within an ecosystem increases linearly with the ratio of total biomass to primary productivity (Eq. **1**) so all ecosystems fall along a single line with slope = 1.0. Position of different ecosystem types along this line vary: residence times increase with increasing body sizes of the organisms and decrease with increasing environmental temperature. (*C*) If the temperature remains constant, residence times of different ecosystems generally increase with increasing body sizes of the primary producers, from pelagic marine ecosystems with tiny phytoplankton to forests with large trees. The slope of this relationship is <1/4, because animal consumers contribute proportionately more to total biomass in pelagic marine ecosystems, whereas trees dominate the biomass of forests. (*D*) If total biomass remains constant, residence times of different ecosystems decrease with increasing environmental temperature.

the component organisms and on aspects of trophic organization, such as the number of trophic levels and amount of cycling. The exact residence time for any ecosystem can easily be calculated by applying Eq. **4** and substituting appropriate values for the uptake rate, body mass, and body temperature of the organisms (which we assume to be equal to environmental temperature for all organisms except endothermic birds and mammals) to obtain

$$\hat{t}_{eco} = B_{eco}/P_{pro} = \sum M_{ind} \Big/ \sum P_{pro} = \sum M_{ind} \Big/ \sum \left(P_0 M_{pro}^{\beta} e^{-(E/kT)}\right). \quad [5]$$

The above theory makes four predictions for residence times that are shown schematically in Fig. 2:

1) For individual organisms, Eq. **4** predicts that residence time or half-life of carbon and other elements increases with increasing body size, with a slope of $\alpha \sim 1/4$ (Fig. 2*A*), and decreases with increasing temperature, with $E \sim 0.65$ eV.
2) For ecosystems, Eqs. **1** and **5** predict that $\hat{t}_{eco} = B_{eco}/P_{eco}$, so in a graph of residence times as a function of the ratio of total biomass to GPP, all ecosystems fall along a single line through the origin with slope = 1.0 (Fig. 2*B*).
3) For ecosystems, it follows from Eq. **5** that residence time is positively correlated with the body size of the primary producers, provided they account for a large fraction of total ecosystem biomass. In such cases, for example in forests dominated by trees, residence time scales with producer body mass, with $\alpha \sim 1/4$. However, when producers are small, such as pelagic systems with phytoplankton, they comprise a smaller fraction of total biomass, and the slope of this relationship is <1/4 (Fig. 2*C*).
4) For ecosystems, Eq. **5** predicts that residence time decreases exponentially with environmental temperature, and therefore with the body temperatures of all organisms except for endothermic birds and mammals, so residence times are longer in cold high-latitude than warm tropical ecosystems (Fig. 2*D*).

Although residence time was our primary focus, we also modeled how organismal metabolism affects two other emergent properties of ecosystems: TST and extent of recycling, as measured by the FCI (30–32). TST is the sum of all trophic flows in the system. FCI gives the percentage of molecules of organic carbon (or energy) that is recycled through the decomposer loop, in which microbes consume nonliving organic detritus and are themselves consumed by heterotrophic consumers (e.g., the second trophic level in the Forest and Pelagic 2 networks in Fig. 1). We now derive TST and FCI in terms of the flow of carbon into the system from photosynthesis (P), the metabolic induced flow of carbon at each trophic level (P_i), the number of trophic levels (n), and the efficiency of carbon transfer between trophic levels (TTE). TTE is expressed as a fraction of the carbon or energy transferred between two trophic compartments. Due to the second law of thermodynamics and the limited efficiency of metabolic biochemistry, TTE is always less than 1 and empirically often ranges between 0.01 and 0.2. We distinguish the TTE for three different fluxes of carbon: (*i*) the proportion of carbon leaving one trophic level and going to the next highest level is $t = (P_{i+1}/P_i)$, where P_i and P_{i+1} are the gross uptake rates of two successive trophic levels; (*ii*) the proportion leaving each trophic level and going to decomposers is d_1; and (*iii*) the proportion leaving decomposers and going to level 2 is d_2. Here, we assume that t, d_1, and d_2 are constant. Now the uptake of carbon by level 2 (i.e., P_2) can be divided into that coming directly from producers, Pt; that coming from producers via decomposers, Pd_1d_2; and that coming from higher levels via decomposers, $P_2d_1d_2\,(1 + t + t^2 + \ldots + t^{n-2})$, which is a geometric series. Hence, $P_2 = P(t + d_1d_2) + P_2d_1d_2\,(1 - t^{n-1})/(1 - t)$, i.e., $P_2 = P(t + d_1d_2)(1 - t)/[1 - t - d_1d_2\,(1 - t^{n-1})]$, and therefore

$$\mathrm{TST} = \left(P + P_2 \frac{1 - t^{n-1}}{1 - t}\right)(1 + d_1). \quad [6]$$

FCI is given by the sum of the flows through each compartment that have previously passed through them ($\mathrm{TST_C}$) multiplied by 100 and divided by TST. In cases such as Fig. 1 where there is just one compartment at each trophic level and the flow from decomposers goes only to level 2, $\mathrm{TST_c}$ is given by

$$TST_c = \frac{d}{1 - t}\left(Pd_1\left(1 - t^{n-1}\right) + P_2\left\{d_1\frac{\left(1 - t^{n-1}\right)^2}{1 - t} + \frac{1 - t^{2n-2}}{1 - t^2} - \frac{t^{n-1} - t^{2n-2}}{1 - t}\right\}\right). \quad [7]$$

See *SI Appendix* for proof. The above expressions for TST and FCI have not previously been derived for ecosystems. More generally our theory predicts

5) Because flows between successive trophic levels decrease rapidly up the trophic network (Fig. 1), TST is determined primarily by variation in GPP, which constitutes the largest fraction of TST. Therefore, TST should be strongly positively correlated with GPP, and it should secondarily increase with trophic transfer efficiency between trophic levels (t) and the strength of the decomposer recycling loop (Eq. **6**).
6) Recycling of carbon occurs only through the decomposer loop, so FCI must be small. Where there is just one compartment

at each trophic level it follows from Eqs. **6** and **7** that FCI ~ $100d_1d_2(d_1 + t)$ if t, d_1, and d_2 are small (*SI Appendix*).

Numerical Simulations

To explore the implications of our theory, we created numerical models of idealized autotrophy-based ecosystem networks (*SI Appendix*, Table S1; see examples in Fig. 1). We assumed steady-state and enforced mass and energy balance on the inputs and outputs to each trophic compartment and hence throughout each network. We evaluated a wide variety of autotrophy-based networks designed to capture idealized but realistic properties of natural ecosystems: (*i*) terrestrial and marine; (*ii*) primary producers varying in size by 14 orders of magnitude from unicellular algae to grasses to trees; (*iii*) consumers varying in size by 14 orders of magnitude from zooplankton and insects to elephants and whales; (*iv*) environmental temperatures ranging from 7 °C to 27 °C; (*v*) containing both ectothermic consumers with body temperatures equal to environmental temperature and endothermic consumers with body temperatures equal to 37 °C; and (*vi*) with various amounts of recycling of detritus through the decomposer loop. Metabolic rate was assumed to vary with body mass and temperature according to Eq. **3**. Four of these networks and their parameters are shown in Fig. 1, with details for all networks provided in *SI Appendix*, Table S1. Methods used to construct the networks and run simulations are described below.

Results of the numerical simulation models supported all of the above predictions. Residence times scaled linearly as the ratio of total biomass to GPP with a slope of 1.0, so $\hat{t}_{eco} = B_{eco}/P_{eco}$ (Fig. 3*A*). Residence time was positively correlated with the body size of the primary producers. The slope of this relationship was <1/4 as predicted, because tiny phytoplankton comprised a lower fraction of total ecosystem biomass in pelagic marine ecosystems with than did large trees in forest ecosystems (Fig. 3*B*).

System properties calculated from the numerical models using Ecological Network Analysis (33) matched those calculated from Eqs. **6** and **7**. The numerical models also supported the above predictions for TST and recycling (FCI). TST was positively correlated with GPP (r = 0.73), and also positively correlated with FCI (r = 0.54). TST was mainly determined by GPP, but also increased as the strength of the decomposer loop increased (Fig. 3*C*). An advantage of using Eq. **7** or its approximation with FCI ~ $100d_1d_2(d_1 + t)$ is that this shows explicitly the individual contributions to FCI made by the trophic transfer efficiencies t, d_1, and d_2. FCI was always low; it varied from about 0% to 11% (*SI Appendix*, Table S1), as the percentage of carbon flowing through the decomposers varied from 0% to 10%.

The numerical models confirmed the predictions of the analytical theory that average residence times of carbon molecules in ecosystems vary (*i*) by orders of magnitude with the body sizes of the primary producers, from weeks in pelagic marine ecosystems with minute phytoplankton to centuries in forests with giant trees; and (*ii*) with trophic structure, increasing with number of trophic levels and body sizes of top predators. The numerical models also supported our theoretical predictions for total system throughflow and recycling.

Empirical Validation

The ultimate test of our theory will be its ability to predict and explain properties of real ecosystems. We performed preliminary validation by comparing theoretical predictions with available data (Fig. 4). The prediction that residence times within individual organisms scale with body mass with $\alpha \sim 1/4$ was confirmed by compiling and analyzing published data from physiological studies of half-life of carbon and nitrogen in animals (Fig. 4*A*). The dependence of residence time in ecosystems on the body sizes of primary producers was assessed using a large existing dataset (10). As predicted, the observed $\alpha = 0.21$ was somewhat less than 1/4 (Fig. 4*B*). The predicted dependence of ecosystem residence time on environmental temperature was also supported; the data in Fig. 4*B* were already temperature-corrected using Eq. **3**, which substantially reduced variation around the regression line. The prediction that $\hat{t}_{eco} = B_{eco}/P_{eco}$ was evaluated using a different but overlapping dataset (12). A plot of average residence times of carbon in the ecosystems ($\hat{t}_{eco}$) as a function of total biomass (B_{eco}) over the uptake rate (GPP, or B_{pro}) showed the data clustering around the predicted linear relationship with slope = 1.0 (95% CI includes slope = 1.0; Fig. 4*C*). Overall, the empirical data showed that residence time of carbon in both individual organisms and entire ecosystems increased with increasing system biomass. Residence time in ecosystems increased by about four orders of magnitude, from 0.05 to 100 yr, as the size of primary producers increased from tiny algae in pelagic marine ecosystems to large trees in forests.

Discussion

The above metabolic theory of ecosystem properties provides a robust basis for estimating the flux and storage of carbon, other materials, and energy in terrestrial, marine, and freshwater ecosystems throughout the world. The theory makes two important advances over previous treatments. It shows (*i*) how carbon residence time and other whole-ecosystem properties depend on biological metabolism and specifically on the effects of body sizes and temperatures of the organisms in the different trophic levels; and consequently, (*ii*) that residence time increases linearly with the ratio of two ecosystem-level properties, total biomass, and gross primary production, so that that $\hat{t}_{eco} = B_{eco}/P_{eco}$ and all ecosystems fall along the same line with slope = 1.0. Additionally, it predicts that the absolute values of residence time (i.e., the position along the line) increase by several orders of magnitude with increasing body sizes of the primary producers (from algae to large trees) and by a factor of about 40 with

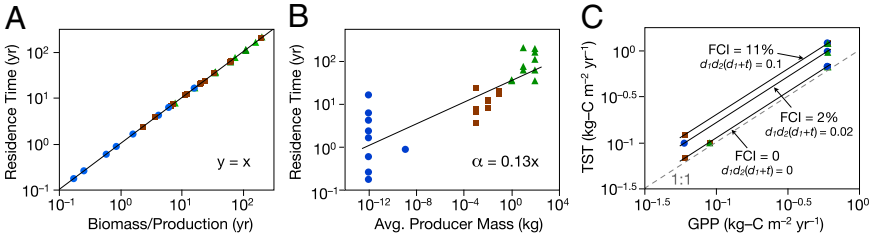

Fig. 3. Tests of the theoretical predictions in Fig. 2 *C* and *D* with outputs of numerical simulation models of 37 idealized ecosystems. Symbol color and shape as in Fig. 2*A*. Solid black lines are GLM regression fit. (*A*) In a graph of residence times as a function of the ratio of total biomass to GPP, all ecosystems fell along a single line with slope = 1.0, so $\hat{t}_{eco} = B_{eco}/P_{eco}$. (*B*) Residence time was positively correlated with the body size of the primary producers divided by GPP with $\alpha = 0.13$, so <1/4 because of relatively long residence times in pelagic marine ecosystems. (*C*) TST increased primarily with increasing GPP and secondarily with the strength of the decomposer recycling loop. All 37 models are plotted here.

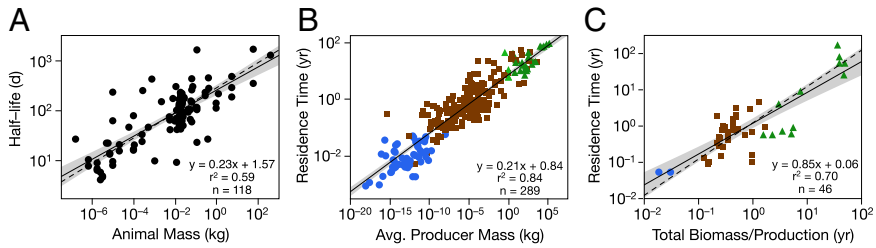

Fig. 4. Empirical data for the residence time of carbon and nitrogen for diverse organisms and ecosystem types. Symbol color and shape as in Fig. 2*A*. Solid black lines are GLM regression fits (gray shading is the 95% confidence band), and black dotted lines are our predicted relationships from our theory. (*A*) Within individual organisms the half-life of carbon and nitrogen increases with body mass with a slope of 0. 23 ± 0.03 95% CI (this includes our predicted slope of 0.25, see prediction 1 in main text). These data have been temperature corrected to 15°C and include a large diversity of tissue types (*Materials and Methods* and *SI Appendix*, Table S2). As we also predict, in entire ecosystems, carbon residence times increase with (*B*) increasing body size of the primary producers (slope is 0.21 ± 0.02 95% CI; expected slope is <0.25 depending on the network, see prediction 3 in main text), data replotted from Allen et al. (10), and (*C*) the ratio of total biomass to primary production (slope is 0.85 ± 0.17 95% CI, see prediction 2 in main text). Production is GPP, determined by doubling NPP values in ref. 12 as per ref. 45. For terrestrial systems, biomass = plant and herbivore biomass. For freshwater pelagic systems, biomass = 3 × producer mass (46).

decreasing environmental temperature (from 40 °C to 0 °C). The predictions are relatively insensitive to the precise scaling of metabolic rate with body size and temperature (values of β and E in Eq. **3**), but somewhat more sensitive to variation in the trophic transfer efficiency between levels, t, and the strength of the decomposer recycling loop $d_1d_2(d_1 + t)$. These predictions are supported by numerical simulation models parameterized with realistic values and by empirical data for real ecosystems.

There is abundant scope to test, extend, and apply our theory. We have evaluated the theory using data from only a modest number of simulated and real autotroph-based ecosystems and analyzing the effect of only a few variables. However, because the theory incorporates theoretically and empirically well-established scaling relations, it can be generalized and applied to a wide variety of systems. For example, it can be extended to other elements in addition to carbon and used to address roles of organisms in nutrient cycling. It can be applied to subsystems within ecosystems, such as single trophic levels or individual organisms (see analysis of residence times of carbon and nitrogen molecules within individual organisms in Fig. 4*A*). Finally, the theory can be applied to address the roles of different kinds of organisms in heterotrophy-based ecosystems, such as the soil and deep sea, where the input of carbon is in preformed organic molecules (detritus) rather than CO_2 fixed in photosynthesis.

Additionally instead of carbon, units of energy or other elements could be used, for example, to explore metabolic effects on nutrient cycling. The theory suggests ways to parameterize and evaluate the accuracy of empirically derived trophic networks. For example, Fig. 4*B* shows that the predicted linear relationship between residence time and the ratio of total biomass to primary productivity, $\hat{t}_{eco} = B_{eco}/P_{eco}$, is strongly supported, but there is considerable unexplained residual variation. All of our analyses support Eq. **1**; the deviations from exact linear scaling in Fig. 4*B* are presumably due to violations of model assumptions, such as steady-state or mass balance, or to measurement errors. Because we demonstrated that Eq. **1** is robustly supported by mathematical theory, numerical simulations, and empirical evidence, deviations from exact linear scaling in Fig. 4*B* are presumably due to violations of model assumptions, such as steady-state or mass balance, or to measurement errors. Although there are many datasets on ecosystem properties (34), most do not contain information on the body sizes and temperatures of the organisms in each trophic compartment, making them problematic for rigorous empirical evaluation of our theory. There are also significant challenges in precisely measuring GPP, total biomass, and residence time for entire ecosystems (34). The assumption of steady state is especially critical, and it can potentially be evaluated by estimating mass and energy balance at different levels, from individual organisms to trophic compartments to the entire ecosystem. To account accurately for the carbon budget, it is important not only to include all photosynthesis, respiration, and fluxes between trophic levels but also any net export or storage of organic carbon.

Our theory extends the bottom-up individual-based framework of metabolic theory (10, 17, 35) to ecosystems to incorporate organisms and their metabolism explicitly into ecological systems theory (15, 16, 20, 21, 31). It reveals how the size and temperature of the plants, animals, and microbes in different trophic compartments affect carbon residence time, and other emergent ecosystem properties such as TST and recycling (FCI). Systems ecologists have predicted that TST and FCI increase over time as ecosystems reorganize during ecological succession or evolve over geological time (15, 16, 21). Our theory and numerical models show that, although this may be true, the magnitudes of changes are limited by powerful metabolic constraints: TST by GPP and FCI by $d_1d_2(d_1 + t)$. TST is predicted to increase over primary and secondary succession, due primarily to an increase in GPP. Recycling is also expected to increase as ecosystems age. Over both ecological and evolutionary time the number of species and metabolic pathways should increase as different microbes colonize and evolve, consuming detrital resources more completely by adding specialized pathways to obtain energy from diverse and refractory organic compounds (such as lignin or chitin). The magnitude of recycling of carbon and energy through microbial loops is modest and strongly constrained by the Second Law of Thermodynamics as shown by Finn (32) and above in the powerful constraint on $d_1d_2(d_1 + t)$ (Fig. 1 and Eq. **7**). However, our analyses apply only to cycling of organic carbon or energy, which are dissipated in the trophic network as organic molecules are metabolized. A much greater proportion of nutrients, such as nitrogen or phosphorous, may be recycled (32).

Our theory not only generates testable predictions that are supported by data from real systems, it also provides a powerful basis for assessing natural spatial and temporal variation and impacts of human activities on the carbon cycle. With respect to natural variation, the model should provide a straightforward and robust basis for quantitatively estimating the flux rates and residence times of carbon in different ecosystems based on the body sizes of the dominant organisms (especially the primary producers) and temperature. Collection and synthesis of such data should provide a quantitative basis for assessing the contributions of different ecosystem types and geographic regions (e.g., tropical vs. high latitude, marine vs. terrestrial, forest vs. grassland) to the global carbon cycle. Our theory should also help predict human impacts on the carbon cycle on scales from local ecosystems to the biosphere. For example, overharvesting of large animals can significantly alter ecosystem biomass and GPP, impacting carbon residence times (3, 36–38). Both deforestation, which replaces

forests with agricultural fields and grasslands (39–42), and a warmer climate, which increases metabolic rates, should decrease the residence time of carbon in local ecosystems and in the biosphere as a whole. More generally, our theory is a synthesis of systems and metabolic approaches that shows explicitly and quantitatively how organisms control the carbon cycle at all scales from individuals to ecosystems to the biosphere.

Materials and Methods

Numerical Model. Fig. 1 represents four examples of how we modeled the carbon flows between the compartments of ecosystems in our numerical simulations. All individuals within a compartment were for simplicity assumed to have the same individual body mass m. The order of calculations was as follows: (*i*) calculate the carbon uptake P_{ind} of each individual primary producer (kg C/ind·y) using Eq. **3** with parameter values $P_0 = 2.16 \times 10^9$ (25); $k = 8.62 \times 10^{-5}$ eV/K; $E = 0.65$ eV; ectotherm $T = 7$ °C or 20 °C or 27 °C or 37 °C; $\beta = 0.67$ or 0.75; (*ii*) calculate total number of individuals in the compartment, assuming net primary production = 1/2 GPP (kg C/y·m^2), and then $n = 0.5$ GPP/P_{ind} (ind/m^2) (43, 44); (*iii*) calculate total biomass in the compartment, $X = N \times M$ (kg/m^2); (*iv*) using a trophic transfer efficiency t, calculate carbon flow to the next trophic level ($t = 0.1$ for all TTEs not associated with the decomposers, but some models $t = 0.01$ between trophic levels 1 and 2 only; *SI Appendix*, Table S1); and (*v*) repeat steps *i*–*iv*, replacing primary producers by the individuals in the next trophic level. For models with decomposers, all compartments transferred $d_1 = 0.40$ to decomposers, and the decomposer trophic transfer efficiencies were assumed to be either $d_2 = 0.1$ or 0.5 depending on model objective. Thirty-six such models were constructed. Once all carbon storages and flows (intercompartmental, input, and output) were known for the balanced model, ecological analysis software (33) was used to calculate TST, FCI, and residence time. An Excel spreadsheet was used to calculate the parameters for each trophic network (Fig. 1 and *SI Appendix*, Table S1 and Fig. S1).

Empirical Data. Data to test how body size affects residence times of C and N in individual organisms (Fig. 4*A*) were obtained from the literature (*SI Appendix*, Table S2). These data were recorded as half-lifes—the amount of time required for the stable-isotopic signature of tissue to reach a midpoint between the enriched and original value—and were not converted to residence times because of differences between studies in how half-life was calculated. Data in Fig. 4*A* were temperature corrected to 15 °C using Eq. **3**. Empirical evaluation of our predictions for residence times in ecosystems (Fig. 4 *B* and *C*) requires high-quality data on residence time (or turnover rate), total biomass, and GPP for real ecosystems composed of organisms of varying size operating at different environmental temperatures. Despite a plethora of empirical whole-ecosystem models, especially in marine habitats (30), only a few studies provide independently measured estimates of all three variables. From a large dataset compiled by Cebrian et al. (12), we obtained the relevant data for 46 ecosystems representing a variety of habitats (terrestrial and marine), environmental temperatures (temperate to tropical), and organism body sizes (phytoplankton to trees and whales). The predicted dependence of ecosystem residence time on the body sizes of primary producers was evaluated using a different but overlapping dataset (10).

ACKNOWLEDGMENTS. We thank the members and, especially, organizer J. Shevtsov of the 2013 National Center for Ecological Analysis and Synthesis working group on Ecological Energetics for thoughtful discussions that led to this paper, J. Cebrian and K. Anderson-Teixeira for generously providing data used in Fig. 4, and M. O'Connor and J. Shevtsov for helpful comments on the manuscript. This work was supported by National Science Foundation Macrosystems Biology Grant EF 1065836.

1. Parry ML, Canziani OF, Palutikof JP, van der Linden PJ, Hanson CE (2007) *Climate Change 2007: Impacts, Adaptation and Vulnerability. Contribution of Working Group II to the Fourth Assessment Report of the Intergovernmental Panel on Climate Change* (Cambridge Univ Press, Cambridge, UK).
2. Schmidt MW, et al. (2011) Persistence of soil organic matter as an ecosystem property. *Nature* 478(7367):49–56.
3. Schmitz OJ, et al. (2013) Animating the carbon cycle. *Ecosystems (NY)* 17(2):344–359.
4. Paine RT (1966) Food web complexity and species diversity. *Am Nat* 100(910):65–75.
5. Sheldon RW, Parsons TR (1967) A continuous size spectrum for particulate matter in the sea. *J Fish Res Board Can* 24(5):909–915.
6. Yodzis P, Innes S (1992) Body size and consumer resource dynamics. *Am Nat* 139(6): 1151–1175.
7. Jones CG, Lawton JH, Shachak M (1994) Organisms as ecosystem engineers. *Oikos* 69:373–386.
8. Legendre L, Michaud J (1998) Flux of biogenic carbon in oceans: Size-dependent regulation by pelagic food webs. *Mar Ecol Prog Ser* 164:1–11.
9. Kerr SR, Dickie LM (2001) *The Biomass Spectrum: A Predator-Prey Theory of Aquatic Production* (Columbia Univ Press, New York).
10. Allen AP, Gillooly JF, Brown JH (2005) Linking the global carbon cycle to individual metabolism. *Funct Ecol* 19(2):202–213.
11. Jennings S, et al. (2008) Global-scale predictions of community and ecosystem properties from simple ecological theory. *Proc Biol Sci* 275(1641):1375–1383.
12. Cebrian J, et al. (2009) Producer nutritional quality controls ecosystem trophic structure. *PLoS ONE* 4(3):e4929.
13. Beaugrand G, Edwards M, Legendre L (2010) Marine biodiversity, ecosystem functioning, and carbon cycles. *Proc Natl Acad Sci USA* 107(22):10120–10124.
14. Boit A, Martinez ND, Williams RJ, Gaedke U (2012) Mechanistic theory and modelling of complex food-web dynamics in Lake Constance. *Ecol Lett* 15(6):594–602.
15. Odum HT (1994) *Ecological and General Systems* (Univ Press of Colorado, Niwot, CO).
16. Jørgensen SE (2009) *Ecosystem Ecology* (Academic, Waltham, MA).
17. Brown JH, Gillooly JF, Allen AP, Savage VM, West GB (2004) Toward a metabolic theory of ecology. *Ecology* 85(7):1771–1789.
18. Sibly RM, Brown JH, Kodric-Brown A (2012) *Metabolic Ecology: A Scaling Approach* (Wiley-Blackwell, Oxford).
19. Peters RH (1983) *The Ecological Implications of Body Size* (Cambridge Univ Press, Cambridge, UK).
20. Lindeman RL (1942) The trophic-dynamic aspect of ecology. *Ecology* 23(4):399–417.
21. Odum EP (1969) The strategy of ecosystem development. *Science* 164(3877):262–270.
22. Odum HT, Odum EP (1955) Trophic structure and productivity of a windward coral reef community on Eniwetok Atoll. *Ecol Monogr* 25(3):291.
23. Sheldon RW, Prakash A, Sutcliffe WH (1972) The size distribution of particles in the ocean. *Limnol Oceanogr* 17(3):327–340.
24. Sheldon RW, Sutcliffe WH, Paranjape MA (1977) Structure of pelagic food-chain and relationship between plankton and fish production. *J Fish Res Board Can* 34(12):2344–2353.
25. Ernest SKM, et al. (2003) Thermodynamic and metabolic effects on the scaling of production and population energy use. *Ecol Lett* 6(11):990–995.
26. Peters RH, Wassenberg K (1983) The effect of body size on animal abundance. *Oecologia* 60(1):89–96.
27. Gillooly JF, Brown JH, West GB, Savage VM, Charnov EL (2001) Effects of size and temperature on metabolic rate. *Science* 293(5538):2248–2251.
28. Brown JH, Sibly RM (2012) The metabolic theory of ecology and its central equation. *Metabolic Ecology: A Scaling Approach*, eds Sibly RM, Brown JH, Kodric-Brown A (Wiley-Blackwell, Oxford), pp 21–33.
29. Dell AI, Pawar S, Savage VM (2011) Systematic variation in the temperature dependence of physiological and ecological traits. *Proc Natl Acad Sci USA* 108(26): 10591–10596.
30. Christensen V, Walters CJ, Pauly D (2005) *Ecopath with Ecosim: A User's Guide* (Fisheries Centre, Univ of British Columbia, Vancouver).
31. Finn JT (1976) Measures of ecosystem structure and function derived from analysis of flows. *J Theor Biol* 56(2):363–380.
32. Ulanowicz RE (1986) *Growth and Development: Ecosystems Phenomenology* (Springer, New York).
33. Lau MK, Borrett SR, Hines DE (2014) enaR: An R package for ecosystem network analysis. *Methods in Ecology and Evolution* 5(11):1206–1213.
34. Houghton RA (2003) Why are estimates of the terrestrial carbon balance so different? *Glob Change Biol* 9(4):500–509.
35. Anderson-Teixeira KJ, Vitousek PM (2012) Ecosystems. *Metabolic Ecology: A Scaling Approach*, eds Sibly RM, Brown JH, Kodric-Brown A (Wiley-Blackwell, Oxford), pp 99–111.
36. Roman J, Palumbi SR (2003) Whales before whaling in the North Atlantic. *Science* 301(5632):508–510.
37. Estes JA, et al. (2011) Trophic downgrading of planet Earth. *Science* 333(6040):301–306.
38. Ripple WJ, et al. (2014) Status and ecological effects of the world's largest carnivores. *Science* 343(6167):1241484.
39. Angelsen A, Kaimowitz D (2001) *Agricultural Technologies and Tropical Deforestation* (CABI Publishing, New York).
40. Achard F, et al. (2002) Determination of deforestation rates of the world's humid tropical forests. *Science* 297(5583):999–1002.
41. Geist HJ, Lambin EF (2002) Proximate causes and underlying driving forces of tropical deforestation. *Bioscience* 52(2):143.
42. Hansen MC, et al. (2013) High-resolution global maps of 21st-century forest cover change. *Science* 342(6160):850–853.
43. Waring RH, Landsberg JJ, Williams M (1998) Net primary production of forests: A constant fraction of gross primary production? *Tree Physiol* 18(2):129–134.
44. Cheng W, Sims DA, Luo Y, Coleman JS, Johnson DW (2000) Photosynthesis, respiration, and net primary production of sunflower stands in ambient and elevated atmospheric CO2 concentrations: An invariant NPP:GPP ratio? *Glob Change Biol* 6(8): 931–941.
45. Zhang Y, Xu M, Chen H, Adams J (2009) Global pattern of NPP to GPP ratio derived from MODIS data: Effects of ecosystem type, geographical location and climate. *Glob Ecol Biogeogr* 18(3):280–290.
46. Jonsson T, Cohen JE, Carpenter SR (2005) Food webs, body size, and species abundance in ecological community description. *Adv Ecol Res* 33(36):1–84.

Chapter IV

‘Metabolic asymmetry drives the distribution of marine predators’

The ocean is populated by large predators with diverse ancestries and thermoregulatory strategies. Nowhere else on earth do co-occurring endothermic, ectothermic, and mesothermic apex predators coexist, compete, and prey upon each other. Patterns of coexistence and exclusion offer clues to the macroevolutionary pressures behind the radiation of endothermy and high energy lifestyles.

In my fourth chapter of my dissertation, I examine the role of energetics in the distribution of competing marine predators. I compile distributional data for over a thousand predatory marine mammals, birds, sharks, fish and reptiles. After demonstrating a compelling empirical pattern, I derive foraging theory to account for the high richness and abundance of endotherms in cold, thermally stressful waters. I argue that favorable metabolic asymmetries underlie this pattern and draw upon metabolic and ecosystem data on mammal consumption to support my model.

Metabolic asymmetry drives the distribution of marine predators

John M. Grady*, Ara S. Winter*, Brian S. Maitner[§], Kristin Kaschner[†], Felisa A. Smith*, Helen J. Wearing*, Derek P. Tittensor[‡], Anthony I. Dell[Φ], James H. Brown*

*University of New Mexico, Albuquerque, NM, USA.

[§]University of Arizona, Tucson, AZ, USA.

[†]University of Freiburg, Freiburg, Germany

[‡]Dalhousie University, Halifax, Nova Scotia, Canada

[Φ]National Great Rivers Research and Education Center, East Alton, IL, USA

Endothermic mammalian and avian lineages have independently invaded the sea over a dozen times during the Cenozoic and are ecologically significant predators in many habitats. Remarkably, the radiation of endotherms has occurred primarily in cold, thermally stressful waters, counter to general biogeographic patterns of animal diversity. Here we show that energetic constraints on foraging lead to metabolic and foraging asymmetries that favor endotherms in cold waters. We compile a large spatial database of over one thousand species of predatory fish, sharks, reptiles, mammals and birds to assess global patterns of distribution and foraging at sea, and derive theory to link metabolism to ecosystem consumption rates. After controlling for food availability and other factors, thermal drivers of consumption lead to 1–2 orders of magnitude increase in mammal abundance and prey capture from the equator to the poles. This corresponds to an increase in morphological and phylogenetic diversity in cold waters as prey become easier to capture and predators less dangerous. An increase in

abundance and foraging breadth best accounts for the striking patterns of richness in marine endotherms.

Marine systems are home to a diversity of top predators that span all major thermoregulatory guilds, including ectothermic sharks and reptiles, mesothermic tuna and marlin, and endothermic mammals and birds. Perhaps most striking is the diversity of marine endotherms. Mammals and birds which have independently invaded the sea over a dozen times despite numerous hurdles to entry, including high rates of heat loss from water (~24x greater than air), lack of available oxygen and energy costs associated with surfacing to breathe, incumbent predators and competitors, inefficient locomotion, and, for many taxa, energetic and geographic restrictions imposed by terrestrial birth[1-3]. Remarkably, marine endotherms have largely diversified in cold temperate waters despite the thermal stress it imposes; this pattern runs counter to nearly all biogeographic trends of diversity in major taxa. They dominate predatory richness at large body sizes (Fig. 1) and the energy flux through upper trophic levels in cold seas[4,5].

To account for this physiological, ecological, and biogeographic puzzle, and to better understand the selective advantages of endothermy, we first document empirical patterns of distribution of apex predators and highlight their covariation with thermoregulation. We then build on more qualitative theory[6] to derive principles that link individual metabolism to ecology at scales from foraging of individual animals to trophic fluxes through ecosystems and global patterns of diversity.

Empirical Patterns

Ecologists have long noted that biodiversity on land tends to peak in the tropics, particularly within the productive and structurally complex tropical rainforests[7]. This pattern holds for virtually all major multicellular taxa on land, including mammals, birds, reptiles, amphibians, plants, insects and fungi[8,9]. In the ocean, similar patterns are generally observed, with peak richness for fish, sharks, coral, seagrass, and mangroves occurring in the coastal tropics; in particular, within the productive and structurally complex reefs of the Indo-Pacific[10]. The recent availability of new spatial data permits broader and more finely resolved analysis of top predators, including addition of new teleost, squamate and avian clades. Our synthesis of ectotherms reinforces prior assessments, with groupers (Epinephalinae), barracuda (Sphyraena), jacks (*Caranx* and *Seriola* in Carangidae), and sea snakes (Hydrophiini and Latidicauda) all showing peak diversity in the warm, coastal waters of the Indo–Pacific (Fig. 2). In contrast, endotherms are generally most diverse in colder, high-latitude oceans. Pinnipeds are virtually absent from the tropics, and all major clades of birds that pursue prey via swimming (penguins, auks, cormorants, grebes, ducks, and loons), rather than aerial diving, are predominantly temperate (Fig. 2, S1). Indeed, not a single species of penguin, auk or pinniped inhabits in the tropical central Indo-Pacific, the center of marine biodiversity. Of the 10 families of marine cetaceans, only dolphins (Delphinidae) are predominantly tropical (Fig. S2). An integrative measure of phylogenetic diversity (PD)[11], which measures total cladogram branch length, demonstrates a strong temperate bias to marine endotherm diversity (Fig. S3). Mesothermic tuna (Thunnini), billfish

(Istiophoridae and Xiphiidae), mackerel sharks (Lamnidae), and thresher sharks (*Alopius vulpinus* and *A. superciliosus*), which use metabolic heat production to elevate their body temperature but do not defend a thermal set point[12,13], have intermediate, cosmopolitan ranges that lack a strong latitudinal signal.

Some ecologists have posited that endotherms, with their high-energy demands, are generally restricted to temperate seas because they are more productive (see [14] and references therein). While high productivity may be necessary for endotherm populations, it is not sufficient. Analysis of annual pelagic NPP at global scales reveals a very weak latitudinal signal that is actually higher in the tropics for some production models (Fig. S4, S5). Similarly, fishery catch rates, a measure of fish productivity, also bears little relationship to latitude or sea surface temperature[15]. Records of benthic productivity in tropical coral reefs are among the highest annual rates of benthic marine productivity recorded[16], rivaling temperate, kelp-dominated coastal systems[17]. Finally, the diversity of oceanic dolphins and aerial-foraging seabirds, which thrive in the tropics (Fig. S2, S6), attests to the availability of sufficient food to support endotherm populations, if it can be procured.

As an alternative to the energy supply hypothesis, we propose that patterns of diversity in large marine predators are mostly due to the effects of environmental temperature on the energetic costs and benefits of foraging. We present a conceptual framework showing how key physiological and behavioral components of predation differ between endotherms and ectotherms and how these differences can account for their contrasting biogeographic patterns. We first consider the elements of foraging,

then link relevant rates to environmental variables, and finally to patterns of global diversity. The resulting hierarchy of mechanistic models makes testable predictions for the different levels of interaction: from individual foraging to ecosystem energy fluxes and biogeographic patterns of species richness.

A Metabolic Model of Vertebrate Predation in Marine Ecosystems

Foraging and locomotion, like all activity, is supported by metabolism, the processing of energy and materials to sustain life. Temperature *T* drives the kinetics of metabolic and organismal rates *R*, as:

(1) $$R = R_0 e^{-E0k/T}$$

where R_0 is a normalization constant, E_0 is a metabolic 'activation energy' (~0.65 eV), *k* is Boltzmann's constant, and *R* is corrected for body size effects[18,19]. Ecological rates tend to be somewhat higher, with a mean activation energy of ~1 eV for competitive and predatory interactions[20].

Two fundamental components of foraging are the encounter rate of prey (E_n) and the capture per encounter ratio (C_a/E_n), which comprise the maximum individual consumption rate (C_{Ind}), also known as the Type I functional response[21] (Fig. 3). Both of these components reflect the metabolic rates of locomotory muscles that govern organismal speed. The encounter rate is a function of the density of prey (D_{prey}) and the routine velocities (*V*) of predator and prey, which determines the rate at which predator and prey paths intersect (I_{Path}):

(2) $$E_n \propto D_{Prey} I_{Path} \propto D_{Prey} \sqrt{{V_{Pred}}^2 + {V_{Prey}}^2}$$

Swimming speed is a well-studied behavioral parameter that directly mediates prey capture and escape[22]. We expect the capture per encounter ratio to increase as the ratio of predator to prey burst speed (S_{Pred}/S_{Prey}) increases. For ectothermic hunters chasing ectothermic prey, $S_{Pred,Ecto}/S_{Prey,Ecto}$ does not generally vary across thermal gradients, as both predators and prey speeds shift in a similar fashion with temperature. But for endothermic hunters this is not the case. Instead, endothermic predators will be relatively faster than prey in cold waters, reflecting their asymmetric metabolic response to water temperature (Fig. 4). While the exact relationship between $S_{Pred,Endo}/S_{Prey,Ecto}$ and C_a/E_n has received little attention, this is expected to be a positive relationship: e.g., $C_a/E_n \propto (S_{Pred,Endo}/S_{Prey,Ecto})^{\alpha}$, where $\alpha > 0$.

For endothermic predators feeding on mobile ectothermic prey we can substitute Eq. 1 into Eq. 2 to reveal the temperature dependence of path intersection:

(3) $$I_{Path} \propto \sqrt{K^2 + v_{r0}e^{-2E/kT}}$$

where v_{r0} is a normalization constant, K is a constant representing routine swimming speed of endotherms (~1.5 m/s)[23]. We can also use Eq. 1 to show the temperature dependence on capture per encounter ratio for endothermic hunters of ectotherms:

(4) $$\frac{C_a}{E_n} \propto \left(\frac{S_{Pred,Endo}}{S_{Prey,Ecto}}\right)^{\alpha} \propto e^{E_1/kT}$$

Here E_1 is some integrative function of E_0 (i.e., $E_1 = \alpha E_0$). Because capture involves multiple, potentially multiplicative rates (e.g. detection and pursuit), E_1 may be higher than metabolic activation energies of 0.65 eV, and closer to observed ecological rates of 1 eV. Note that Eq. 3 and 4 indicate opposing responses to consumption with water

temperature; path intersection rates fall in cold water as prey speeds decline but endotherm capture per encounter ratios will increase as sluggish prey become easier to capture.

While individual consumption is limited by handling and satiation in nature, maximum consumption rates C_{Ind} are indicative of food that can potentially be converted into offspring. Consequently, C_{Ind} is relevant for linking individuals to population growth rates. The response of C_{Ind} to water temperature is determined by the relative magnitude of the respective foraging components. Substitution of empirical data for routine swimming speed into Eq. 3 indicates a ~40% decline in path interaction rates from the tropics to the poles (i.e, 30 to 0 ºC; see Methods). But if $E_1 \geq E_0$, as studies suggests[20], this decline is more than offset by the ≥15fold increase in capture per encounter values. Therefore, we expect endotherms to generally increase their consumption rate in colder waters, controlling for other environmental factors.

To link endotherm per capita consumption to ecosystem consumption, we recognize that total endotherm consumption C_{Tot} is limited by prey production P_{Prey} and assume that maximum per capita consumption rates (C_{Ind}) function as a rate variable, yielding a logistic-type equation:

(5) $$C_{Tot} = \frac{P_{Prey}}{1+be^{-\ln(C_{Ind})}}$$

where b is a coefficient and $C_{Ind} \propto (I_{Path})(D_{Prey})(S_{Pred}/S_{Prey})$. To isolate the role of water temperature and facilitate analysis, we rearrange and log transform Eq. 5 and substitute from Eq. 3 & 4 to generate the linear model:

(6) $$\ln\left(\frac{P_{Prey}}{C_{Pred}} - 1\right) + \ln(I_{Path}) = \ln(B) - \left(\frac{E_1}{kT}\right)$$

To test model predictions, we analyzed ecosystem data on marine mammals. Mammal consumption C_{Tot} was determined from abundance counts and habitat preferences of pinnipeds and small toothed whales[24,25], while P_{prey} was calculated from Net Primary Production (NPP) values, assuming 10% trophic transfer efficiency[26]. Among cetaceans, we restricted our analysis to small toothed whales (e.g., dolphins and porpoises), which feed at a trophic level of ~4 and whose thermal environment for feeding generally corresponds to sea surface temperature[27]. Values for D_{Prey} are difficult to gather, but we considered chlorophyll density as a potential proxy.

Tests: Linking Consumption to Richness

The thermal sensitivity of total mammal consumption is similar to that of individual trophic interactions. The fitted slope yields an activation energy of 1.03, close to E ~1 observed for ecological rates[20]. This translates to a 80fold increase in consumption from the equator to poles due to temperature (Fig. S7; $\ln(P_{prey}/C_{Tot} - 1) + \ln(I_{path}) = 46.12 - 1.043(1/kT)$, $r^2 = 0.71$, n = 25,847). Inclusion of the additional predictor variables of distance to shoreline and ocean depth does not significantly change the temperature coefficient (CI: -1.051 to -1.035 for original vs. -1.050 to -1.034 with additional predictors). A 4.6x increase in chlorophyll from the equator to the poles (Fig. S8), a possible proxy for prey density, could potentially reduce the magnitude to 17fold. Collectively, the results indicate a substantial 1 to 2 orders magnitude increase in total endotherm consumption and abundance from the tropics to the poles due to temperature.

The increase in mammal consumption in colder waters reflects the marked increase in abundance as water temperature drops (Fig. S7). Ecologically, marine mammals shift from minor players in the tropical seas that consume, on average, less than 1% of available of food, to major predators near the poles, ingesting one fifth of all food (Fig. 5). These results are conservative, as potential food lost to planktivorous baleen whales, marine birds and human harvest further limits the prey available to pinnipeds and toothed whales. With the exception of dolphins, marine endotherms are generally rare or absent until mid-temperate latitudes, suggestive of thermal filtering (Fig. 2).

The disparate patterns of biogeography among thermoregulatory guilds can be visually summarized by plotting the ratio of endotherm to ectotherm richness (Fig. 6). Marine mammals and birds dominate apex predator richness in coastal habitats above 30º latitude or below 20 ºC sea surface temperature. Fitting the endotherm/ectotherm richness ratio against temperature and distance from shore reveals a 32fold shift in diversity towards endothermy from 30 to 0 ºC [$ln(ratio) = -34.96 + 0.769(1/kT) + 0.432(ln(distance))$; $r^2 = 0.70$, n = 25,048]. As indicated by the positive slope for distance to shore, endotherms are also favored in the open ocean, even comprising the majority of richness in tropical open seas where dolphins are diverse. These pelagic habitats are also home to an array of high-power, mesothermic tuna, billfish and sharks (e.g., mako and thresher sharks). The evolution of mesothermy among pelagic fish, which often pursue prey in clear open waters, is indicative of the advantages gained by elevated metabolism when prey cannot hide and locomotory power is at a premium.

Our model indicates that the success of endotherms in cold and open waters is primarily due to the locomotory and sensory benefits that increases the capture per prey encounter ratio. Muscle contraction rates, acceleration, and routine swimming speeds increase in an approximately exponential fashion with temperature in ectotherms and close to theoretically expected values (Fig. S9). In contrast, endothermic burst speeds are insensitive to ambient temperature, generating a performance asymmetry that favors endotherms in cold waters (Fig. 4). Visual rates in fish, including flicker fusion frequency and saccadic eye movement, also increase with temperature at rates equaling or exceeding theoretical predictions (Fig. S10). The ecological significance of elevated sensory rates are underscored by the unique mesothermic physiology of billfish, which metabolically elevate temperatures in their eyes and brain, but no other organ, to increase visual processing speeds[28]. Overall, the thermal sensitivity of metabolism favors endotherm foraging where prey are slow, stupid, and cold.

Beneficial metabolic asymmetries granted by cold waters are not restricted to endotherms foraging on ectotherms. Indeed, many species of ectothermic sharks are capable of preying on marine mammals and birds. Figure 4a suggests that predation pressure from sharks will decline as endotherms move away from the warm tropics and sharks become slower. This may result in behavioral shifts in predatory sharks, from pursuit in the warm tropics to ambush in cold temperate seas. This is perhaps best illustrated by polar Greenland and sleeper sharks, whose very slow swimming speeds[29] suggests successful hunting occurs largely when warm-bodied prey are caught napping.

Conversely, high predation pressure by tropical Galapagos and tiger sharks is likely an important factor in the slow recovery of the endangered Hawaiian monk seal[30].

The systematic increase in marine mammal abundance in colder water latitudes holds the key to understanding how endotherms diversified more rapidly in higher latitudes (Fig S7). Larger populations sizes reduce local extinction risks and permit niche specialization, allowing multiple species to coexist by pursuing different prey[31,32]. For instance, incipient speciation of killer whales (*Orcinus orca*) is in progress in the eastern North Pacific, where 'transient' mammal-feeding populations overlap but do not interbreed with fish-eating 'residents' or 'offshore' populations that specialize on sharks and large teleosts[33]. Further, the absence of many endotherm families in the tropics (Fig. S11) indicates that thermal constraints on foraging may place strong limits on the potential of endotherms with certain body plans or foraging strategies to enter and radiate in warm waters.

Consideration of burst speeds offers additional insight into variation in endotherm distributions and diversity. Among endotherms, warm shallows seas are primarily limited to oceanic dolphins (Fig 2, S2), which possess burst speeds of nearly twice the rate of pinnipeds and penguins (Fig. 4B). One straightforward consequence of their elevated speeds is an expansion of their thermal range and prey base. In addition, dolphins have uniquely large brains that assist in cooperative foraging, such as herding fish, which mitigates locomotory challenges posed by fleet tropical prey[34]. Compared to dolphins, swimming birds, otters, and pinnipeds are all relatively slow and solitary foragers of benthic and pelagic prey. These families are rare or absent from warm-water

habitats (Fig 2, S1), despite high production rates along many tropical coastlines (Fig. S4). Instead, tropical waters are feeding grounds for several families of birds that forage by aerial plunging or alighting on surfaces (Fig. S6). Plunge-diving species, such as gannets, can attain exceptional speeds upon entry to water (~24 m/s)[35], and can readily depart waters if threatened. Further, sperm whales (Physeteridae & Kogiidae), which forage in deep, cold waters at all latitudes, are not expected to be limited to high latitudes and are, indeed, cosmopolitan (Fig. S2). Likewise, sirenians, whose large bulk protects them from many predatory sharks, are able to forage for immobile seagrass in warm tropical seas.

Finally, global patterns of mammal consumption and theory shed light on the competitive interactions between predatory endotherms and ectotherms. According to resource-competition theory[36], ectothermic sharks are potentially lethal competitors for endotherms because their slow metabolism permits them to reduce prey densities low enough to exclude endotherms. Yet endotherms thrive in polar waters where ectotherm metabolism is lowest and their potential prey-reduction abilities are greatest (Fig. 5B). This likely reflects the advantages high locomotory and sensory rates offer in permitting endotherms (and mesotherms) to more quickly access transient food resources, interfere, and/or consume their competitors' offspring. At least in productive environments, it appears that where metabolic power diverges endotherms thrive and ectotherms dwindle.

Conclusion

Both foraging theory and global patterns of consumption point towards a common mechanism underlying high endotherm diversity in cold seas. Warm waters reduce food accessibility and expose endotherms to dangerous ectothermic predators. The consequence is a decline in total endotherm abundance that limits opportunities for niche specialization and speciation. Further, warm waters impose an environmental filter that bars entry to taxa with certain body plans and foraging styles. In particular, solitary and slower-moving birds and mammals are disadvantaged in the warm tropics, leading to a sharp decline in familial richness and phylogenetic diversity. The consequence for marine endotherms is a striking departure from the general biogeographic rule of richness peaking in the tropics.

Methods

Range distributions of large predatory ectotherms, mesotherm and endotherms were collected for our analysis. Distributions for birds were acquired from BirdLife International (www.birdlife.org) and all mammal, reptile and shark data from the IUCN (www.iucnredlist.org). Analyses of teleost clades were restricted to taxa with at least 10 species, of which the majority were capable of reaching 1 meter in length. The bulk of fish spatial data was also acquired from the IUCN, but missing species of barracuda and jacks were supplemented from Aquamaps (www.aquamaps.org), which utilizes observation data stored in OBIS (www.iobis.org). Small toothed whales examined here include all members of Odontoceti except *Physeter* and Ziphiidae. Data on locomotory and metabolic rates were compiled from the literature including speeds for pinnipeds[37-

[42], penguins[43-46], and dolphins[47,48] (see also citations in the supplemental captions). Contraction time t and body length L can be used to calculate maximum speed S, where $S = 0.7L/2t$.[49] This formula was used to generate the burst swimming speeds of fish shown Figure 4B, based on muscular contraction rates reported from Wardle[49]. Fish data for Fig 4B includes one species of tuna, but at small sizes where tuna are effectively ectothermic. See also Figure S9. Routine velocities for endotherms to calculate I_{Path} were taken from the literature (~1.5 m/s)[23]. For fish, the average routine swimming speeds of an important forage fish, Atlantic mackerel (*Scomber scombrus*; 23 cm fork length) was used to represent prey routine speed[50]. To generate prey routine speeds at all temperature the following formula was applied: Speed = $B_0 e^{-0.65/0.00008617T}$ where speed = 0.287 m/s at 283.16 Kelvin.

Mammal total consumption data was determined from compilation of abundance records, niche modeling of habitat preferences, and metabolic scaling with body size[24,25]. Niche preferences for distance to land (e.g., coastal vs pelagic), distance from ice, water temperature preferences, and evolutionary origin were gathered from the literature and used to construct range maps for marine mammals and a density function that spread abundances across space. Food availability was not considered in determining patterns of mammal spatial abundance; therefore, analysis of scaling consumption with prey density and production merits further study. Analyses were performed in R *v.* 3.2.4[51], QGIS *v.* 2.12.1[52] and JMP *v.*12.1.0[53].

Figures

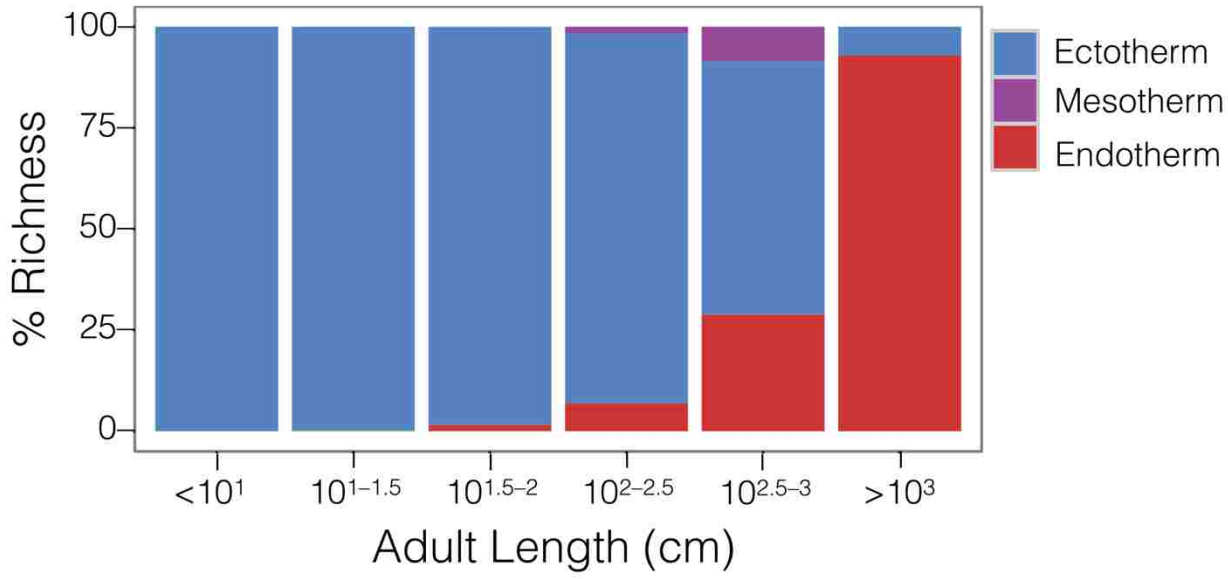

Figure 1. Global marine diversity for thermoregulatory guilds at varying body sizes. The total diversity of marine taxa was compiled from the literature, including marine fish and sharks[54], reptiles[55-57], mammals[58,59] and birds[60 59] and percentages of marine diversity were calculated for each length bin. For reptiles and fish, which often continue to grow after sexually mature, maximum body length was recorded; for mammals and birds adult size was recorded. Body length data for some species of fish were not available. The percentage of species without length data was determined, and a correction was applied by adding a value corresponding to the missing percentage to each bin. Each bin represents one half an order of magnitude of length, where $10^{0.5}$ cm equals 3.16 cm, $10^{1.5}$ cm = 31.6 cm, etc.

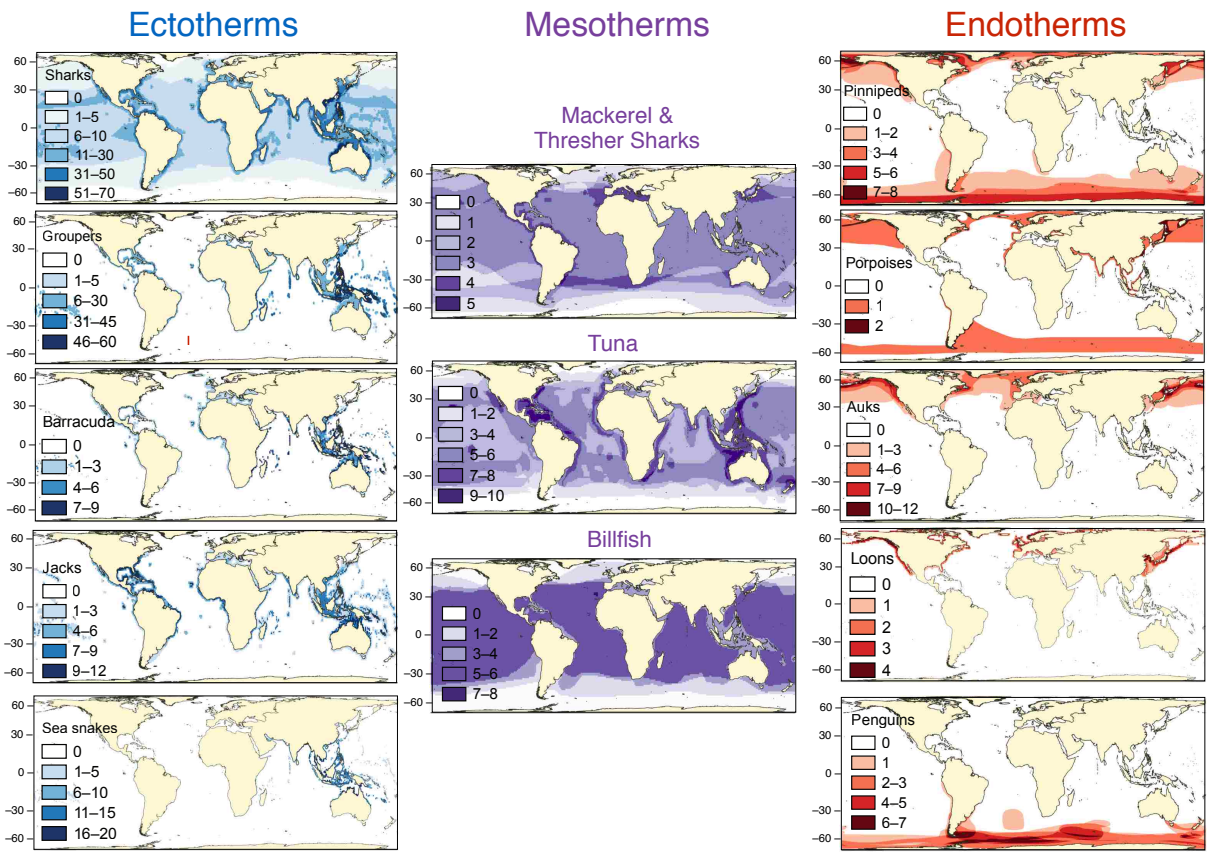

Figure 2. Global patterns of richness in large marine predators. Ectothermic apex predators are most diverse in tropical and warm-temperate coastal habitats, particularly in the Indo-Pacific region. Mesothermic predators (see text) are equally diverse in the tropics and mid-temperate latitudes, only declining above 45º. Endothermic marine mammals and swimming birds are generally absent or low diversity in the tropics, with diversity peaking above 30º.

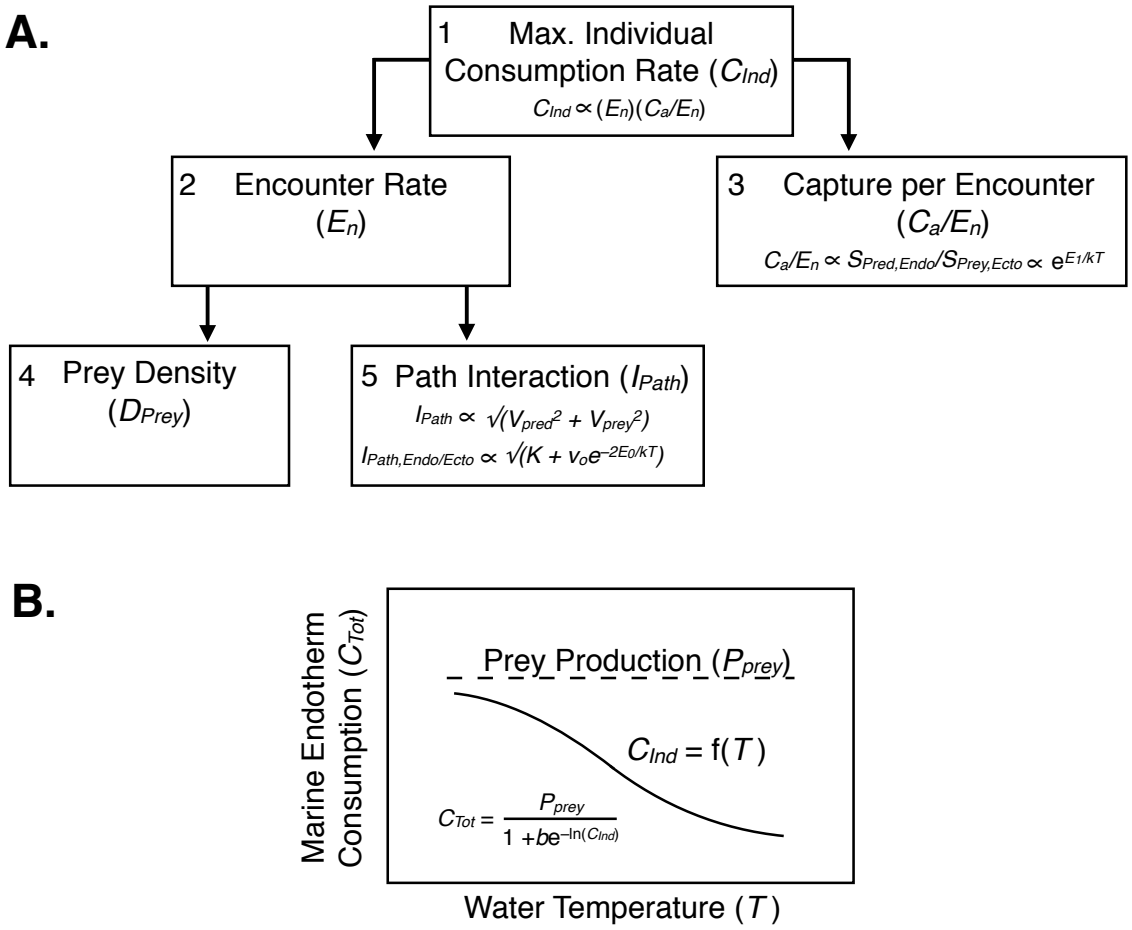

Figure 3. Diagram of foraging model. **A.** The maximum consumption rate C_{Ind} (1) is the product of the encounter rate E_n (2), capture per encounter ratio C_a/E_n (3) and prey mass per capture (not shown). The encounter rate can be further decomposed into prey density (4) and the path interaction I_{Path} rate (5). The capture per encounter ratio is proportional to the relative burst speed of predator vs. prey (S_{Pred}/S_{Prey}), and I_{path} is proportional to the root mean square of predator and prey speeds. Since prey speed is sensitive to ambient thermal shifts, both E_n and C_a/E_n will be functions of water temperature T. **B.** C_{Ind} acts as a rate and prey production as a limit to generate a logistic-type response of total endotherm consumption to water temperature.

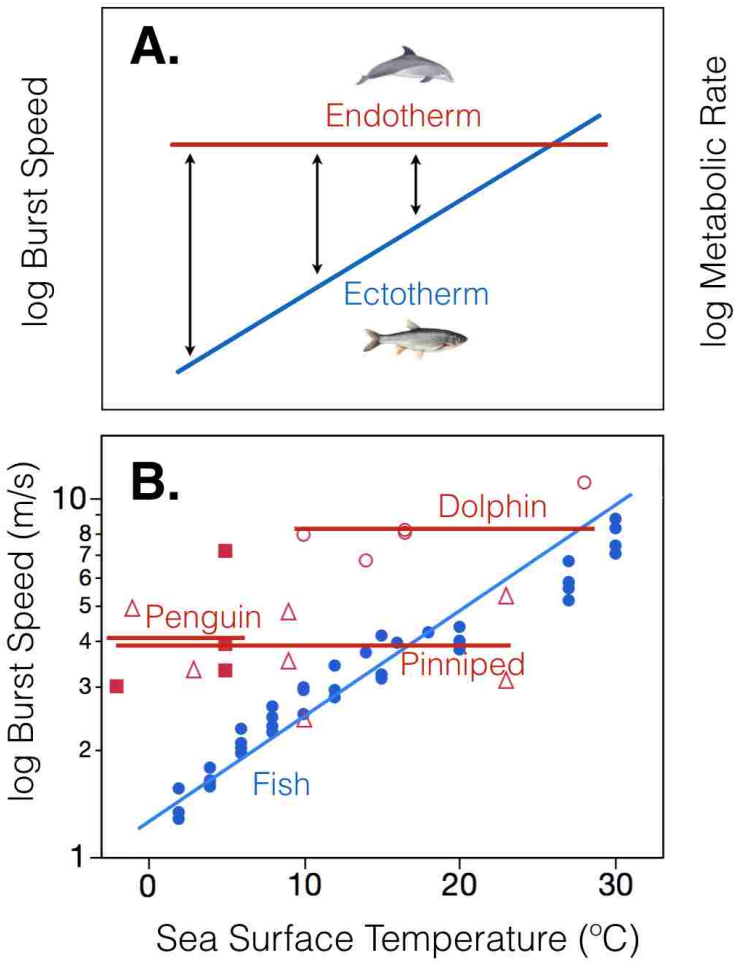

Figure 4. Metabolic asymmetry between endotherms and ectotherms. A. Endotherm metabolic and performance rates are predicted to be insensitive to water temperature, while ectotherm rates generally respond in an exponential fashion (*sensu* [20]). Thus S_{Pred}/S_{Prey} increases in cold water for endothermic predators and ectothermic prey. **B.** Data from the literature on fish and endotherm speed supports our schematic predictions. The geometric mean burst speed for dolphins[47,48] was 8.2 m/s (stand. dev. = 1.2); penguins[43-46] 4.1 m/s (s. d. = 1.5); pinnipeds[37-42] 3.9 m/s (s. d. = 1.3). For fish[49], 5 species were analyzed, with temperature and species as predictor variables, yielding $\ln(y) = 0.068T$, n = 43, $r^2 = 0.98$ (shown) or $\ln(y) = -0.48(1/kT)$, where T is in kelvins.

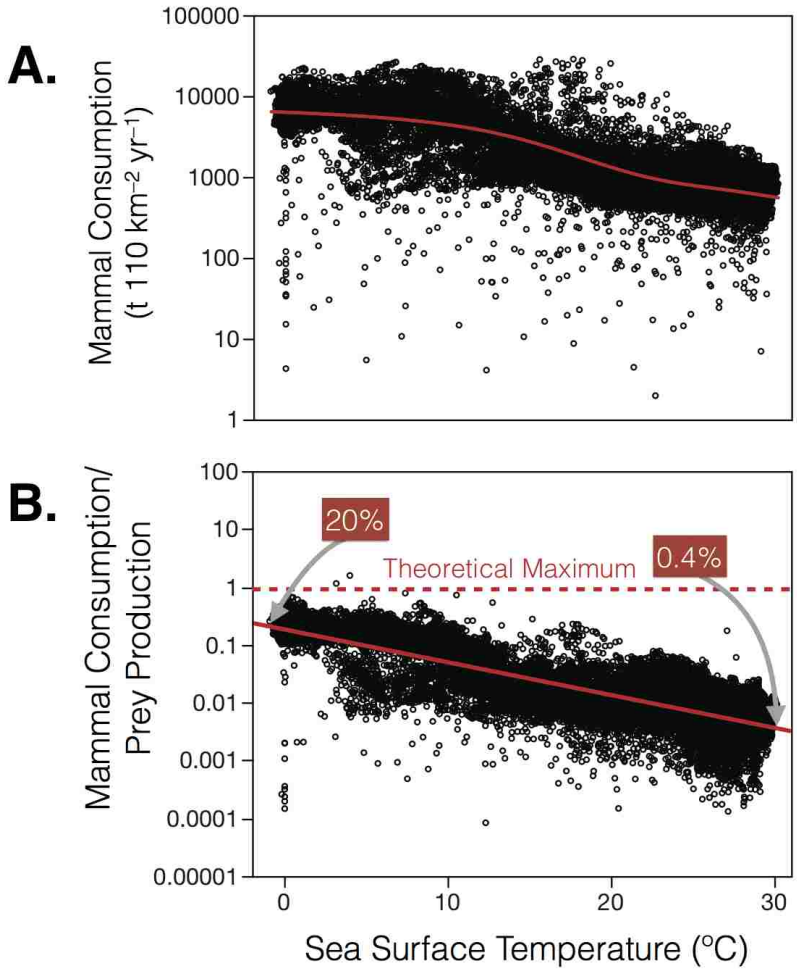

Figure 5. Total consumption in marine mammals. Each point represents data for a 110 km x 110 km cell. **A.** As sea surface temperatures decline, pinnipeds and small odontocetes increase their total consumption, following the theoretical form of Fig 3B: $\ln(\text{consumption}) = \ln(P_{Prey}/(1 + 3.04e^{1.37T}))$, where T is sea surface temperature (ºC) and P_{prey} is spline fit of ln(prey production) vs sea surface temperature (lambda = 100,000). **B.** The fraction of available energy consumed by mammals declines with increasing water temperature, where y = 1.69 – 0.131x, $r^2 = 0.68$, y = 25,849. Prey production rates are calculated from NPP assuming 10% trophic transfer efficiency and mammal trophic level of 4.

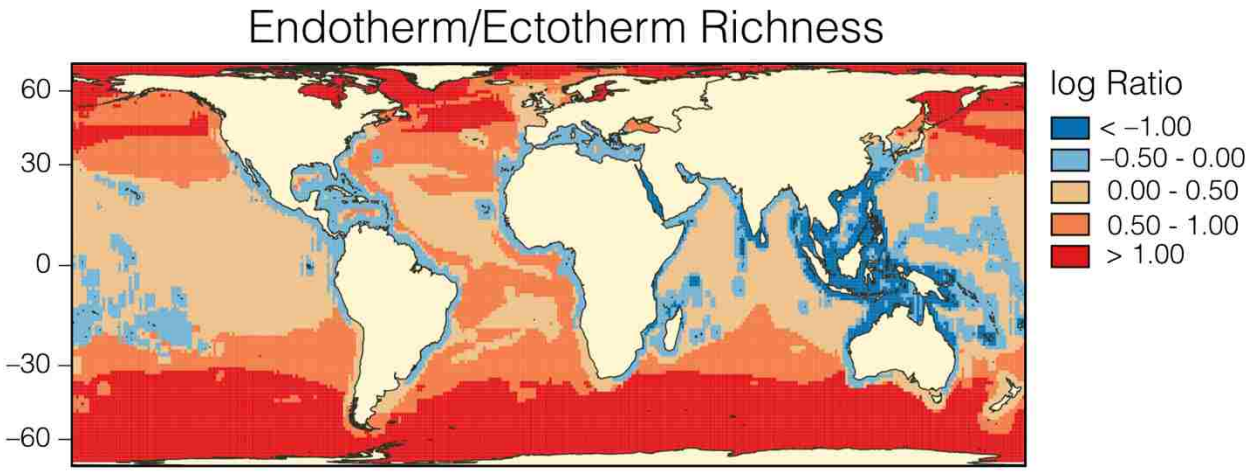

Figure 6. Relative richness of major predatory taxa. Large ectothermic predators (sharks, groupers, barracuda, jacks, sea snakes) contribute the highest fraction of community richness in tropical and subtropical coastal waters (blue), while endothermic swimming birds and mammals dominate cold waters and open oceans (red). In areas where no large predatory ectotherms were recorded, e.g., near coastal Antarctica, the highest ratio value was assigned.

References

1 Pyenson, N. D., Kelley, N. P. & Parham, J. F. Marine tetrapod macroevolution: Physical and biological drivers on 250Ma of invasions and evolution in ocean ecosystems. *Palaeogeogr., Palaeoclimatol., Palaeoecol.* **400**, 1-8 (2014).

2 Jarvis, E. D. *et al.* Whole-genome analyses resolve early branches in the tree of life of modern birds. *Science* **346**, 1320-1331 (2014).

3 Williams, T. M. The evolution of cost efficient swimming in marine mammals: limits to energetic optimization. *Philosophical Transactions of the Royal Society of London B: Biological Sciences* **354**, 193-201 (1999).

4 Estes, J. A., Tinker, M. T., Williams, T. M. & Doak, D. F. Killer whale predation on sea otters linking oceanic and nearshore ecosystems. *Science* **282**, 473-476 (1998).

5 Ainley, D. G., Ballard, G. & Dugger, K. M. Competition among penguins and cetaceans reveals trophic cascades in the western Ross Sea, Antarctica. *Ecology* **87**, 2080-2093 (2006).

6 Cairns, D. K., Gaston, A. J. & Huettmann, F. Endothermy, ectothermy and the global structure of marine vertebrate communities. *Marine Ecology-Progress Series* **356**, 239 (2008).

7 Pianka, E. R. Latitudinal gradients in species diversity: a review of concepts. *Am. Nat.*, 33-46 (1966).

8 Hillebrand, H. On the generality of the latitudinal diversity gradient. *The American Naturalist* **163**, 192-211 (2004).

9 Tedersoo, L. *et al.* Global diversity and geography of soil fungi. *Science* **346**, 1256688 (2014).

10 Tittensor, D. P. *et al.* Global patterns and predictors of marine biodiversity across taxa. *Nature* **466**, 1098-1101 (2010).

11 Faith, D. P. Conservation evaluation and phylogenetic diversity. *Biol. Conserv.* **61**, 1-10 (1992).

12 Grady, J. M., Enquist, B. J., Dettweiler-Robinson, E., Wright, N. A. & Smith, F. A. Evidence for mesothermy in dinosaurs. *Science* **344**, 1268-1272 (2014).

13 Bernal, D., Dickson, K. A., Shadwick, R. E. & Graham, J. B. Review: analysis of the evolutionary convergence for high performance swimming in lamnid sharks and tunas. *Comparative Biochemistry and Physiology Part A: Molecular & Integrative Physiology* **129**, 695-726 (2001).

14 Berta, A., Sumich, J. L. & Kovacs, K. M. *Marine Mammals: Evolutionary Biology*. 3 edn, 135 - 146 (Academic Press, 2015).

15 Worm, B. *et al.* Rebuilding global fisheries. *Science* **325**, 578-585 (2009).

16 Hatcher, B. G. Coral reef primary productivity. A hierarchy of pattern and process. *Trends Ecol. Evol.* **5**, 149-155 (1990).

17 Dayton, P. K. Ecology of kelp communities. *Annu. Rev. Ecol. Syst.*, 215-245 (1985).

18 Gillooly, J. F., Brown, J. H., West, G. B., Savage, V. M. & Charnov, E. L. Effects of size and temperature on metabolic rate. *Science* **293**, 2248-2251 (2001).

19 Dell, A. I., Pawar, S. & Savage, V. M. Systematic variation in the temperature dependence of physiological and ecological traits. *Proceedings of the National Academy of Sciences* **108**, 10591-10596 (2011).

20 Burnside, W. R., Erhardt, E. B., Hammond, S. T. & Brown, J. H. Rates of biotic interactions scale predictably with temperature despite variation. *Oikos* **123**, 1449-1456 (2014).

21 Holling, C. S. Some characteristics of simple types of predation and parasitism. *The Canadian Entomologist* **91**, 385-398 (1959).

22 Domenici, P. & Blake, R. The kinematics and performance of fish fast-start swimming. *J. Exp. Biol.* **200**, 1165-1178 (1997).

23 Sato, K. *et al.* Stroke frequency, but not swimming speed, is related to body size in free-ranging seabirds, pinnipeds and cetaceans. *Proceedings of the Royal Society of London B: Biological Sciences* **274**, 471-477 (2007).

24 Kaschner, K. *Modelling and mapping of resource overlap between marine mammals and fisheries on a global scale*, (2004).

25 Kaschner, K., Watson, R., Trites, A. & Pauly, D. Mapping world-wide distributions of marine mammal species using a relative environmental suitability (RES) model. *Mar. Ecol. Prog. Ser.* **316**, 2-3 (2006).

26 Pauly, D. & Christensen, V. Primary production required to sustain global fisheries. *Nature* **374**, 255-257 (1995).

27 Pauly, D., Trites, A., Capuli, E. & Christensen, V. Diet composition and trophic levels of marine mammals. *ICES Journal of Marine Science: Journal du Conseil* **55**, 467-481 (1998).

28 Block, B. Billfish brain and eye heater: a new look at nonshivering heat production. *Physiology* **2**, 208-213 (1987).

29 Watanabe, Y. Y., Lydersen, C., Fisk, A. T. & Kovacs, K. M. The slowest fish: swim speed and tail-beat frequency of Greenland sharks. *J. Exp. Mar. Biol. Ecol.* **426**, 5-11 (2012).

30 Bertilsson-Friedman, P. Distribution and frequencies of shark-inflicted injuries to the endangered Hawaiian monk seal (*Monachus schauinslandi*). *J. Zool.* **268**, 361-368 (2006).

31 Wright, D. H. Species-energy theory: an extension of species-area theory. *Oikos*, 496-506 (1983).

32 Hutchinson, G. E. Homage to Santa Rosalia or why are there so many kinds of animals? *The American Naturalist* **93**, 145-159 (1959).

33 Moura, A. *et al.* Phylogenomics of the killer whale indicates ecotype divergence in sympatry. *Heredity* **114**, 48-55 (2015).

34 Marino, L. *et al.* Cetaceans have complex brains for complex cognition. *PLoS Biol.* **5**, e139 (2007).

35 Lee, D. N. & Reddish, P. E. Plummeting gannets: a paradigm of ecological optics. *Nature* **2930**, 293-294 (1981).

36 Tilman, D. *Resource competition and community structure*. (Princeton University Press, 1982).

37 Gallon, S. L. *et al.* How fast does a seal swim? Variations in swimming behaviour under differing foraging conditions. *J. Exp. Biol.* **210**, 3285-3294 (2007).

38 Feldkamp, S. D. Swimming in the California sea lion: morphometrics, drag and energetics. *J. Exp. Biol.* **131**, 117-135 (1987).

39 Cheneval, O., Blake, R., Trites, A. & Chan, K. Turning maneuvers in Steller sea lions (*Eumatopias jubatus*). *Mar. Mamm. Sci.* **23**, 94-109 (2007).

40 Ponganis, P. J. *et al.* Swimming velocities in otariids. *Canadian Journal of Zoology* **68**, 2105-2112 (1990).

41 Boyd, I., Reid, K. & Bevan, R. Swimming speed and allocation of time during the dive cycle in Antarctic fur seals. *Anim. Behav.* **50**, 769-784 (1995).

42 Crocker, D., Gales, N. & Costa, D. Swimming speed and foraging strategies of New Zealand sea lions (*Phocarctos hookeri*). *J. Zool.* **254**, 267-277 (2001).

43 Ropert-Coudert, Y. *et al.* Preliminary investigations of prey pursuit and capture by king penguins at sea. *Polar bioscience* **13**, 101-112 (2000).

44 Kooyman, G. L. *et al.* Heart rates and swim speeds of emperor penguins diving under sea ice. *J. Exp. Biol.* **165**, 161-180 (1992).

45 Culik, B. & Wilson, R. P. Swimming energetics and performance of instrumented Adélie penguins (*Pygoscelis adeliae*). *J. Exp. Biol.* **158**, 355-368 (1991).

46 Wilson, R. P., Ropert-Coudert, Y. & Kato, A. Rush and grab strategies in foraging marine endotherms: the case for haste in penguins. *Anim. Behav.* **63**, 85-95 (2002).

47 Fish, F. E. & Hui, C. A. Dolphin swimming–a review. *Mamm. Rev.* **21**, 181-195 (1991).

48 Rohr, J., Fish, F. & Gilpatrick, J. Maximum swim speeds of captive and free-ranging delphinids: Critical analysis of extraordinary performance. *Mar. Mamm. Sci.* **18**, 1-19 (2002).

49 Wardle, C. in *Environmental Physiology of Fishes* (ed MA Ali) 519-531 (Springer, 1980).

50 Macy, W. K., Sutherland, S. J. & Durbin, E. G. Effects of zooplankton size and concentration and light intensity on the feeding behavior of Atlantic mackerel *Scomber scombrus*. *Mar. Ecol. Prog. Ser.* **172**, 89-100 (1998).

51 R: A language and environment for statistical computing. R Foundation for Statistical Computing (R Foundation for Statistical Computing, Vienna, Austria, 2012).

52 Quantum GIS Geographic Information System (2016).

53 JMP Pro v. 9.0 (SAS Institute, Cary, NC, 1998–2014).

54 Froese, R. & Pauly, D. *FishBase 2000: concepts, design and data sources*. (International Center for Living Aquatic Resources Management, 2000).

55 Uetz, P. & Hošek, J. e. (2016).

56 Rasmussen, A. R. in *Bony fishes part 4 (Labridae to Latimeriidae), estuarine crocodiles, sea turtles, sea snakes and marine mammals* Vol. 6 *The Living Marine Resources of the Western Central Pacific: FAO Species Identification Guide for Fishery Purposes.* (eds K. E. Carpenter & V. H. Niem) 3987–4008 (Food and Agriculture Organization of the United Nations, 2001).

57 Pritchard, C. H. & Mortimer, J. A. in *Research and Management Techniques for the Conservation of Sea Turtles* Vol. 4 (eds KL Eckert, KA Bjorndal, FA Abreu-Grobois, & M Donnelly) 21-40 (SSC/IUCN Marine Turtle Specialist Group, 1999).

58 Perrin, W. F. (http://www.marinespecies.org/cetacea, 2016).

59 Myhrvold, N. P. *et al.* An amniote life-history database to perform comparative analyses with birds, mammals, and reptiles. *Ecology* **96**, 3109-3109 (2015).

60 del Hoyo, J., Elliot, A., Sargatal, J., Christie, D. A. & de Juana, E. (Lynx Edicions, Barcelona, 2016).

61 Lambert, O., Muizon, C. & Bianucci, G. The most basal beaked whale *Ninoziphius platyrostris* Muizon, 1983: clues on the evolutionary history of the family Ziphiidae (Cetacea: Odontoceti). *Zool. J. Linn. Soc.* **167**, 569-598 (2013).

62 Behrenfeld, M. J. & Falkowski, P. G. Photosynthetic rates derived from satellite-based chlorophyll concentration. *Limnol. Oceanogr.* **42**, 1-20 (1997).

63 Behrenfield, M. (http://www.science.oregonstate.edu/ocean.productivity/index.php, 2014).

64 Peck, M. A., Buckley, L. J. & Bengtson, D. A. Effects of temperature and body size on the swimming speed of larval and juvenile Atlantic cod (*Gadus morhua*):

implications for individual-based modelling. *Environ. Biol. Fishes* **75**, 419-429 (2006).

65 Fritsches, K. A., Brill, R. W. & Warrant, E. J. Warm eyes provide superior vision in swordfishes. *Curr. Biol.* **15**, 55-58 (2005).

66 Hanyu, I. & Ali, M. Electroretinogram and its flicker fusion frequency at different temperatures in light-adapted salmon (*Salmo salar*). *Journal of Cellular and Comparative Physiology* **63**, 309-321 (1964).

67 Montgomery, J. C., McVean, A. R. & McCarthy, D. The effects of lowered temperature on spontaneous eye movements in a teleost fish. *Comparative Biochemistry and Physiology Part A: Physiology* **75**, 363-368 (1983).

68 Friedlander, M., Kotchabhakdi, N. & Prosser, C. Effects of cold and heat on behavior and cerebellar function in goldfish. *Journal of Comparative Physiology* **112**, 19-45 (1976).

Supplemental Materials and Methods

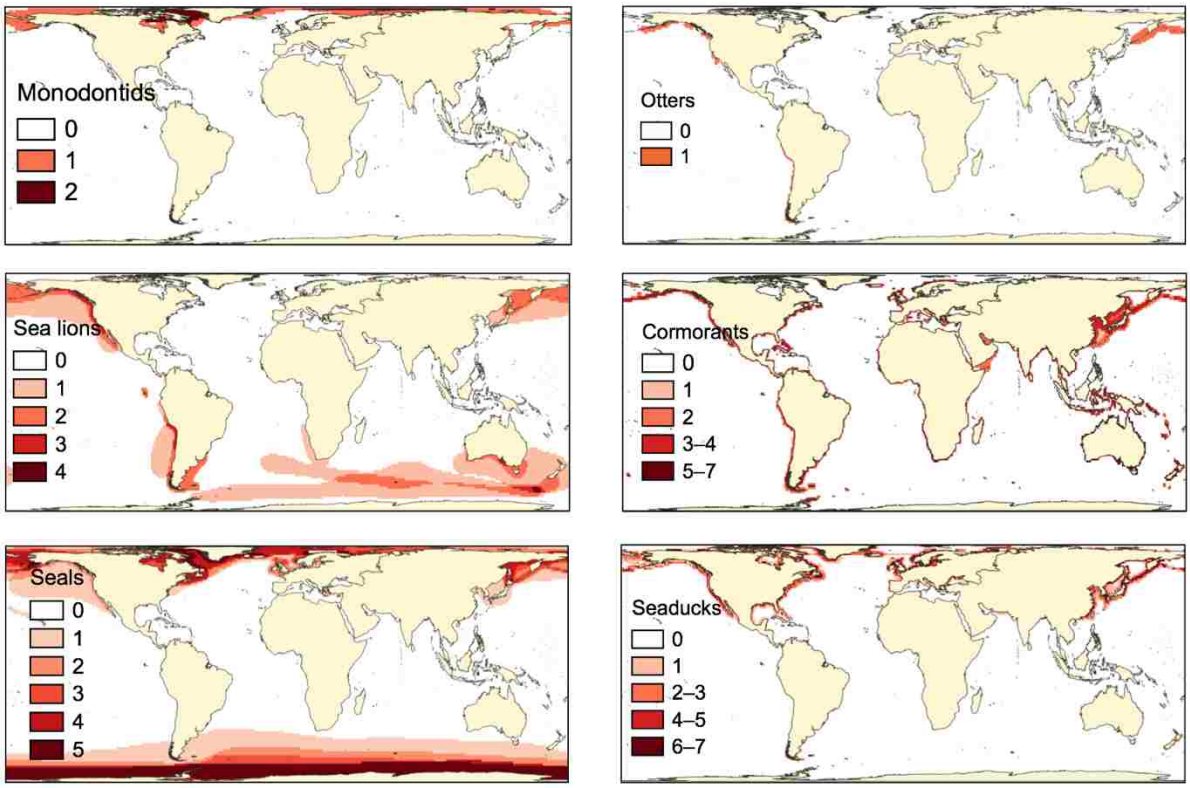

Figure S1. Additional richness patterns in marine mammals and swimming birds.

Monodontids are composed of narwhals and belugas. Sea lions are Otarriidae, seals are Phocidae, cormorants are Phalacrocoracidae, and marine ducks are within Anatidae, primarily Merginae.

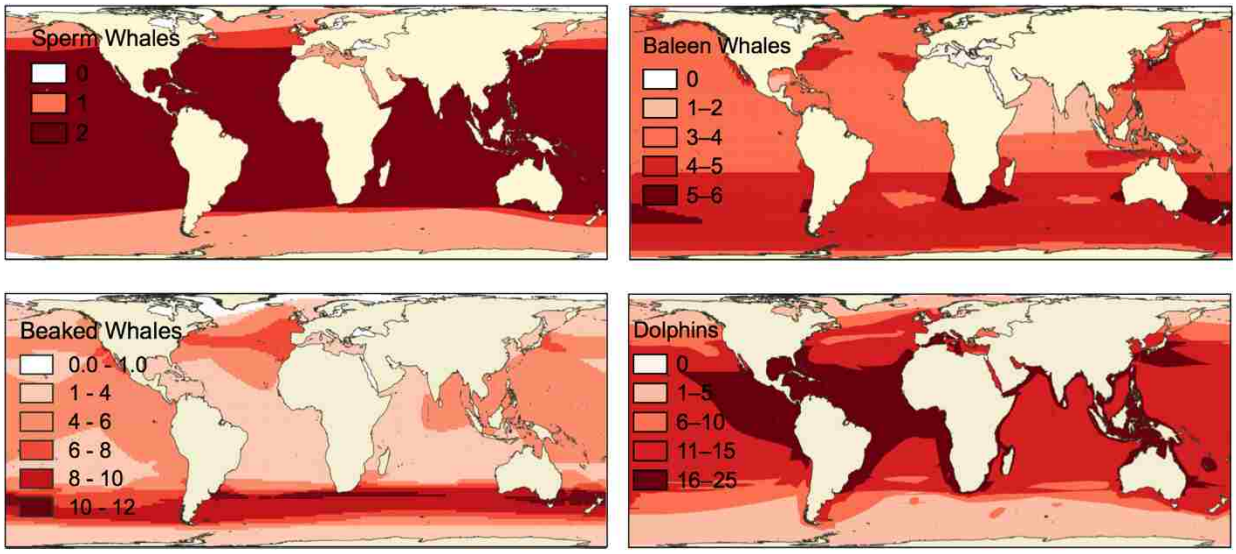

Figure S2. Mammal exceptions that prove the rule. Marine mammals that forage in deep, cold waters or are large planktonic feeders are not expected to show a systematic bias towards temperate waters. Sperm whales (Physeteridae & Kogiidae) are cosmopolitan, beaked whales (Ziphiidae) are found at all latitudes but show peak diversity in low southern latitudes, which may reflect its evolutionary origin[61]. Baleen whales (Mysticeti) largely feed in temperate latitudes where swarms of zooplankton can be found, though many migrate to warm waters to breed. Dolphins (Delphinidae) are exceptionally fast and cooperative, and are able to exploit prey items in tropical as well as temperate seas.

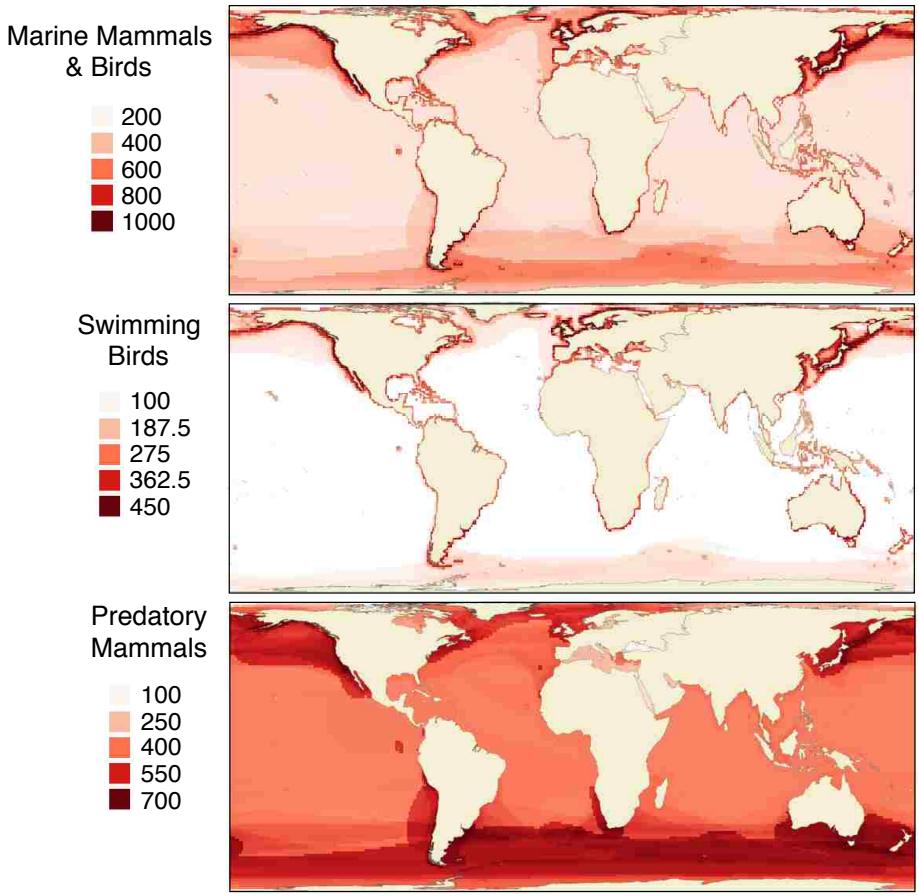

Figure S3. Phylogenetic diversity (PD) of predatory marine mammals and swimming birds. PD is a widely used measure of phylogenetic diversity that is defined as the minimum total length of phylogenetic branches that characterize the species of interest. It incorporates diversity among deeper nodes of the tree in addition to diversity at the branch tips.

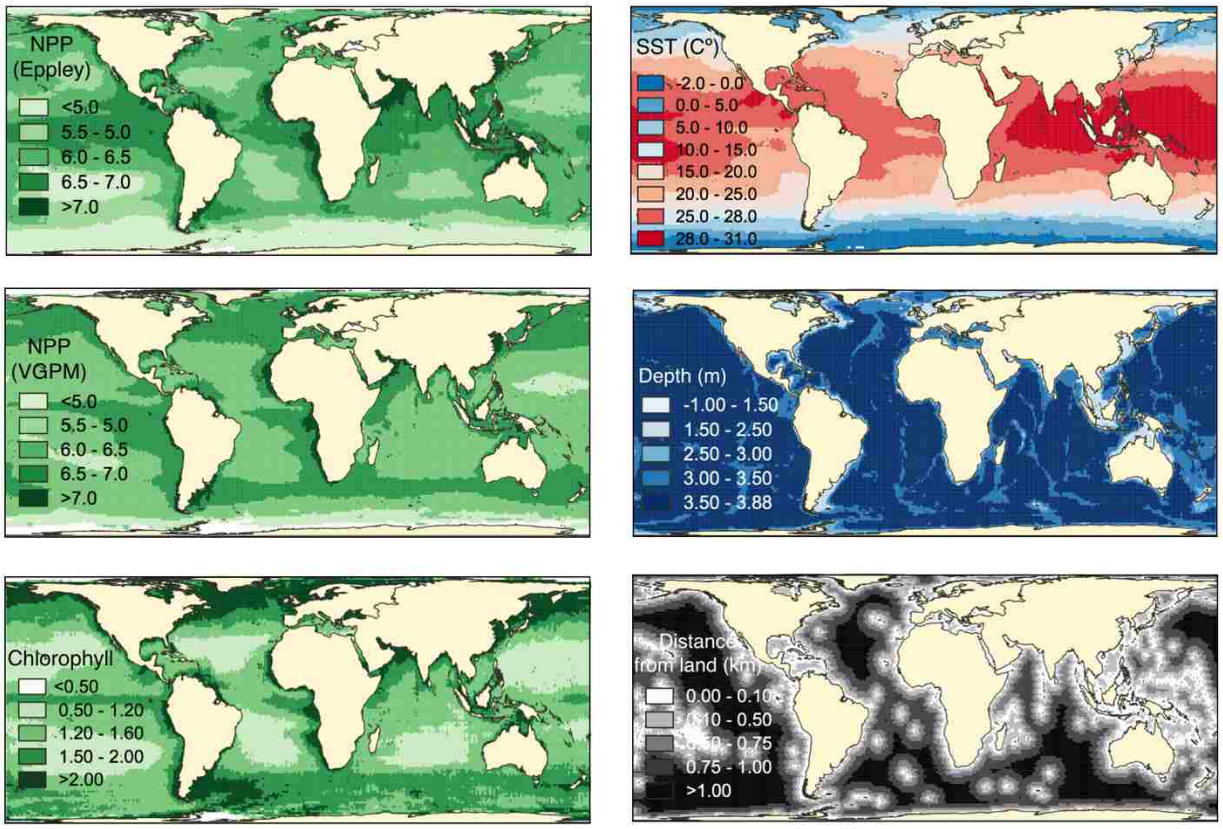

Figure S4. Environmental predictors of endotherm consumption and richness. All values are log transformed, the Eppley and VGPM (vertically generated production model) are two common models of marine net primary production. Units for Chlorophyll *a* are mg m^{-3}, for NPP t*C* $(110\ km)^{-2}\ yr^{-1}$. Chlorophyll is a density or average, while NPP is a total (sum).

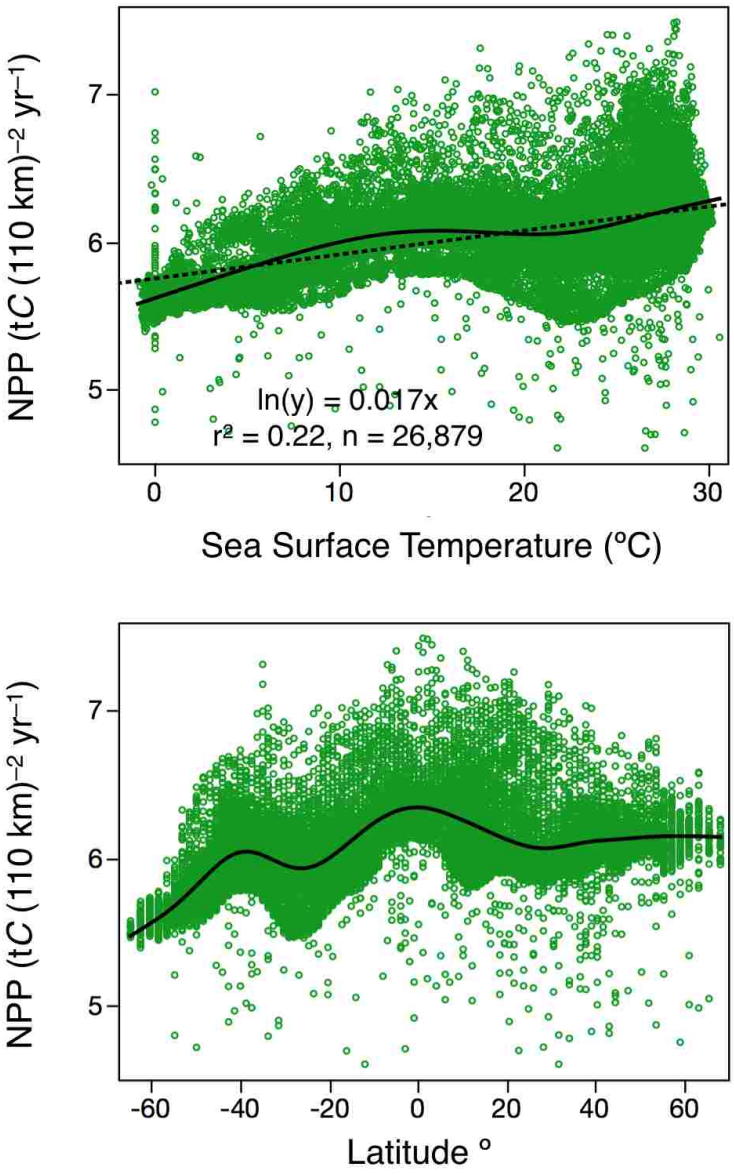

Figure S5. Plots of Net Primary Production (NPP) with sea surface temperature (SST) and latitude. SST and latitude are only weak predictors of NPP, and in the wrong direction to explain elevated endothermic consumption and richness in cold waters. NPP is derived from the Eppley model[62,63]; NPP for cells that experience ice cover were not considered. Splines fits are solid, lambda = 100,000.

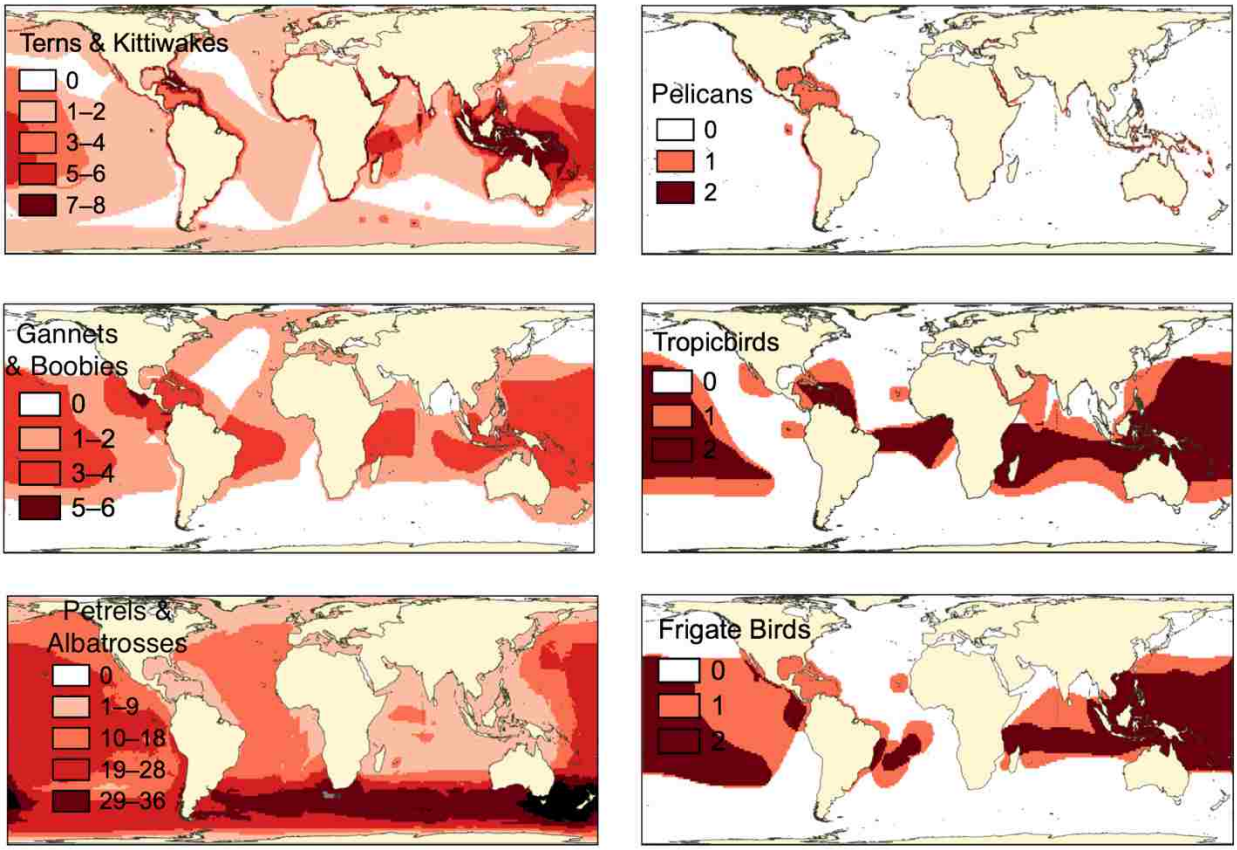

Figure S6. Avian exceptions that prove the rule. Aerial feeding birds can opportunistically feed on surface foods or capture fish with fast plunging dives. This strategy permits species to live throughout the globe, and show diverse distributions. Most families are predominantly tropical, although some families within Procellariiformes (petrels and albatrosses), show peak diversity in southern seas. Terns and kittiwakes belong to Laridae, gannets and boobies comprise Sulidae, pelicans are Pelecanidae, Tropicbirds are Phaethontidae, and frigate birds are Fregatidae.

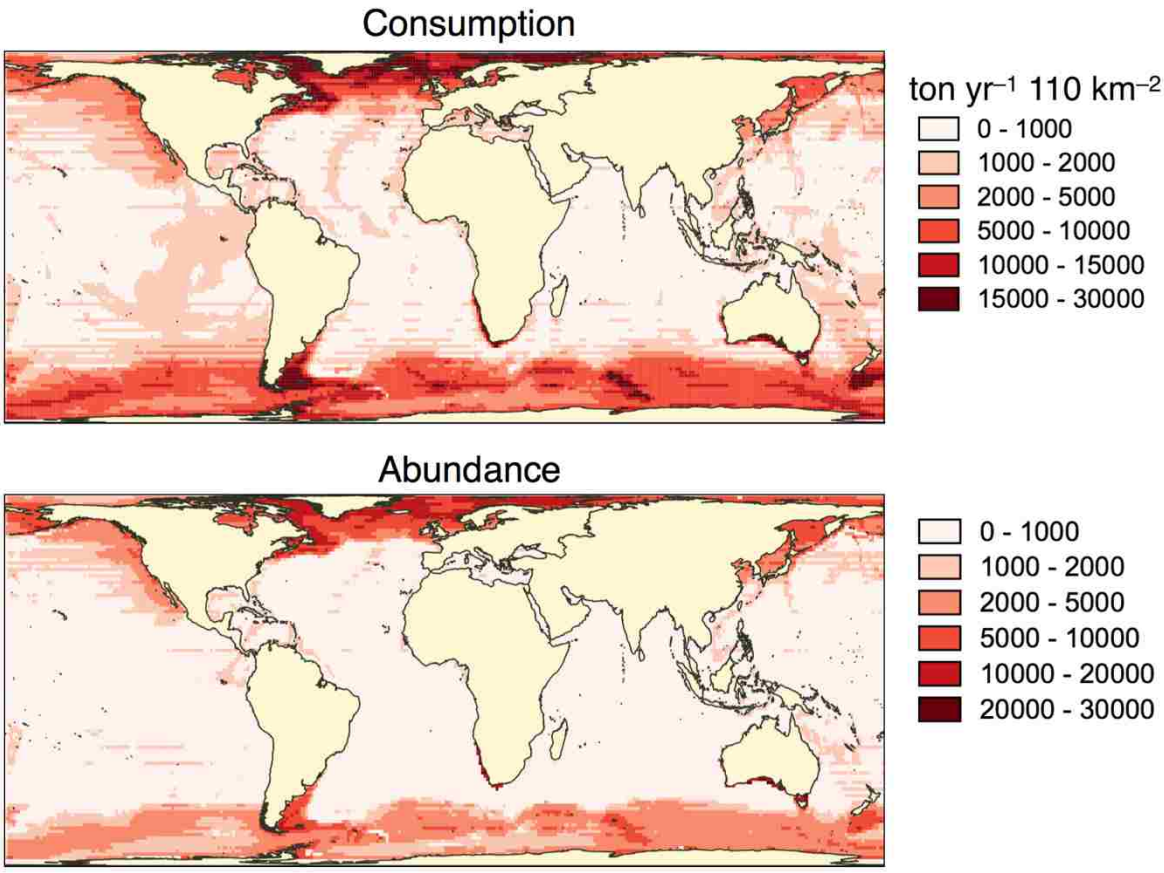

Figure S7. Global patterns of marine mammal abundance and consumption. Pinniped and small odontocete abundance and consumption increase towards high latitudes with cold surface waters.

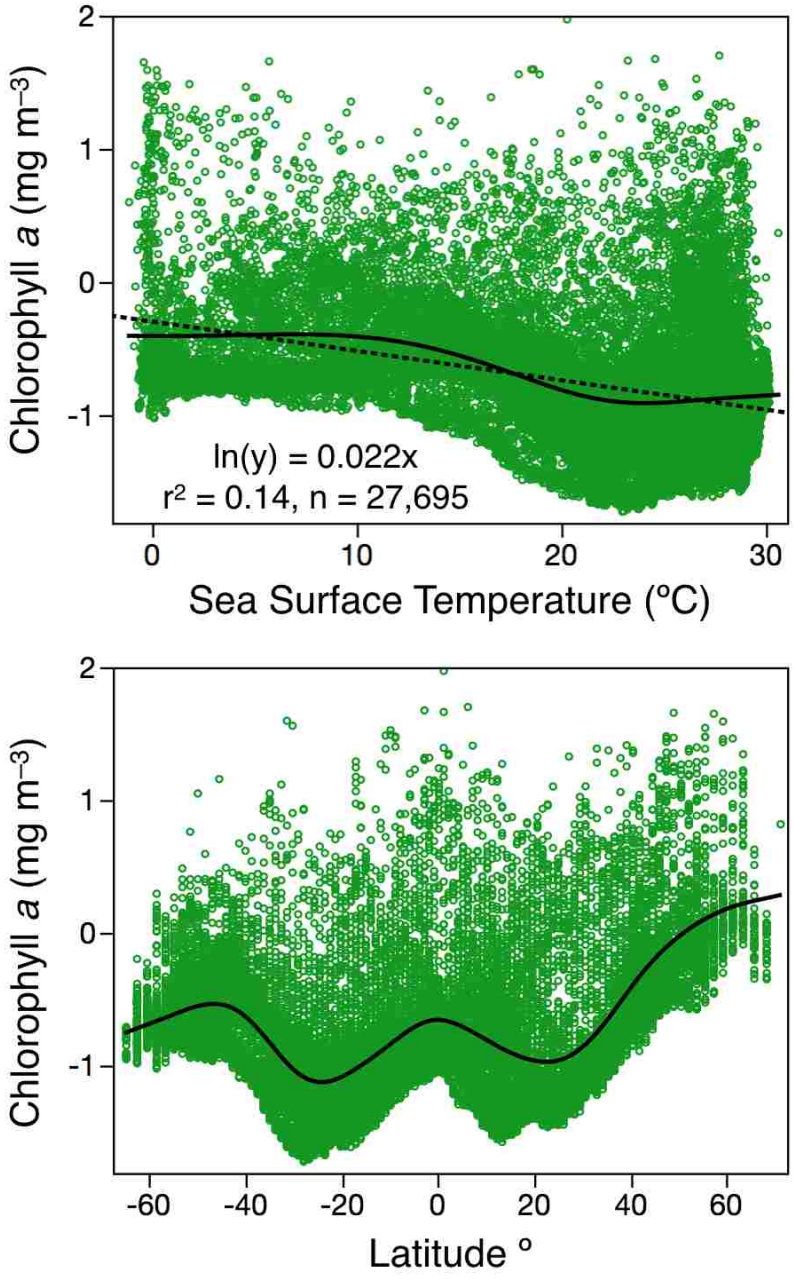

Figure S8. Global patterns of chlorophyll density. Chlorophyll density shows a complicated relationship with temperature and latitude. Forcing a linear regression against temperature (top, dashed line), chlorophyll density declines 4.6fold from 0 to 30 ºC.

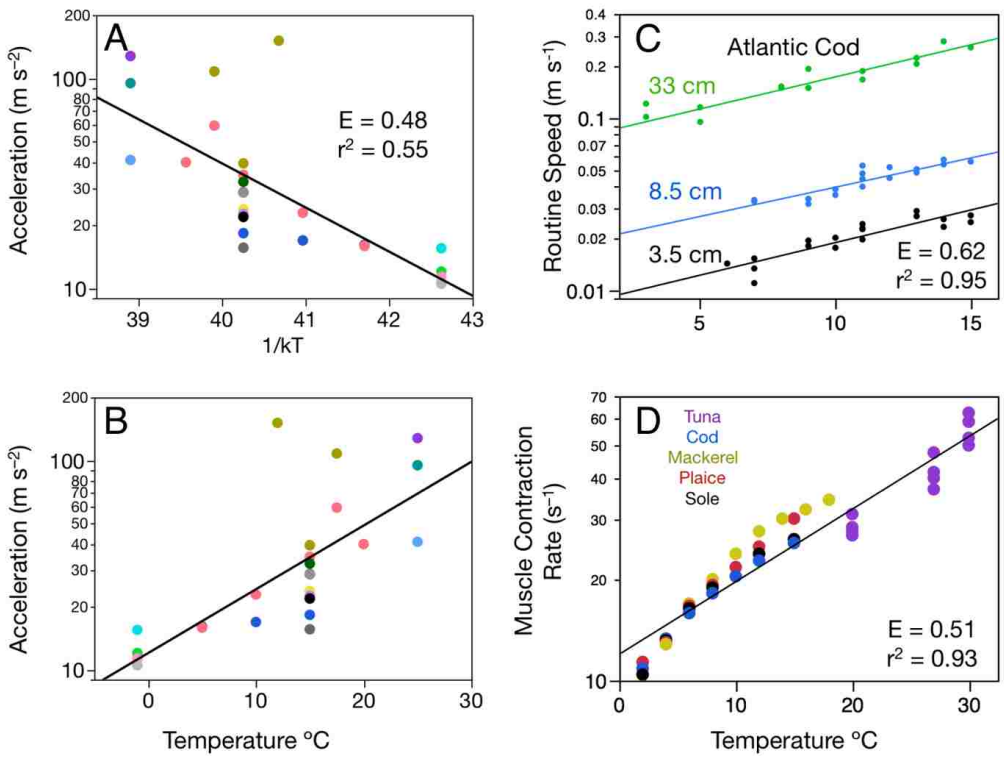

Figure S9. Thermal dependence of metabolic rates. Metabolic rates generally increase in an exponential fashion with temperature. Metabolic theory suggests the rate of increase corresponds to an 'activation energy' *E* of 0.65 eV. This value can be determined by plotting against 1/*kT* (inverse temperature), where *k* is Boltzmann's constant and *T* is temperature in Kelvins, and the slope corresponds to *E* (upper left panel). For ease of understanding, all calculations where performed using inverse temperature but are shown in the conventional manner with temperature in Celsius on the x axis. Note that the **A** and **B** depict the same data. Acceleration (**A** & **B**) is considered to be a mass-independent rate in fish[22], so standardization of body size is not necessary, but for speed (**C** & **D**) it is important to control for size. In the bottom right, all individuals range in length from 35 – 43 cm. Date for **A** & **B** is from [22]; **C** from [64], **D** from Wardle[49].

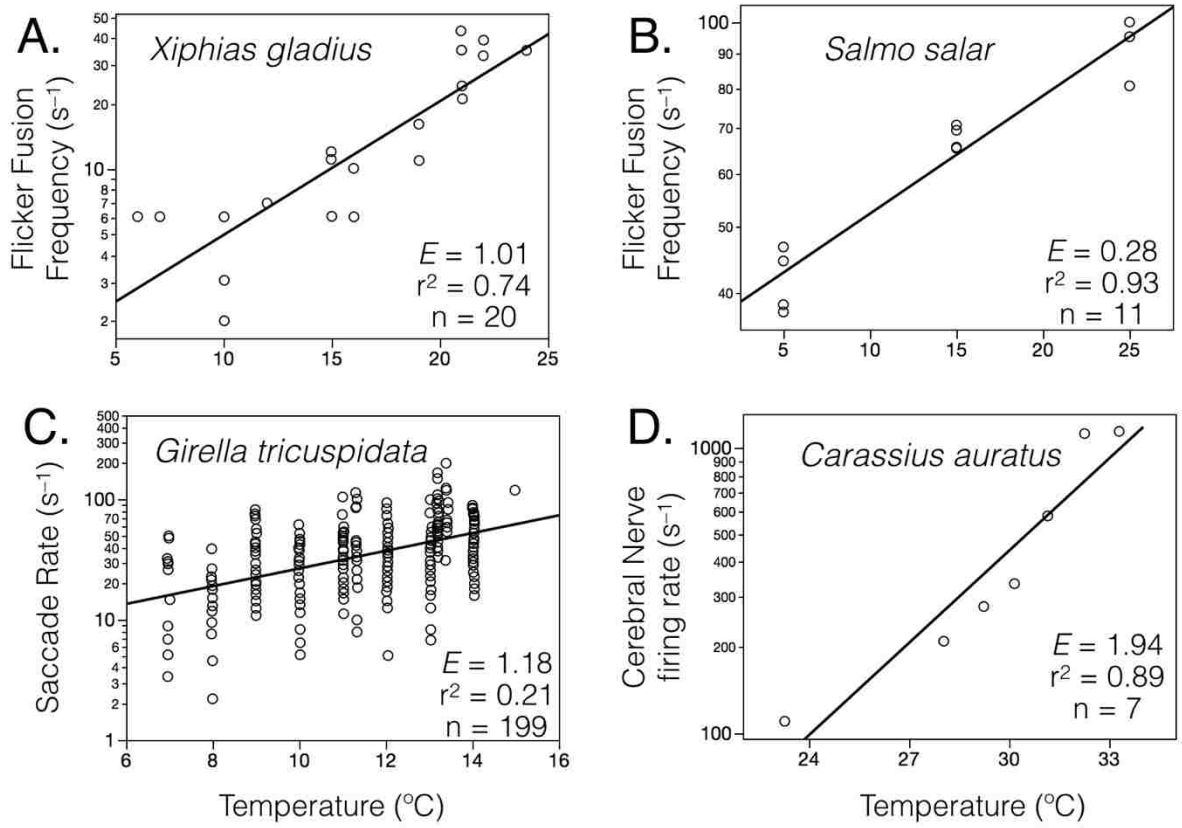

Figure S10. Thermal dependence of visual detection and processing speeds. Activation energies (*E*) are determined by plotting rates against inverse temperature 1/*kT*, where *k* is Boltzmann constant (eV) and *T* is kelvins; for clarity rates are shown plotted against temperature ºC. Data for **A** is from [65], **B** from [66], **C** from [67] and **D** from [68].

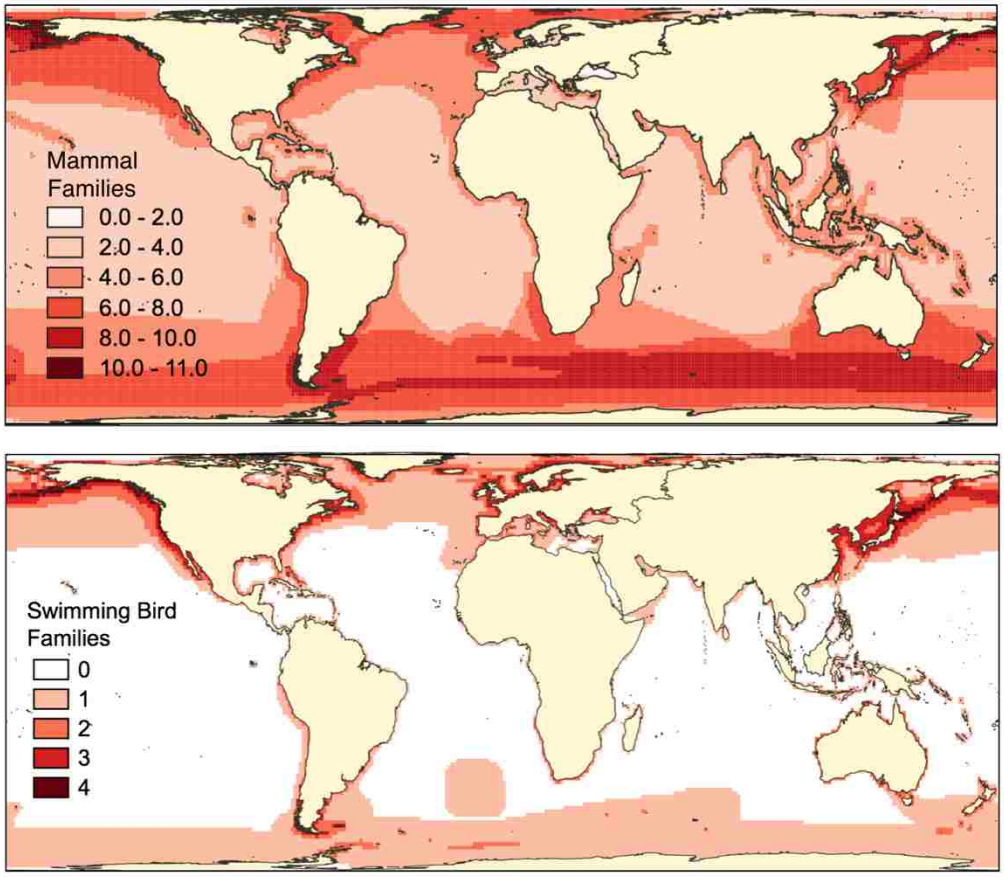

Fig S11. Familial level richness in predatory marine mammals and swimming birds.

Marine mammal families include families of cetaceans, pinnipeds, and otters; bird families include penguins, auks, ducks, grebes, loons and cormorants.

Conclusion

Energy sustains life, and an energetic approach to ecology can shed light on many puzzling features of nature. In chapter I, I linked growth rates to respiration to show that dinosaurs had an intermediate metabolism and thermal physiology. In chapter II, I present an extensive dataset on vertebrate growth and metabolism and discuss various challenges methodological and conceptual challenges to ascertaining and linking these two metrics. In chapter III, I and colleagues demonstrate quantitatively how individual metabolism gives rise to the ecosystem rate of carbon flux. Finally, in chapter IV, I show how the metabolic asymmetry between marine endotherms and ectotherms leads to favorable foraging conditions for endotherms in colder oceans. This, in turn, gives rise to starkly different patterns of biogeography and biodiversity. Throughout each of these chapters, energy has been the common theme underlying these various topics in macroecology.